Isotopic composition of Pb in tree rings of Norway spruce (*Picea abies)* from the Fensfjorden area, western Norway

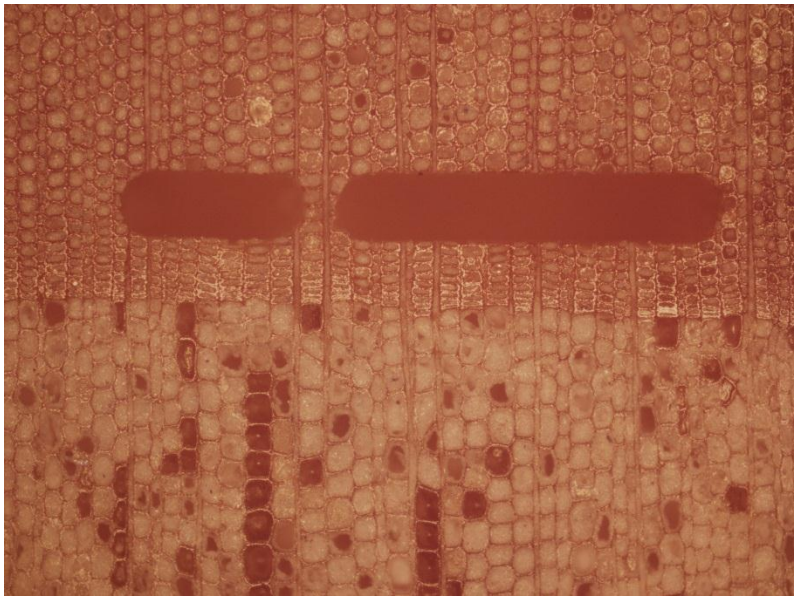

Hugo Vika Gjesteland

Master thesis

Depeartment of Earth Science

University of Bergen

2012

I. Acknowledgment

This master-thesis was conducted at the Institute of Geoscience, University of Bergen, under the instructions of Professor Jan Kosler.

When starting the work I did not know much about trees and their potential of recording past atmospheric changes in lead content and composition. However, over the last year I've gained some interesting results from tree ring analysis of two Norway spruces, collected in Nord-Hordaland in the vicinity of Statoil's Mongstad refinery.

First of all I want to thank Professor Jan Kosler for guidance and discussions over the last year, and for always keeping an open office door. You have been very helpful.

I want to thank my friends for supporting me throughout the study, and especially Thomas Karlsson for proofreading. Finally I want to thank my family and grandparents for being helpful and supporting throughout six years of study at the Institute of Geoscience.

Hugo Vika Gjesteland Bergen, 01.06.2012

II. Abstract

The annual growth of tree rings makes the trees as possible archive of the past atmospheric pollution. However, several aspects addressed in literature such as post-depositional mobility of Pb, intra-ring heterogeneity and possible detoxification mechanisms can make the interpretation on past atmospheric pollution, difficult. Annual rings of two Norway spruce (*Picea Abies*) trees 43 and 42 years old located 10.1 km north-northwest and 17.8 km east-southeast of Mongstad refinery, respectively, were analysed by laser ablation inductively coupled plasma mass spectrometer (LA-ICP-MS) for lead isotopic composition, and $^{63}Cu/^{12}C$, $^{66}Zn/^{12}C$ and $^{44}Ca/^{24}Mg$ elemental ratios. These two trees, recorded $^{206}Pb/^{207}Pb$ ratios between 1.13 and 1.32, and 1.12 and 1.29, respectively, but showed no systematic trend towards higher or lower ratios from the innermost to the outermost tree ring. For all ratios, only the $^{208}Pb/^{12}C$ (for tree #1) and $^{44}Ca/^{24}Mg$ (for tree #1 and #2) ratios showed pronounced trends. The $^{208}Pb/^{12}C$ ratio of tree #1 increased from 1968 and peaked in the year 1979, followed by a steady decrease toward the present (2010), and showed significant correlation with the lead content and the pH of precipitation in the area. The $^{44}Ca/^{24}Mg$ of tree #1 and #2 demonstrated showed a systematically decrease from 1968-2010 and showed significant correlation with the pH of the precipitation. Comparison of the lead isotopic composition of the tree rings with that recorded by mosses in the same area during the time period 1975-2000 showed significant differences. Most of the tree rings plotted have higher $^{206}Pb/^{207}Pb$ and $^{208}Pb/^{207}Pb$ ratios relative to the Norwegian peat bogs (<1691-1991), and also show some overlap with the relatively higher recorded ratios of a Greenlandic ice core (7313 BC to 1523 AD). The tree rings have also higher Pb isotopic ratios compared to the European aerosols. Comparisons with the $^{206}Pb/^{207}Pb$ ratios recorded by the Scottish peat bogs and mosses covering the same time period as the trees did not reveal any similarity. The onset of production at Mongstad refinery in 1975 and the subsequent expansion in the refinery production and occasional accidents in the factory did not have any significant impact on lead isotopic composition of the tree rings, nor on the $^{208}Pb/^{12}C$, $^{63}Cu/^{12}C$, $^{66}Zn/^{12}C$ or the $^{44}Ca/^{24}Mg$ ratios. Pollution associated with the Mongstad refinery may be minor compared to the long range pollution by atmospheric aerosols. In order to differentiate between pollution sources and natural sources, local soil and bedrock measurements and a chemical and isotopic analysis of Pb in oil that is being refined at Mongstad, should be carried out.

Table of Contents

1 Introduction

Lead in the environment stems from natural sources and can be released to the environment through anthropogenic activity. Emissions from anthropogenic activity along with natural "emissions" such as volcanic emissions, soil erosion, forest fire debris, biogenic emission and oceanic emission may contribute to the overall lead composition of the atmosphere (Rasmussen, 1998). Lead has four naturally occurring isotopes: ^{204}Pb, ^{206}Pb, ^{207}Pb and ^{208}Pb. Among these, only ^{204}Pb is non-radiogenic. The others, ^{206}Pb, ^{207}Pb and ^{208}Pb are the stable nuclides at the end of the ^{238}U, ^{235}U and ^{232}Th decay series, respectively (White, 1998). Depending on the geological system, the age of the system, and the initial chemical composition (Bollhofer and Rosman, 2001b), the amount of lead isotopes will vary, yielding different and characteristic isotopic ratios of the individual system/reservoirs (White, 1998). As a consequence of this, and because lead is not affected to a measurable extent by natural fractionation processes (Bollhofer and Rosman, 2001a), lead isotopes may be used as tracers in deciding the main contributing sources of lead pollution.

According to Komarek et al. (2008), atmospheric lead pollution is estimated to be approximately 5000 years old, and increased significantly during the industrial revolution (1750-1850) and even more when leaded gasoline became common practice in the 1920s (Dunlap et al., 1999). By the 1960s and 1970s, leaded gasoline was considered the most important source of atmospheric lead pollution, but the relative contribution of industrial emission increased when abolishment of leaded gasoline started (Nriagu, 1990).

The annual growth of tree rings and the assumption that they record and preserve the annual uptake of trace-metals and heavy metals, makes trees possible "archives" recording past and present pollution. Among tree species, conifers are regarded as having the greatest potential for dendroanalysis (have fewer ray cells (Legge et al., 1984)) due to its primitive nature of wood (Cutter and Guyette, 1993), but successful attempts with oaks, and maples (Watmough and Hutchinson, 1996, Watmough et al., 1998) have also been performed. However, several factors may discredit the use of tree rings as an environmental archive. A short summary of factors include the influence of the sapwood/heartwood boundary (Nabais et al., 1999), intra-ring variability/heterogeneity, possible detoxification mechanisms i.e. inward transportation of elements (Stewart, 1966) and detoxification via bark shedding (Hagemeyer and Weinand, 1996), inter and intra element mobility between tree-rings (possible through ray cells (Legge et al., 1984)), variation with stem level above ground (this can however be omitted by comparing tree-rings at the same stem height).

2 Aim of study

This study will attempt to evaluate possible pollution from Statoil's refinery located at Mongstad in Hordaland and test whether it is possible to distinguish pollution originating from Mongstad refinery from other sources, e.g. local sources such as transport or geology, and distal sources abroad. This will be addressed by investigating the lead content and lead isotopes recorded by annual tree rings of two Norwegian spruces (*Picea Abies*). In addition, content variations of heavy metals/trace metals in the tree rings will be investigated.

A final objective will be to evaluate the reliability of tree rings as an environmental archive. This will be addressed by comparisons with historic records of pollution, i.e. peat bogs, mosses and ice-cores. In addition data from operated weather stations or climatic stations will be used to support the conclusions.

3 Background

3.1 The Study Site

3.1.1 Location

Figure 3-1 shows a topographical map of the study area and the respective location of the two collected tree boles of Norwegian spruce (*Picea Abies*). Tree #1 and #2 are located approx. 10.1 km north-northwest and 17.8 km east-southeast of the Mongstad refinery, respectively. Geographical coordinates are listed in Table 3-1.

	Geographical coordinates
Tree #1	60°53'55.98"N, 5° 2'14.22"E
Tree #2	60°46'13.56"N, 5°21'4.74"E

Table 3-1 Geographical coordinates of Tree #1 and #2.

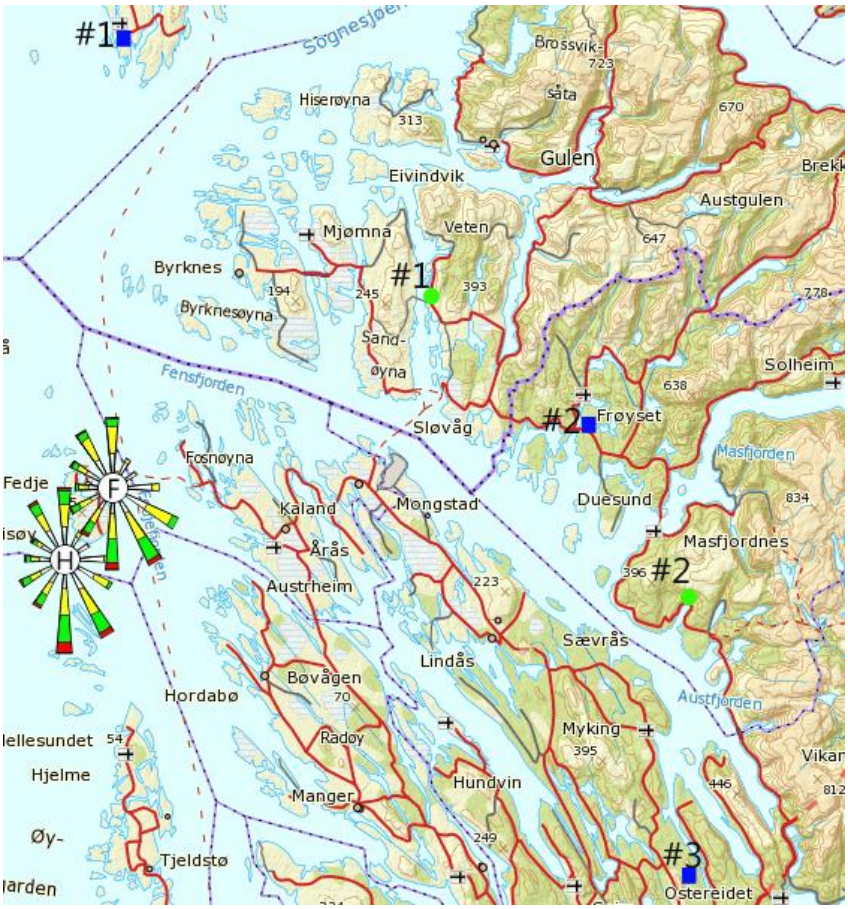

Figure 3-1 Topographical map of the Mongstad area. Green filled circles: Tree #1 and #2, blue squares: weather stations recording precipitation data, #1= Ytre Solund, #2=Frøyset, #3=Eikanger – Myr. Hellisøy (H) and Fedje (F) denote the locations of the two stations recording wind data.

3.1.2 Bedrock geology

The study area is part of *The Western Gneiss*-region, and the two trees, #1 and #2, were collected just outside the Bergen Arc, situated on metamorphosed (Caledonian orogeny) Precambrian rocks. Rocks surrounding tree #1, consist of monzogranitic to granodioritic gneisses, sometimes bonded, and quartzitic gneisses and quartzites, granitic dikes and augen gneiss. The rocks encompassing the area surrounding tree #2, are dioritic to granitic gneisses, with occurring heterogeneous veins of migmatite. In the heights northeast of tree #2, a lens of meta-sandstone and mica schist occurs.

No rock samples were collected for the two sites. Whole rock lead content and lead isotopic composition were not available for the study area. Lead concentration and lead isotopic composition only exist for the highly radiogenic minerals, like zircon, used for dating. These will not be representative for the whole rock lead isotopic composition. Therefore, the influence of local bedrock geology on the lead isotope composition of the tree rings is difficult to assess.

3.1.3 Soil type

According to Norwegian-Institute-of-Forests-and-Lanscape (2007), no municipal maps showing soil characteristics (depth to bedrock and distribution) within Gulen and Masfjorden exist. However, a sedimentary map from NGU covers both the localities. This map shows that tree #1 and #2 grew in an area classified as having thin sedimentary cover. Regarding lead isotopic ratios of soils in Norway, Steinnes et al. (2005) refers to a study performed by Steinnes et al., though unpublished, that the $^{206}Pb/^{207}Pb$ ratios of the C-horizon from different parts of Norway (not specified which places), vary between 1.20-1.73.

3.1.4 Weather conditions

The amount of precipitation and prevailing wind direction will control the geographical distribution of lead. Some lead particles may be transported over great distances, and some particles will fall to the ground during periods of rain. Emitted flue-gases and particles from Mongstad or other pollution sources can be removed from the atmosphere by dry (usually deposited locally) and wet deposition (carried over greater distances) (Slinn, 1977, Larsen, 2000). Precipitation data for Eikanger-Myr, Frøyset and Ytre-Solund weather-stations are plotted in Figure 3-2. As the Ytre-Solund weather station covers the whole life-span of both trees and because the weather stations in the area demonstrate similar records over time, this particular station will be used in this study. From 1965 to 2011 the amount of

precipitation here varied between 1284.4 (min. in 1996) and 2521.1 mm (max. in 1967), but no systematic trend is observed. The wind-roses of Figure 3-1, H (Hellesøy Lighthouse) and F (Fedje), display two different periods, 1965-2005 and 2004-2011, respectively. However, they show very similar wind distribution. Southern and southeastern winds appear to dominate, followed by western and northern winds.

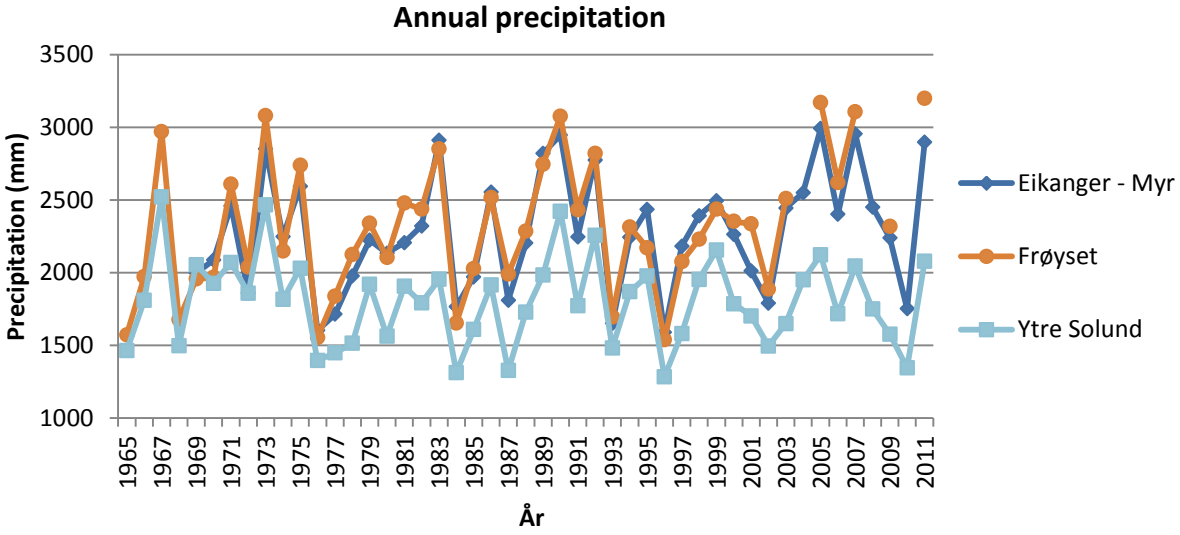

Figure 3-2 Annual precipitation data from weather stations published by Meterologisk-institutt (2012).

3.1.5 Mongstad oil refinery

3.1.5.1 History and accidents at Mongstad oil refinery

Before the 1970s Mongstad did not have any significant industry. Neptun Canning, a cannery, was put into operation in 1927 and provided work for up to 60 people- the largest place of work in the rural district for 45 years (Kolstad, 1999). Before the building of Mongstad refinery, the North-Hordaland district witnessed a great depopulation due to lack of industry and the planned closing of the Neptune Canning factory (Bjørnevoll and Mongstad administrasjon, 2004, Kolstad, 1999). Hydro and British Petroleum (BP) started the building of Mongstad refinery in 1972 and it was officially opened on the 25. September 1975. In the beginning, the capacity of the refinery was 4 million tons crude oil per year (Kolstad, 1999), and in 1989 it increased from 6.5 to 10 million tons crude oil per year. Figure 3-3 lists accidents and relevant information regarding operation of the Mongstad refinery, some of these which may have influenced the lead content in the tree rings. Also listed are relevant events which may have had an effect on the lead content of the trees.

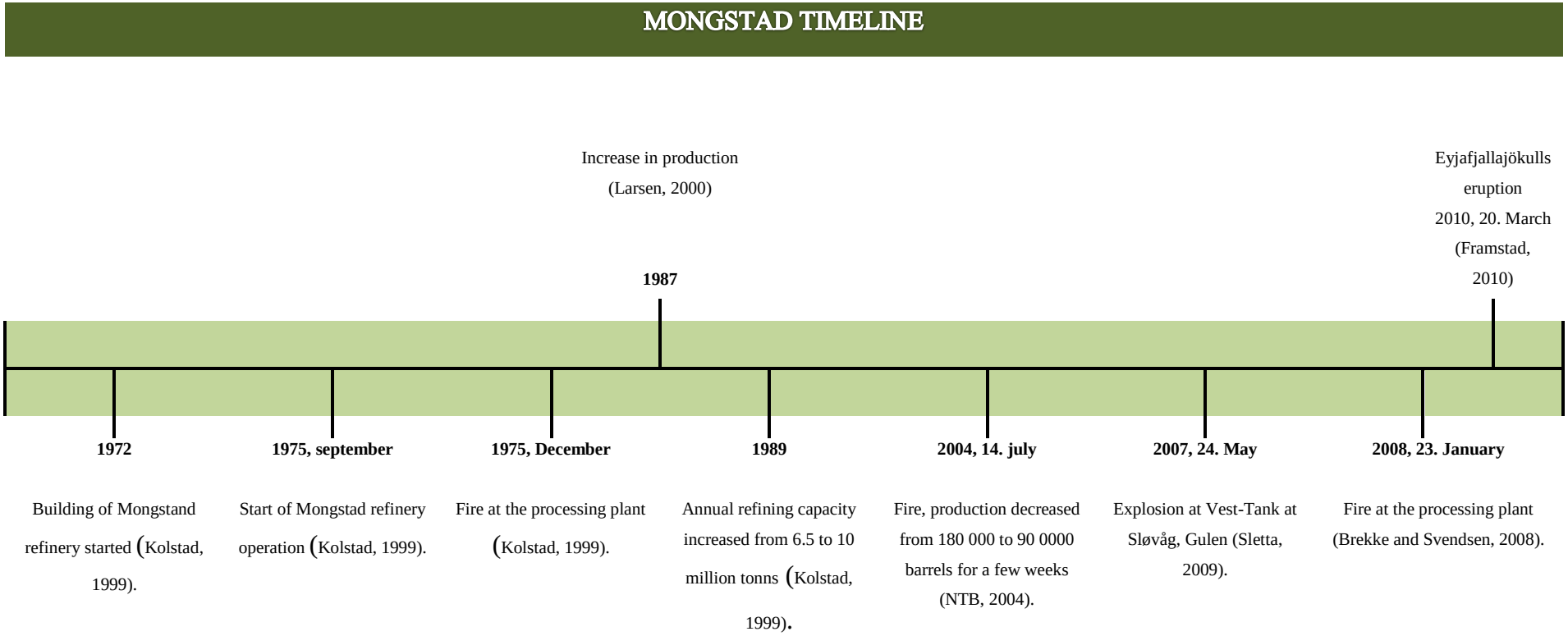

Figure 3-3 Timeline representing the history of the Mongstad refinery, and related accidents. Also listed are relevant event which may have had an impact on the lead content of the two trees. The distance between the events is not to scale.

3.2 Lead in nature

3.2.1 General

3.2.1.1 The natural isotopes of lead

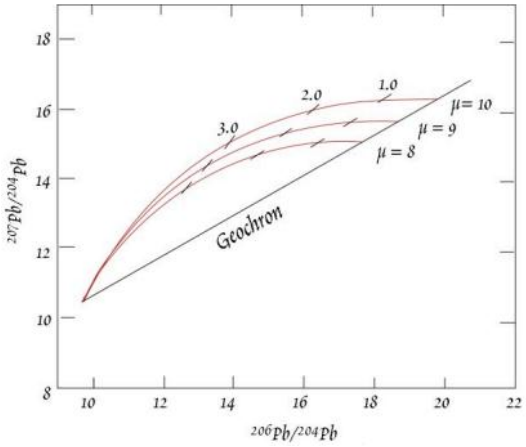

Figure 3-4 The evolution of $^{207}Pb/^{204}Pb$ and $^{206}Pb/^{204}Pb$ through time shown for three μ ($\mu = \frac{238U}{204Pb}$) values. Figure from White (1998).

Lead belongs to group number 14 in the periodic system, and it is the most studied heavy metal (Aberg et al., 1999). It has four natural isotopes ^{204}Pb, ^{206}Pb, ^{207}Pb and ^{208}Pb. Among these, only ^{204}Pb is non-radiogenic. The others, ^{206}Pb, ^{207}Pb and ^{208}Pb are the stable nuclides at the end of the ^{238}U, ^{235}U and ^{232}Th decay series, respectively (White, 1998). ^{204}Pb is the least naturally occurring isotope of Pb, with abundance of only 1%, while the ^{208}Pb, ^{206}Pb and ^{207}Pb isotopes comprise 52%, 24% and 23% of the naturally occurring lead, respectively (Komarek et al., 2008). Depending on geological system, age of the system, and the initial chemical composition (Bollhofer and Rosman, 2001b), the amount of lead isotopes will differ, yielding different and characteristic isotopic ratios of the individual systems/reservoirs (White, 1998). Figure 3-4 show the evolution of $^{207}Pb/^{204}Pb$ and $^{206}Pb/^{204}Pb$ through time.

3.2.1.2 Lead and heavy metals in soil profiles

Figure 3-5 shows an idealized developed soil profile. The upper two horizons, O- and E-horizons, tend to form the bulk of the rhizosphere, which is the depth to which plant roots may extend. The uppermost horizon, the O-horizon, is rich in organic matter and is best developed where decomposition rate is slow, i.e. in soils depleted in O_2 (White, 1998). Going downward we enter the E-horizon – the zone of leaching – which contains a variety of minerals, organic compounds and the humus. The underlying B-horizon is the zone of accumulation, and compared to the overlying E-horizon it is richer in clays and poorer in organic matter. The last horizon before encountering the bedrock is the C-horizon, which is only weathered rock.

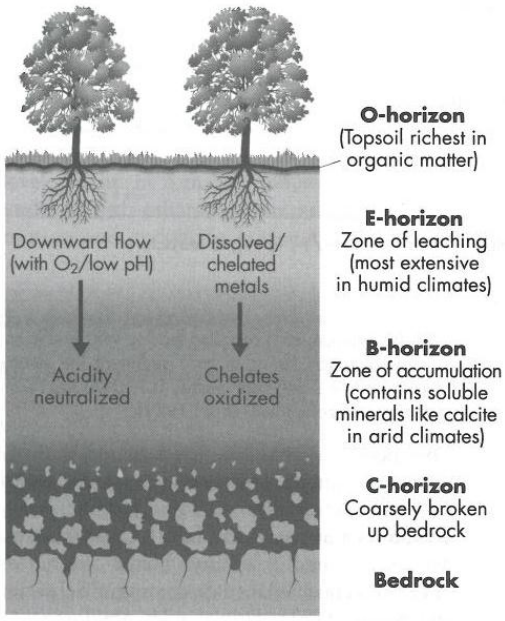

Figure 3-5 A sketch of an idealized soil profile (Konhauser, 2007) .

The abundance of natural heavy metals and nutrients in soils depend on the geological source of the parent material (Motto et al., 1970). According to Adriano (1986), lead generally accumulates in the upper parts of the soil surface, more specifically in the upper few centimeters. Most of the anthropogenic lead is considered to reside in the topsoil horizons (Hutchinson and Whitby, 1977). According to Lepp (1975), airborne lead occurs most commonly in particulate form.

However, lead- (and other elements) and nutrient uptake by the root system is to a certain extent regulated by edaphic- (abiotic factors) and biological factors (e.g, microbes) of the soil (Lepp, 1975, Taiz and Zeiger, 2007), which affect the bioavailability of the element. These factors involve interactions between soil microbes, plant roots, fungi, pH, the presence and degree of both organic and inorganic colloidal particles, available nutrients and heavy metals, and competition between cations. Other factors such as climate and topography, also affect the distribution of heavy metals and nutrients in soils (Adriano, 1986). Colloidal particles have predominantly negative charges which may adsorb and immobilize nutrients and heavy metals through cation-exchange (McBride et al., 1997, Taiz and Zeiger, 2007). In addition to cation exchange reactions, heavy metals may form chelate complexes. This may lower the bioavailability of the specific metal involved (Alloway, 1995). The pH of the soil affects the stability of metal-organic complexes; high pH increases complexation (Berggren et al., 1990).

3.2.2 General lead pollution history

According to Komarek et al. (2008), atmospheric pollution is estimated to be approximately 5000 years old, first introduced in southwestern Asia. It was estimated a Pb production of 200 tons a year, which increased during the time of the Roman Empire to 80 000 tons a year. Figure 3-6 illustrates the lead production from 5000 years before present. The lead production increased significantly from about 500 years ago. This coincides with the industrial revolution (1750-1850). During the 20th century lead emission increased predominantly by the increasing use of leaded gasoline (introduced in the 1920s (Dunlap et al., 1999)) followed by the increased industrial activity (Komarek et al., 2008). Figure 3-6b shows the lead production in terms of gasoline in the US. The column diagram in Figure 3-6c illustrates the significant amount of emitted lead associated with leaded gasoline in 1983.

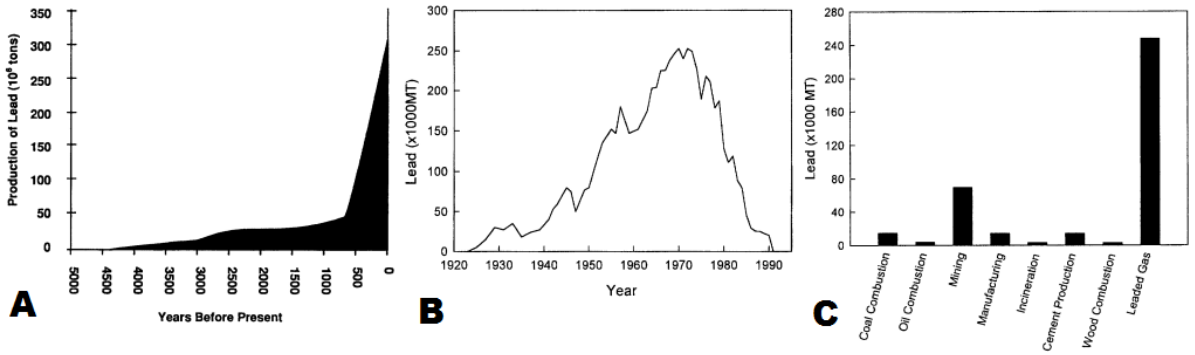

Figure 3-6 Three diagram showing cumulative lead production and discharge (A) from 5000 years before present, lead consumption in terms of gasoline in the US (B), and the worldwide lead emission to the atmosphere from various sources in 1983. All diagrams from Smith and Flegal (1995).

In Norway, the dominating pollution sources from the 17th century to about 1925 are considered to have been coal burning and ore-smelting, both from England and from The Continent (Aberg et al., 2004). Continuing from 1925 until 1950, Aberg et al. (2004), claim that waste burning, in addition to coal burning and ore-smelting comes into play. From the 1950 till present day, leaded gasoline, waste incineration, and coal- and coke-burning are considered the most contributing sources of pollution (Aberg et al., 2004). According to Steinnes (2001), long-range atmospheric transport of trace-elements is the dominating source of contamination in Norway. The elements, zinc, arsenic, selenium, molybdenum, cadmium, tin, antimony, tellurium, thallium, lead and bismuth are considered to emanate from Europe. On the other hand, the elements, chromium, nickel, and copper originate from point sources within Norway. Also, point-sources located in northwestern Russia, close to the

Norway/Russia border, are considered to contribute with pollutants to the Norwegian environment (Steinnes, 2001).

3.2.3 Lead content in gasoline used in Norway

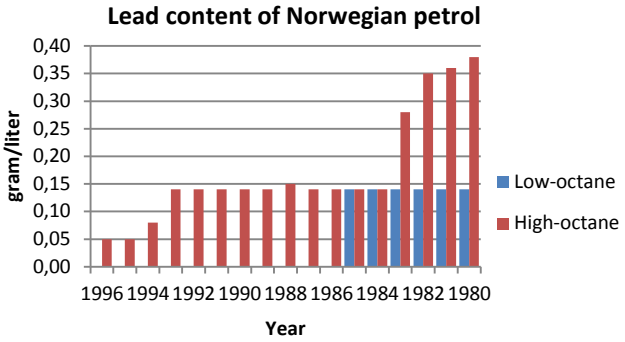

Figure 3-7 Avarage lead content of leaded gasoline used in Norway. Data from Statistisk sentralbyrå (2002).

Figure 3-7 demonstrates the average Pb content of leaded gasoline used in Norway. Sale of low-octane gasoline terminated in 1987, while that of high-octane continued until 1997, when replaced by petrol containing a Pb substitute (Statistisk sentralbyrå, 2002). The Norwegian leaded gasoline had a $^{206}Pb/^{207}Pb$ ratio between 1.07-1.10 (Aberg et al., 2004).

3.2.4 The pH and the lead content of precipitation

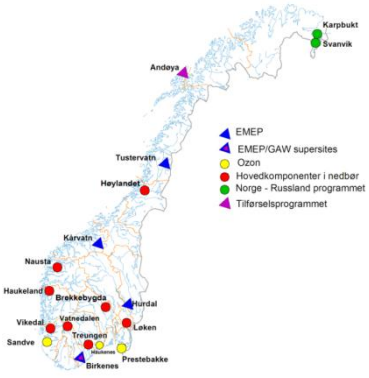

Figure 3-8 Location of stations operated by KLIF. Figure from Schartau (2011b).

Stations operated by KLIF (Climate and Pollution agency of Norway) are shown in Figure 3-8. However, not all stations perform the same type of measurements, and preferably, the stations located along the southwestern coast of Norway should be used in this study. Figure 3-9 shows variation in rainwater pH as well as composition in terms of ammonia, sulphate (corrected for seasalt), and nitrate at Haukeland. Data between 1976 and 1982 are, however, missing. The pH increases from the 70s to the present, with a corresponding decrease in sulphate concentration. Figure 3-10 demonstrates Pb concentrations of precipitation in terms of µg/l measured at various stations (Birkenes, Nordmoen/Hurdal, Kårvatn and Svanvik) in the period 1976-2010. At Birkenes, a steep decline in Pb concentration is registered in the period between 1976 and 1986. By means of data from Birkenes station (located in southernmost Norway, see Figure 3-8), Steinnes (2001) points out that air concentrations of heavy metals in 1978-1979 were highest during periods of south-easterly to south-westerly wind directions. This was also the case for a study performed during 1985-1986. Steinnes et al. (2005)

calculated that only 11.7% for 1978-1979 and 11.8% for 1985-1986 of the integrated amount of lead in Norway emanated from sources within Norway. Also, regular monitoring of 27 elements in precipitation of 1989-1990 at 6 stations (Birkenes, Nordmoen, Osen, Kårvatn, Jergul and Svanvik), attributed 42% of the variation in element composition at Birkenes, to long range atmospheric transport (Berg et al., 1994, Steinnes, 2001).

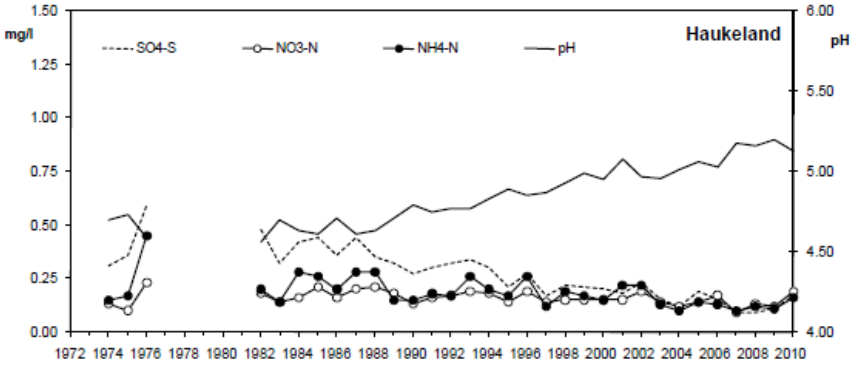

Figure 3-9 Sulphate- (corrected for seasalt), ammonia-, nitrate-concentrations and the pH of precipitation at Haukeland (for location see Figure 3-8). All values are mean values. Figure from Schartau (2011a).

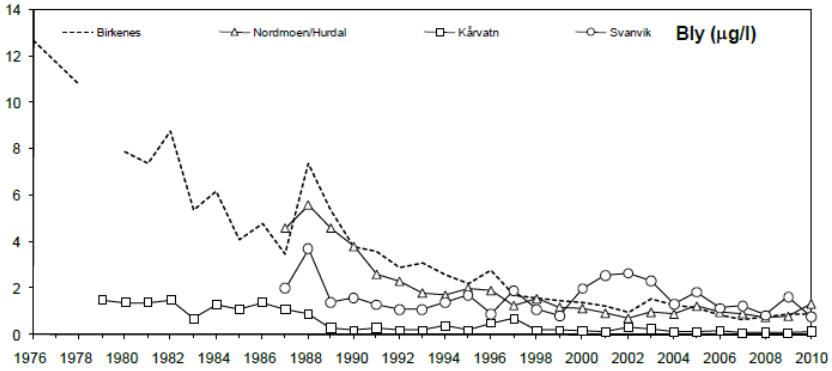

Figure 3-10 Lead concentrations in precipitation measured at different stations in Norway. All values are mean values. For location of these stations see Figure 3-8. Figure from Schartau (2011a).

3.3 Tree physiology

Gymnosperms, producing softwood, and Angiosperms, producing hardwoods, are the two main categories of seed plants, with their names originating from the nature of the seeds (Hoadley, 2000, Taiz and Zeiger, 2007). The name gymnosperm is Greek for "naked seed", which refers to these seeds as "naked" exposure to air, contrary to the angiosperm seeds which are "hidden" inside a fruit. Three types of wood exist: softwood (gymnosperms, i.e.conifers), diffuse porous wood and ring porous wood (e.g. oak) (Watmough, 1999). Diffuse porous- and ring porous wood is often referred to as hardwood.

Gymnosperms are divided into four groups; *Cycadophyta*, *Ginkgophyta*, *Gnetophyta*, and *Coniferophyta*, with the largest group being the *Coniferophyta*. The *Coniferophyta*, known as the conifers (the name is reffering to «cone-bearers»), is comprised of eight families with currently 70 genera and 614 species (Farjon, 2010). Most of the conifers grow in the temperate zone of the northern hemisphere in regions such as Canada, Scandinavia and Russia and include trees as pine, fir, redwood and spruce.

3.3.1 Structure of a seed plant

The vegetative body of a seed plant can be divided into three separate parts: leaf, stem and root, with its general structure shown in Figure 3-11. This can be applied to all seed plants, despite their apparent diversity. Their main function is photosynthesis (leaf), support and transport (stem), and anchorage and absorption of water and minerals (root) (Taiz and Zeiger, 2007). The basic plant form/structure is obtained during a phase called primary growth (this structure is shown in Figure 3-11) at the apical meristems, which involves cell division and cell enlargement (Taiz and Zeiger, 2007). However, when this process is finished, secondary growth may occur. Secondary growth gives rise to the two lateral meristems vascular- and cork cambium (Taiz and Zeiger, 2007). Subsequently, these two meristems form secondary xylem (wood formation) and secondary phloem. Structures and features obtained during secondary growth are shown in Figure 3-13 (section 3.3.2). Some plant terminology encountered during the course of this master-thesis is included in an alphabetically ordered table, Table 3-2.

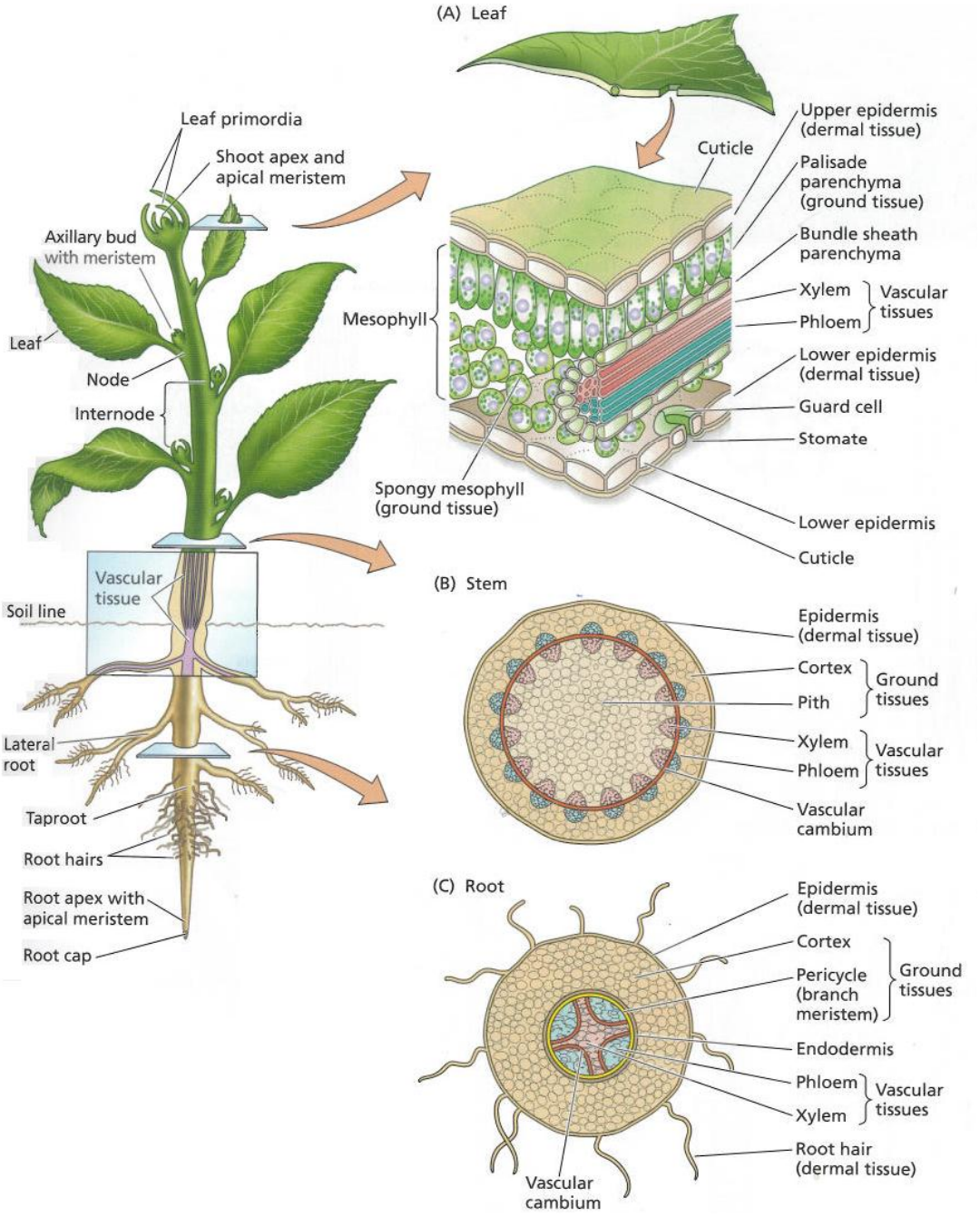

Figure 3-11 The general structure of a seed plant. Cross-sections of stem, root, and leaf show the respective structures and features inside. Figure from Taiz and Zeiger (2007).

PLANT TERMINOLOGY	
Apoplast	A term used to describe the interconnected system containing all the cell walls and their associated water content (Taiz and Zeiger, 2007, Hine, 2008a).
Cork cambium	A lateral meristem forming an outer cork and secondary cortex known as pheolloderm. For location of this meristem, see Figure 3-14. (Hine, 2008a)
Cortex	The tissue between the epidermis and the vascular tissue. Made up of parenchyma cells. (Hine, 2008a).
Dermal tissue	The outermost tissue of a plant body; consist of epidermal cells. (Taiz and Zeiger, 2007).
Embolism	Gas bubbles within the xylem sap (Zimmermann et al., 1971).
Endodermis	The innermost part of the root cortex containing the Casperian strip (Taiz and Zeiger, 2007, Hine, 2008a).
Epidermis (dermal tissue)	The outermost tissue of the plant body (dermal tissue) (Hine, 2008a).
Ground tissue	Consist of parenchyma-, collenchyma- and sclerenchyma cells. The main tissues cortex, pith and primary medullary rays (Hine, 2008a).
Guard cell	Control the opening and closing of leaf pores (stoma) (Taiz and Zeiger, 2007).
Lateral root	A lateral root originating from the taproot (Hine, 2008b).
Mesophyll	The internal tissue of leaves. Consist of parenchyma cells (Hine, 2008a).
Middle lamella	See Figure 3-12
Node	A point on the stem where leaves arise (Hine, 2008a).
Pericycle (branch meristem)	An internal meristematic tissue (Taiz and Zeiger, 2007).
Periderm	The cork cambium, cork and phelloderm make up the periderm layer. Serves as protection. See Figure 3-14 for more information (Hine, 2008a).
Phloem	A vascular tissue conducting products (sugars) from photosynthesis to sites where needed (Hine, 2008a).
Pit-pairs	A pit-pair (see Figure 3-12) is two adjoining pits (circular gaps in the secondary walls), which are microscopic regions of thinned porous primary cell wall and absent secondary cell wall(Taiz and Zeiger, 2007).
Pith	The center of a plant stem consisting of parenchyma tissue (Hine, 2008a).
Plasma membrane	A partially permeable membrane which form the boundary of cells, and regulates the flow of material (Hine, 2008a). See Figure 3-12
Plasmodesmata	Cylindrical pores from 20 to 60 nm in diameter that connect the cytoplasms of adjacent cells (Taiz and Zeiger, 2007).
Primary cell wall	See Figure 3-12
Ray cells	Also known as medullary rays. Function as storage and also conduct food material radially (Hine, 2008a).
Root cap	Protector of the root and directing growth downward. If not present, root may grow upwards (Taiz and Zeiger, 2007).
Root hairs	Microscopic extensions of root epidermal cells (Taiz and Zeiger, 2007).
Stele	A term including features from the end of the cortex to the core of the root. It contains the vascular elements of the root (Taiz and Zeiger, 2007).
Taproot	The main part of the root for which lateral roots or fibrous root systems develop (Hine, 2008a).
Traheids	Xylem tissue of the conifers. Diameters of tracheids range from 20-60 μm. They are about 100 times longer than their respective diameters (Hoadley, 2000). See Figure 3-14 for a visual look.
Vascular cambium	A lateral meristem forming secondary xylem and phloem (Taiz and Zeiger, 2007).
Vascular Tissue	Xylem and phloem make up the vascular tissue (Taiz and Zeiger, 2007).
Xylem	A tissue in vascular plants, transporting water, mineral-nutrients and other elements (Taiz and Zeiger, 2007).

Table 3-2 Some plant terminology encountered during this master-thesis.

3.3.2 Cells and tissues

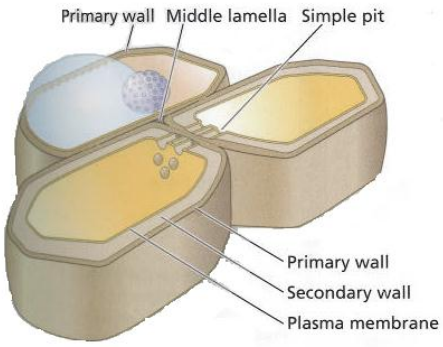

Figure 3-12 Simplified structure of three adjacent cells. For simplicity, the vacuole of only one cell is shown (Taiz and Zeiger, 2007).

Figure 3-12 demonstrates the basic structure of three adjacent plant cells. The walls consist of a primary and a secondary wall, the first being thin while latter is thicker and stronger as a result of the presence of lignin. Each cell is cemented together by a middle lamella. A pit-pair (see Figure 3-12) is two adjoining pits (circular gaps in the secondary walls), which are microscopic regions of thinned porous primary cell wall and absent secondary cell wall. They provide a low-resistance passageway for water between adjacent tracheids (Taiz and Zeiger, 2007). The cytoplasm of adjacent cells in a plant is interconnected to each other by cytoplasmatic bridges, called plasmodesmata. These are cylindrical pores from 40 to 50 nm in diameter. This interconnection is referred to as the symplast (Taiz and Zeiger, 2007). In plants, three major tissue systems are recognized and make up the plant body. These are dermal tissue, ground tissue and vascular tissue. The vascular tissue consists of two types of tissues: xylem and phloem, both extending throughout the plant body (Taiz and Zeiger, 2007). Figure 3-13 shows the basic structures of a tree bole and the corresponding terminology obtained after secondary growth (the formation of wood). Also, a thin section of white pine is shown, displaying the tracheids making up the early- and latewood, ray cells and a resin channel. The ray cells conduct water and solutes radially, and may also store reserves when in surplus, and use them later when needed (Zimmermann et al., 1971). These rays cease to function in the conversion from sapwood to heartwood (Hagemeger, 1995).

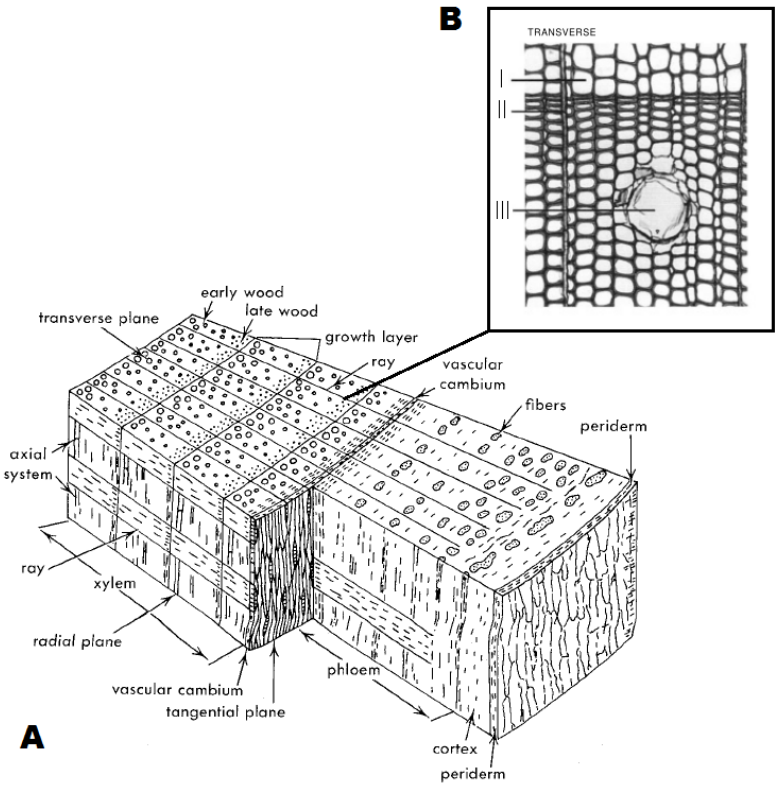

Figure 3-13 Basic structures of an idealized bole of a tree. Note the ray cells, which will be of discussion later in this thesis as possible "channels" for metal mobility. (B) Thin section of white pine (conifer), magnified about 100 times. This figure shows tracheids (I), rays (II), and a resin channel (III). Figure A from Esau (1977), and B from Hoadley (2000).

Xylem functions as a water- and mineral-nutrition conductor, transporting water from the root system and higher up through the stem and finally through the leaves and into the atmosphere (Taiz and Zeiger, 2007). It consists of two types of tracheary elements: tracheids and vessel elements (see Figure 3-14 for structure). For conifers, tracheids function as the water and mineral conducting tissue, and make up more than 90% of the total wood volume (Hoadley, 2000). The rest of conifer wood is made up of ray tissue (Hoadley, 2000). As Figure 3-14 demonstrates, tracheids are elongated cells, and together they overlap and connect through pit-pairs. The composition and anatomical structure of the xylem tissue is not homogenous within a tree stem; it is spatially heterogeneous. Hence, according to Gartner (1995), physical and mechanical properties vary in accordance with xylem composition and structure. This must be taken into account when laser ablation is performed. The other tissue involved in the vascular tissue is the phloem. This tissue, however, translocates the products of photosynthesis, and differ from xylem be means of having living cells when functional (Taiz and Zeiger, 2007).

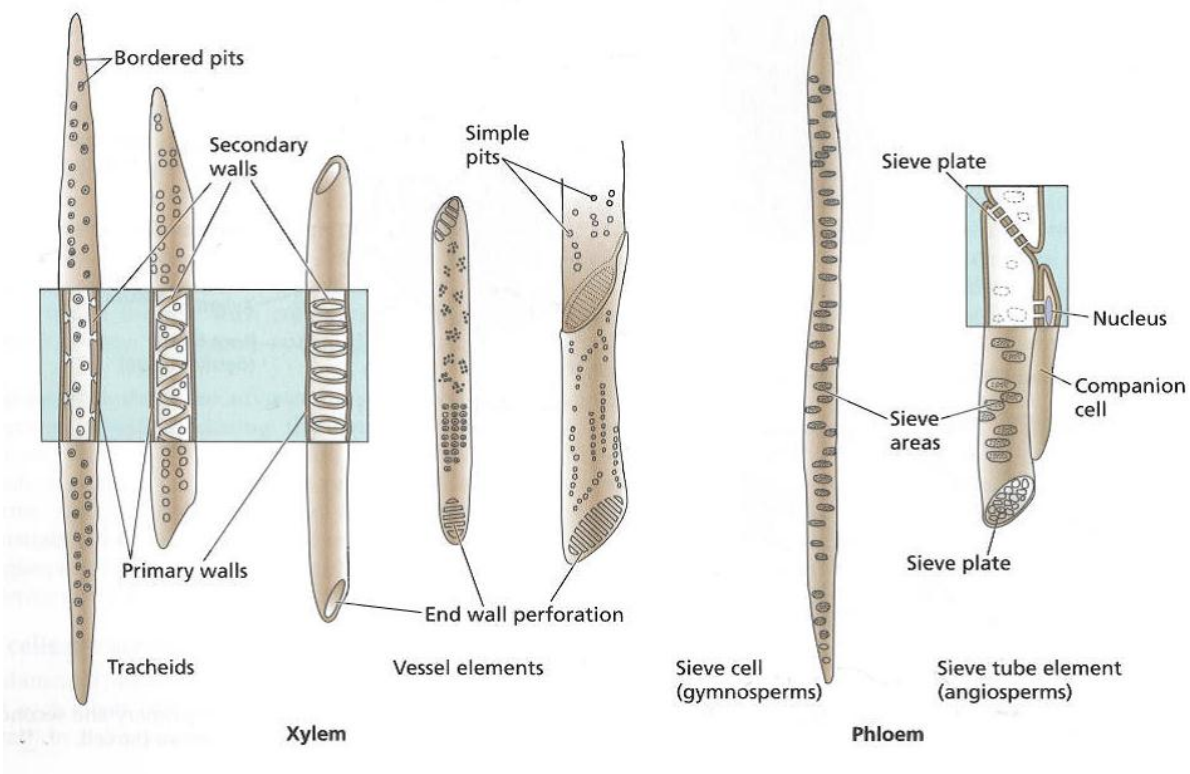

Figure 3-14 The vascular tissues: xylem and phloem, and their different structures (Taiz and Zeiger, 2007).

3.3.3 Formation of tree-rings

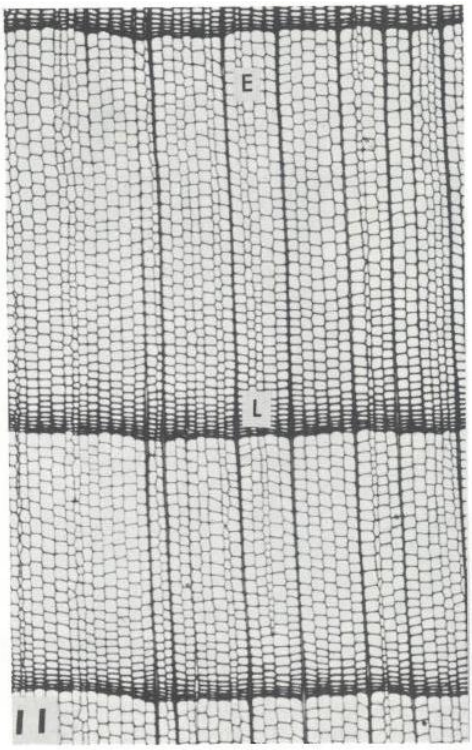

Figure 3-15 The white semi-squares, encapsulated by a black colored margin, are the tracheids elements. E=Earlywood, L=Latewood. Figure from Zimmermann et al. (1971).

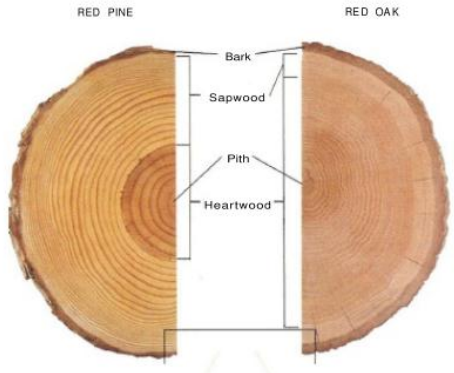

Figure 3-16 Cross-section of red pine (conifer), and red oak (Angiosperm). The heartwood (dark area) and sapwood (light area) width is significant different between the two; the heartwood area of red oak being much wider. From Hoadley (2000).

The formation of tree-rings varies with species, age, latitude and growing conditions (climate, soil, etc.). In the case of conifers growing in the northern hemisphere, annual tree-rings are formed (Zimmermann et al., 1971). Figure 3-15 demonstrates a transverse section of wood of *Pinus Ponderosa* Laws. (a conifer). In conifers, growth rings are elucidated by the distinction between early- and latewood. Earlywood has larger tracheids and cells with thinner cell-walls, and is produced by rapid growth in the early part of the growing season (spring) contrary to latewood which is produced by slower growth in the summer and autumn, hence its denser structure (Zimmermann et al., 1971, Watmough, 1999). This produces the characteristic light coloured- and dark coloured wood, which is clearly shown in Figure 3-15, where the wider and larger tracheids form the earlywood, and the more dense and thick cells form the smaller tracheids elements of the latewood.

Heartwood and sapwood are terms used to distinguish dead and living xylem cells, respectively. Heartwood consists of cells thickened with lignin, providing structural support, while sapwood consists of xylem cells conducting water along with structural support (Hine, 2008a). The time of conversion from sapwood to heartwood, or the time of formation of heartwood, is widely discussed. Longuetaud et al. (2006) investigated the heartwood/sapwood boundary, along with its variation within and between 4 Norway spruce (*Picea abies*) stands in north-eastern France. When plotting the number of heartwood rings vs.

the cambial age of the disc, they obtained a linear relationship with a linear correlation factor of 0.8415. Then, by linear regression they found the heartwood initiation age to be 17 years. For sapwood rings, a mean lifetime of 45 years was estimated by linear regression. This is in correlation with Zimmermann et al. (1971) which states that, quotation, "irreversible embolism seems to have occurred in all tracheids of a given growth ring by the time it has reached the age of 40 years". A study by Cermak et al. (1992), showed that 10-12 out of total 18 xylem rings of Norway spruce were carrying xylem sap. As shown in Figure 3-16, the heartwood/sapwood boundary is considerably different between species, and may also vary within the same species with changing growing conditions (Hoadley, 2000).

Some researchers claim that the heartwood/sapwood boundary is important when inferences on the radial Pb and other heavy metals distribution are to be drawn.

3.3.4 Uptake and transportation of minerals and water

Heavy metals can enter trees through roots, leaves and bark (Lepp, 1975). Water, mineral absorption and uptake by the root system is carried out near the root tips (Taiz and Zeiger, 2007), but as Kahle (1993) points out, uptake and response may vary with application levels, the duration of exposure, the species, age and nutritional status of the plant, transpiration conditions, and other physiological conditions. External factors (climate, topography, bioavailability, etc.) have been discussed earlier in section 3.2.1.2. Water and mineral nutrients can enter the root-system via three pathways: the apoplast-, symplast- or transmembrane pathway, but the precise points of entry for minerals have been of considerable debate (Taiz and Zeiger, 2007). According to Dunn (2007) lead is taken up by root hairs and from the C-horizon at a depth of 1-3 m (Kovalevski, 1987). Three different pathways are shown in Figure 3-17. When loaded into the tracheary elements of the xylem, the ions are translocated in the xylem sap to the shoot or other parts in the plant depending on the biological function. According to Dollar and Lepp, 1977 translocation happens by ion exchange with the xylem wall which carries a negative charge due to the carboxyl groups. Also, metals are most likely transported in a complexed form (Lepp, 1975). Thereof, the quantity of Pb deposited may not represent the total Pb carried within the xylem sap, but a fraction of it; namely, the readily bound ionic form. Entry through roots is considered the major pathway for most elements (Watmough, 1999), and when they enter the xylem they are not necessarily restricted to the outermost tree ring (Lepp, 1975), cf. the sapwood/heartwood boundary discussed in section 3.3.3. This means that trace- and heavy metals may be transported in several adjacent tree rings simultaneously (Hagemeyer and Weinand, 1996).

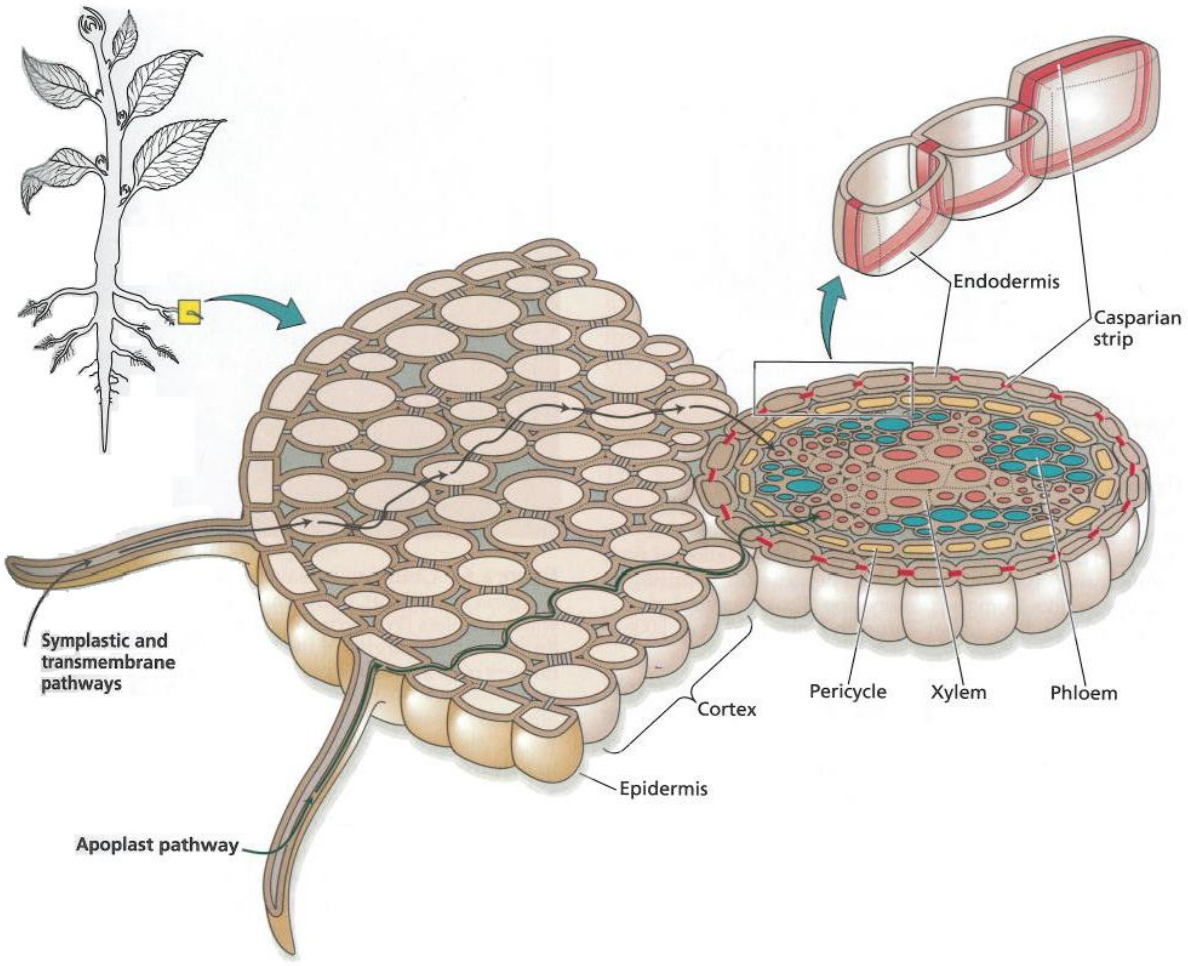

Figure 3-17 Cross-section of a root, showing the apoplastic, symplastic and transmembrane parthways (Taiz and Zeiger, 2007).

However, this varies from species to species, e.g. Ellmore and Ewers (1986) reported that 92±2% of all the fluid transport occurred in the outermost xylem increment of American Elm (*Ulmus Americana*).

In addition to mineral uptake by the root system, leaves can absorb mineral nutrients and heavy metals, in a process referred to as foliar uptake (Lepp, 1975, Taiz and Zeiger, 2007). After foliar uptake, nutrients or other elements are carried from the leaf by the phloem. Then, lateral translocation from the phloem to the outer xylem may take place (Lepp, 1975). However, this is not considered a major pathway for metal uptake. Experimental studies applying dosages of Pb isotopes by means of simulated rainfall, show that only a small amount – one study report 10% (Lin et al., 1995), and another report 1% (Watmough et al., 1999b) - of the isotopes are translocated away from the application area. However, these two studies investigated different elements on different species. The pH may also affect the

amount of translocated metals from the application area (leaf), with low pH increasing the amount (Watmough et al., 1999b).

The final way of incorporate elements into tree rings is by direct deposition on bark, followed by movement, most likely apoplastic, from bark to wood (Lepp, 1975). Lepp and Dollard (1974b) applied ^{210}Pb on the bark surfaces of three different species: alder, beech and birch. In all these, lateral movement of ^{210}Pb from bark to wood occurred. They also observed that this lateral movement appeared to be unaffected by the presence of the active cambial zone; no difference between the dormant season and the growing season. This suggests that the process is a non-metabolic (Lepp and Dollard, 1974b). This mechanism of element incorporation may be important in deciduous trees (Lepp, 1975). However, as pointed out by Watmough (1999), the ratio between bark and root uptake will vary with tree species, soil properties and the chemical composition of rainfall.

Collectively, there are 3 possible ways to incorporate heavy metals in trees: root uptake, foliar uptake and direct deposition on bark. According to Watmough (1999), root uptake is considered the major pathway. Although uptake through bark may be a major pathway, the ratio between root and bark uptake will as mentioned differ and depend on several factors. Considering the above discussion on foliar uptake, this way of incorporating elements seems to be less important.

3.3.5 Deposition of lead and heavy metals in trees

The binding of metals in xylem depends on its form in the xylem sap, i.e. free or in a complexed form with an organic ligand which reduces the affinity of binding (Lepp and Dollard, 1974a), the presence of other metal ions (competition), its ionic charge density and the number of binding sites (Watmough, 1999). The function of xylem as an ion exchange column may slow down or impede movement up the xylem tracheids by months or even years, as pointed out by Momoshima and Bondietti (1990). According to Dunn (2007), lead is stored as pyrophosphate in cell walls.

However, the processes specifically responsible for deposition of lead and other toxic heavy metals in tree rings are currently not known.

3.4 Tree-rings as an environmental archive

The formation of annual tree-rings (cf. section 3.3.3) provides a high resolution method in resolving past pollution. Compared to the geographical distribution of lake sediments, peat bogs and ice cores, the distribution of trees is enormous. In addition to the widespread occurrence, tree-ring analysis is logistically simpler and less costly. However, discrepancies exist in literature on whether tree rings are reliable in terms of past pollution. The reason being that the use of tree-rings in environmental research relies on a fundamental assumption; annual-rings are assumed to preserve the annual uptake of trace-metals and heavy metals, "locking them up" without any further movement. According to Hagemeyer et al. (1992) it is important to not forget that, quotation: "even a very old trunk is still part of a living organism with the ability to control transport and allocation of nutrients effectively". Mobilization of elements after deposition within a tree ring will smear out the historical record of pollution.

Researchers which have presented results and conclusions in favour, or arguing for the usefulness of the use of tree-rings include: Watmough et al. (1999a), Tommasini et al. (2000), Aberg et al. (2004), Savard et al. (2006), Mihaljevic et al. (2008) and Novak et al. (2010). Aberg et al. (2004), Mihaljevic et al. (2008) and Novak et al. (2010). Novak et al. (2010) compared their tree ring data with data from peat cores, and found that they were in agreement. Novak et al. (2010) wrote in their conclusion that factors such as radial mobility, sapwood/heartwood boundary, increase or decrease in ecosystem acidity, and soil buffering, did not seem to render or affect the Pb content in the annual rings of Norway spruce (*Picea abies* L.). Therefore, they conclude that this tree species successfully recorded the historical changes in the Pb deposition/precipitation of the area..

A review by Nabais et al. (1999) discussing whether dendroanalysis provides a source of information regarding environmental pollution, list seasonal variation and the heartwood/sapwood boundary as potential factors influencing the mobility of deposited elements. In terms of seasonal variation, this may be linked or attributed to seasonal changes in the composition of xylem sap. This is because elements bound to the negatively charged xylem walls, may be lost if a stronger ligand is present in the xylem sap. Hagemeyer and Schafer (1995) link changes in elemental distribution to changes in composition and xylem sap quantity. Another paper by Sauter and Vancleve (1992) reports an increase in amino acid content of xylem sap during spring, which again increases the capacity to form metal-complexes. Hagemeyer and Weinand (1996) studied 5 years-old Norway spruce trees (*Picea*

abies) grown in lead contaminated soils. These soil samples varied in the amount of lead ranging from low to medium to high concentration. However, as pointed out by Hagemeyer and Weinand (1996), the highest lead concentration is never observed in the outermost tree ring. Xylem sap flows through several xylem rings at the same time, and it can be assumed that all the annual rings in this case were involved in xylem sap conduction (Hagemeyer and Weinand, 1996). They also measured the lead content in bark, and found that bark contained a higher concentration. The presence of rays between bark and wood (Vanbel, 1990), lead Hagemeyer and Weinand (1996) to suggest that this connection may function as a channel for radial transport; toxic elements are transported to the outer bark which is subsequently shed off, thereof a mechanism for detoxification. Also, translocation of trace metals between adjacent sapwood tree rings has been reported (Hagemeyer and Lohrie, 1995, Donnelly et al., 1990) and the major pathway is thought to be via ray cells (Stewart, 1966). Donnelly et al. (1990) investigated radial translocation of lead in the laboratory, and found that both inward and outward movement occurred.

Collectively, the different aspects which may to a certain degree discredit the use of tree-rings as biomonitors include: mixture of natural geogenic lead and anthropogenic lead (Bindler et al., 2004) sapwood/heartwood boundary, intra-ring variability/heterogeneity, possible detoxification mechanisms (Stewart, 1966, Hagemeyer and Weinand, 1996), element mobility between adjacent tree-rings (possibly through pits in the tracheids), and the variation with stem level above ground (this can however be omitted by comparing tree-rings at the same stem height).

4 Methods of study

4.1 Sample preparation

4.1.1 Preparation of wood samples

Two Norway spruce (*Picea abies*) trees were selected for dendrochemical study (for location of the respective trees see Figure 3-1) by laser ablation inductively coupled plasma mass-spectrometer (LA-ICP-MS). They were harvested in early spring of 2011. Trunk segments ca. 20 cm thick, taken at approximately breast height, were taken to the laboratory. They were dried in the oven at 50°C for 24 hours. The two trunk segments were subsequently sliced into two strips of wood across the stem perpendicular to the growth rings passing through the pith. Then the separate strips of wood were sliced across the light colored wood (earlywood) by razor blade into 2-3 years increments and mounted in 1-inch epoxy blocks and subsequently grinded and polished in order to get flat and smooth surfaces suitable for laser ablation (the epoxy blocks are shown in Figure 4-1). The grinding and polishing of all nine samples were carried out in three steps. First, coarse grinding with a diamond wheel, followed by grinding with silicon carbide (15,14 and 12 microns), and finally with 1 micron aluminum oxide (Buehler) on a soft polishing wheel.

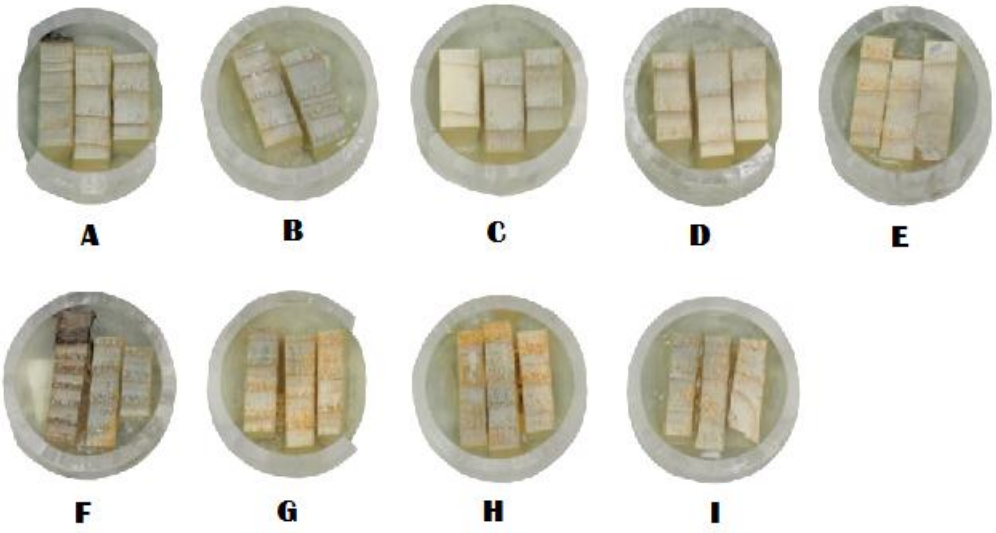

Figure 4-1 Wood increments from the two trees mounted in 1-inch epoxy blocks. The epoxy blocks A-E and F-I contain wood increments from tree #2 and #1, respectively.

4.1.2 Standard and blank preparation

Four different standards and one blank (cellulose powder) were prepared for LA-ICP-MS analysis. The four different standards were the in-house wood standard (Novak et al., 2010), ERM-CD100 wood standard, cellulose powder (α-cellulose from Sigma-Aldrich, Lot # BCBF5683V) mixed with NIST-612, and cellulose powder mixed with BCR-2 (Basalt, Columbia River reference material). NIST is the short abbreviation for National Institute of Standards and Technology. Table 4-1 lists the amount of cellulose, BCR-2 and NIST-612 used when making the cellulose+BCR-2 and cellulose+NIST-612 standards. In Table 4-2, the mean Pb concentration of the three standard materials, BCR-2, NIST-610 and NIST-612 are listed. All the standards were grinded, mixed and homogenized thoroughly while there was no need to grind the already fine-grained homogenized cellulose powder.

	Cellulose (g)	**BCR-2 (g)**	**NIST-612 (g)**
Cellulose + BCR-2	0.1091	0.0109	
Cellulose + NIST-612	0.1008		0.0107

Table 4-1 The making of cellulloce+BCR-2 and cellulose+NIST-612. Weight of cellulose powder, BCR-2, and NIST-612 are listed in the different columns.

	Pb, mean ± 1SD (µg)
BCR-2	11.31 ± 2.02
NIST-610	417 ± 29
NIST-612	38.59 ± 2.64

Table 4-2 Calculated mean concentrations of published data from GEOREM (a Max Planck Institute database for reference materials of geological and environmental interest).

The in-house wood standard, NIST-612 and BCR-2 were grinded with ethanol in a mortar and stored in separate plastic bottles until use. However, this procedure did not work for the ERM-CD100 wood standard. ERM-CD100 wood standard consist of quite long and thin splinters of wood, and had to be grinded into fine powder in order to produce homogenous pellets. This was done in an agate mortar. Before use, the agate mortar was cleaned with ethanol, and a batch of wood splinters were grinded and discarded in order to be sure there was no contaminants left from previous uses, then the wood splinters for standard preparation were introduced into the mill. The fine powdered NIST-612 and BCR-2 were mixed with cellulose and homogenized with ethanol in the mortar. The pellet making was carried out by compressing the powder in a hydraulic press under the weight of ten tons for five minutes.

The pellets were prepared in the following way: from low to higher concentration of lead (see Table 5-6 for concentrations). This was done in order to decrease the level of possible lead contamination and between the makings of each pellet, the apparatus, the piston and other devices in contact with the powder, were thoroughly rinsed with ethanol and dried. Two pellets of each standard and one blank were prepared and stored in plastic boxes before analysis by LA-ICP-MS.

The lead concentrations for NIST-610, cellulose+BCR-2 and cellulose+NIST-612 were calculated by using published data at GEOREM (Table 5-6).

4.2 LA-ICP-MS

Laser ablation of solids using pulses from a laser and transfer of the released material to the inductively coupled plasma mass spectrometry (ICP-MS) in a gas flow, usually of Ar or He, is a very attractive alternative to the nebulization of aqueous sample solutions (Durrant, 1999). The method was first introduced in 1985 and is now a widely used technique in the Earth sciences and various biological and environmental studies. In contrast to the traditional sample dissolution method, this *in situ* method avoids the use of potentially hazardous reagents such as HF, H_3PO_4, and H_2O_2, and reduces the risk of contamination and the loss of volatile elements (Durrant, 1999). It offers reduced sample preparation time, no sample size requirements, increased sample throughput, reduced spectral interferences, *in situ* spatially resolving analysis, and lower limits of detection (LOD) as the samples are not diluted (Vanhaecke and Moens, 1999). The major limitations are the variations of the analyte response during the ablation process, defined as elemental fractionation and calibration typically requires matrix-matched standards (Durrant, 1999).

4.2.1 Principles of LA-ICP-MS

4.2.1.1 Laser principles

Atoms and molecules exist in discrete energy states, and a change from the ground state (lowest energy level, most stable) to a higher energy state, by means of excitation of one or more electrons, followed by spontaneous or stimulated emission of photons, is the basic principle in laser operations. In the case of solid-state laser, which is the type of laser used in this study, excitation occurs within the inner incomplete electron shells (Koechner and Bass, 2003). The ground state is more populated than the higher ones, and to achieve higher energy states, energy has to be supplied to the system in order to maintain this non-equilibrium state. This happens in terms of radiation by an external pump source, a light source, such as a flashlamp, continuous-wave (cw) arc lamp, or diode laser (Koechner and Bass, 2003). When the inverted population is obtained, this material functions as an amplifier, that is, it will amplify incident electromagnetic radiation at the frequency corresponding to the energy level difference. Hence its

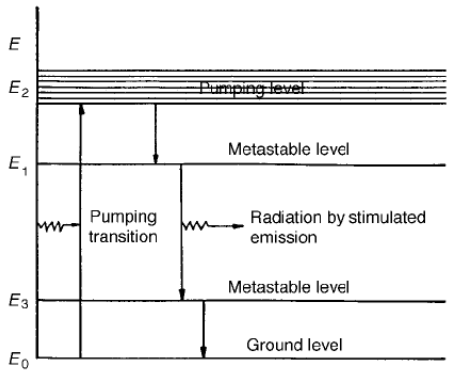

Figure 4-2 The energy levels of a Nd:YAG laser. From (Durrant, 1999).

name LASER: Light Amplification by Stimulated Emission of Radiation (Koechner and Bass, 2003).

The laser used to ablate the tree rings is the solid-state Nd:YAG laser. It is a crystal composed of $Y_3Al_5O_{12}$ (yttrium aluminum garnet), where about 1% of Y^{3+} is substituted by Nd^{3+} (Koechner and Bass, 2003). The energy-level diagram of the the Nd:YAG laser is shown in Figure 4-2. It has four energy levels – with lasing between metastable levels (Durrant, 1999). The lasing of the of Nd:YAG has a fundamental wavelength of 1064.1 nm, and in the case of the apparatus used in this thesis (New Wave UP-213), the final output radiation has a wavelength of 213 nm (frequency quintupled compared to that of 1064.1 nm). The laser can be operated in Q-switch mode which prevents lasing during pumping, allowing the population of E_1 to reach large values (Koechner and Bass, 2003). Figure 4-3 illustrates the schematics of

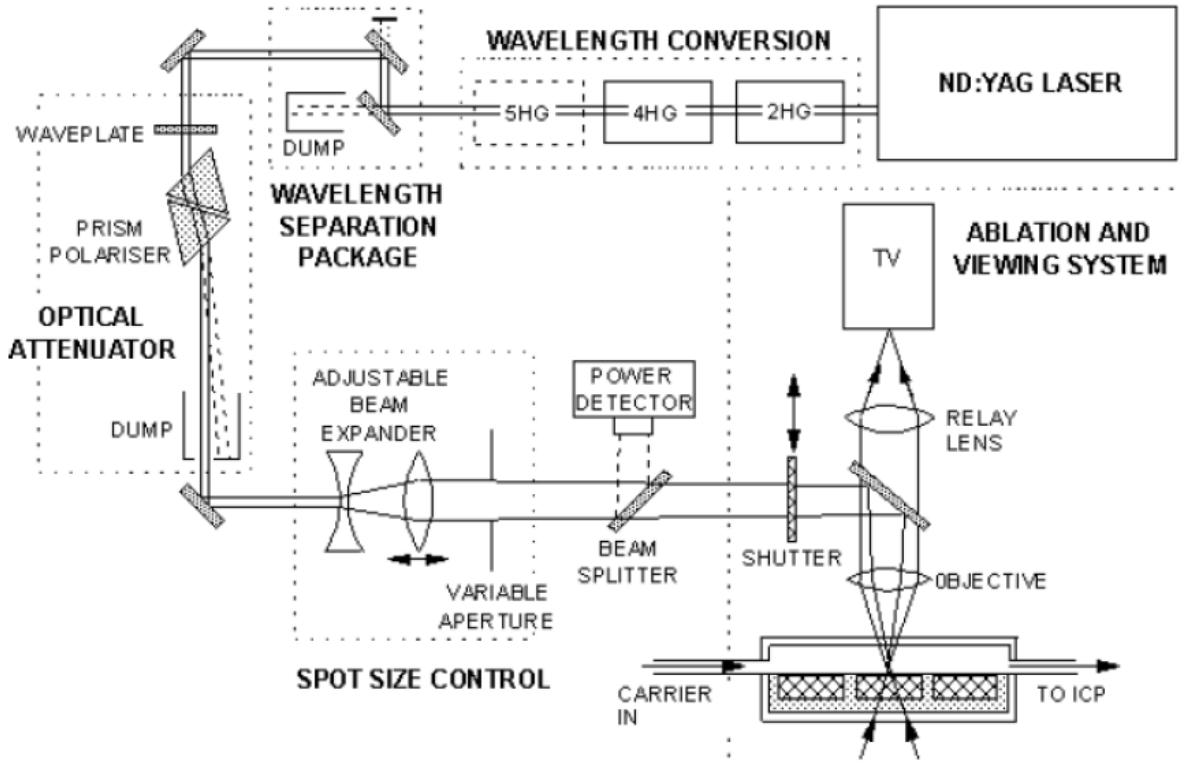

Figure 4-3 Schematics of Nd:YAG laser and the following ablation (Jackson).

a Nd:YAG laser system. When ablation takes place in the sample chamber, the ablated material is carried away by Ar or He gas to the ICP-MS (Durrant, 1999). The radiation-sample interactions depend upon numerous variables, both related to the laser, the sample, and atmosphere within the sample chamber. Considering the laser beam, some important parameters are the wavelength, the energy and the spatial and temporal form. Sample parameters or characteristics are heat capacity, heat of vaporization and thermal conductivity.

Some of the incident radiation is reflected at the sample surface, and the amount of reflected radiation can be decreased by increasing the energy of the laser pulses (Durrant, 1999). Absorption creates photoelectrons and ions may also be emitted. At the sample surface, the energy of the incident laser beam is converted to heat, which first melts the material followed by boiling. However, different elements will vaporize at different rates, and the existence of high temperature gradients along the periphery of laser craters, segregate elements. This may lead to the composition of the ablated material being different from the true value (Durrant, 1999). Absorption can however differ between biological samples and inorganic samples, and biological samples can show little or no evidence of melting or thermal damage (Hoffmann et al., 1994). The ablated material takes the form of droplets and vapour. Ideally, the particles diameters should be between 3µm and 5nm which yield a transport efficiency of > 80% (Durrant, 1999). This is because too large particles would settle out in the ablation cell or in the transfer tube and too small once would be lost by diffusion. The ratio of the amount of material ionized in the ICP-MS to that ablated may be a measure of overall efficiency (Durrant, 1999).

4.2.1.2 Inductively Coupled Plasma-Mass spectrometry principles

Two types of mass-spectrometers were used in this thesis: a single- and a multi-collector, double focusing magnetic sector ICP-MS. The single collector ICP-MS was used for element analysis and the multi collector was used for the lead isotopic analysis. The two mass spectrometers used were Thermo Finnigan Element 2 (single collector) and Thermo Finnigan Neptune (multi collector), their schematics are shown in Figure 4-4.

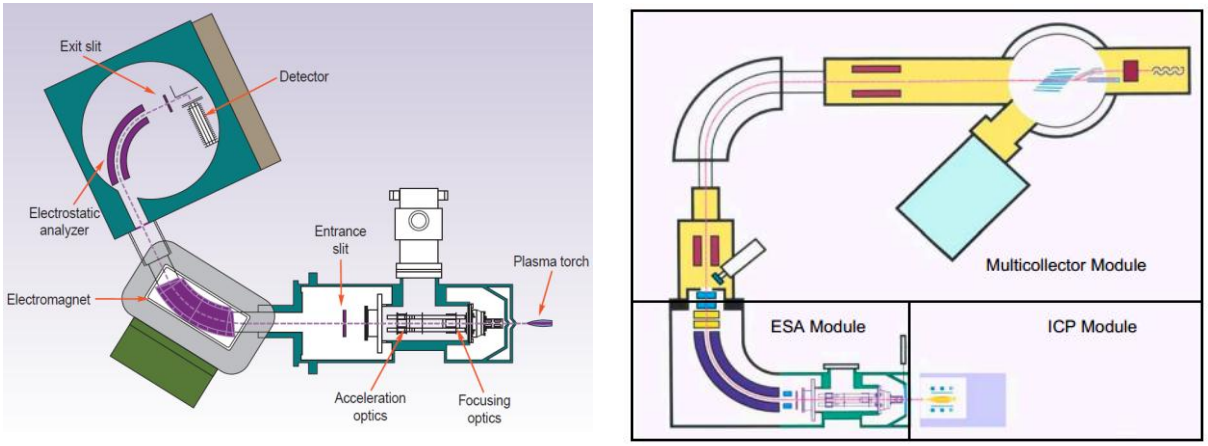

a **B**

Figure 4-4 The schematics of Thermo Finnigan Element 2 (a), and Thermo Finnigan Neptune (b). Both figures are from the manufacturer.

In the ICP-module, the particles from laser ablation or solution droplet are first nebulized. The droplets should be less than 10 µm in diameter to obtain an efficient desolvation, volatilization and atomization. The large droplets are removed by condensation on the walls of the spray chamber and are subsequently pumped into the waste chamber (Finnigan-Neptune-Manual, 2004). The aerosol (solution or laser ablation material) is directed into the injector of the plasma-torch where it is injected into the centre of the argon-plasma, and subsequently atomized and ionized.

In the single and multi-collector ICP-MS the mass analyser is positioned before and after the electrostatic analyser respectively. The separation of ions by mass is controlled by the mass analyser (magnet). The basic principle of a magnetic sector mass analyser is the deflection of a charged particle passing through a magnetic field. Its curvature depends on the intensity of the magnetic field, the mass/charge ration of the ion and its acceleration (Potts, 1987). Equation 4-1 describes the relationship between the kinetic energy of the atom and the force of the magnetic field:

$$\frac{m}{e} = \frac{H^2 r^2}{2V} \qquad \textbf{Equation 4-1}$$

where m and e are the mass and charge of the ion, H the intensity of the magnetic field, r the radius of the ion trajectory, and V the potential gradient (Potts, 1987).

The electrostatic analyser separates the ions according to their kinetic energy. This narrows the energy distribution of the ion beam which results in higher mass resolution. Equation 4-2 describes the radius of curvature of the ion beam:

$$r = \frac{2Ee}{d(KE)} \qquad \textbf{Equation 4-2}$$

where r is the radius of the ion beam, E the voltage difference between the electrostatic plates, d the distance between the plates, e the charge of the ion and KE is the kinetic energy (Potts, 1987).

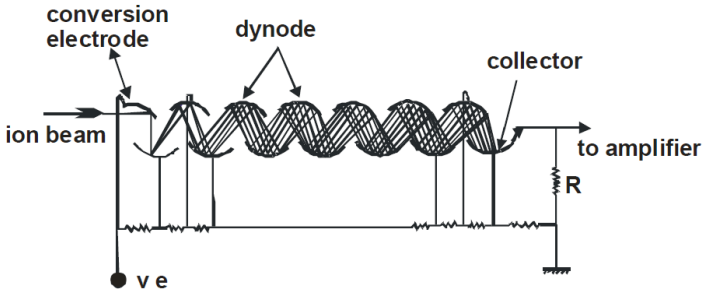

A SEM (Secondary electron multiplier).

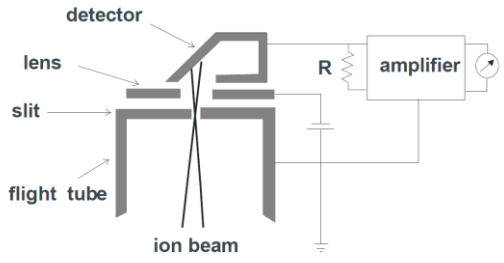

B A farady cup.

Figure 4-5 The detector of Finnigan Neptune multicollector ICP-MS (a) and of Finnigan Element 2 (b). Both figures from Potts (1987).

The single collector ICP-MS uses secondary electron multiplier to detect the ions while the multi collector ICP-MS uses faraday cups as detectors (9 in total). Their geometry are shown in Figure 4-5a and b, respectively.

4.3 Analysis of lead isotopes

The isotopic composition of the individual tree rings was measured using Nd:YAG 213 nm laser (New Wave UP-213) coupled to a Finnigan Neptune multi-collector ICP-MS (Thermo Finnigan). Tuning of the instrument was performed with SRM981 solution standard with 100 ppb of natural Tl with $^{205}Tl/^{203}Tl = 2.3871$ (Dunstan et al., 1980). A sensitivity of 7V was obtained for ^{205}Tl.

	Certificate values from NIST	**Run #1**	**Run #2**
$^{204}Pb/^{206}Pb$	0.059042 ± 0.000037	0.064561 ± 0.000002	0.059049 ± 0.00018
$^{207}Pb/^{206}Pb$	0.91464 ± 0.00033	0.914632 ± 0.00001	0.914633 ± 0.00001
$^{208}Pb/^{206}Pb$	2.1681 ± 0.0008	2.16654 ± 0.000022	2.16654 ± 0.000028

Table 4-3 The results from the solution standard (SRM981+100ppb natural Tl) ICP-MS analysis. The certificated values stem from the certificate of analysis from National Institute of Standards and Technology (NIST). All values are listed with its two standard deviations.

Repeated measurements of the Pb standard solution gave $^{207}Pb/^{206}Pb = 0.914632 \pm 5$ and 0.914633 ± 5 which is in agreement with the recommended value of 0.91464 ± 33 (Table 4-3).

	SRM981+Tl(100 ppb)	**Tree-rings (11.11.09)**	**Tree-rings (11.11.10)**	**Unit**
Extraction	-2000	-2000,0	-2000,0	V
Focus	-668,0	-619,0	-641,0	V
X Deflection	-4,91	-5,42	-6,25	V
Y Deflection	-2,53	-0,83	0,39	V
Shape	210,00	210,00	210,00	V
Rot Quad 1	-16,01	-16,98	-16,98	V
Foc Quad 1	-19,89	-19,89	-19,89	V
Rot Quad 2	0,00	-	-	V
Source Offset	-23,00	-23,00	-23,00	V
Focus Offset	29,70	29,70	29,70	V
Matsuda Plate	0,34	0,34	0,34	V
Cool Gas	15,00	16,00	16,00	L/min
Aux Gas	0,82	0,82	0,82	L/min
Sample Gas	1,220	0,874	0,880	L/min
Add Gas 1	0,00	0,65	0,65	L/min
Add Gas 2	0,00	0,00	0,00	L/min
X-Pos	1,000	1,390	1,200	Mm
Y-Pos	-0,820	-0,440	-0,580	Mm
Z-Pos	-4,000	-4,000	-4,000	Mm
Peri Pump	7,50	7,50	7,50	rpm
RF Power	1250	1250	1250	W

Table 4-4 ICP-MS parameter values used in various analysis.

After tuning and optimum performance was achieved, the laser was connected. Table 4-4 lists the parameters used for the standard solution and the tree-ring analysis. The darker part of the wood (latewood) was selected for LA-ICP-MS analyses because of its denser structure (less porous) with better ablation characteristics. The laser was programmed to scan tracks of 500 µm in length and 100µm in diameter parallel to the tree rings. Figure 4-6 illustrates how the laser was programmed for both the lead isotopic analysis and the element analysis. The rasters were placed in the latewood next to the earlywood/latewood boundary. The analysis of tree #1 and #2 was carried out over two days, and the 6 pellets (standards+blank) were periodically analysed during the course of the analysis. A laser beam with a repetition rate of 20Hz, and fluence of 5J/cm^2, was scanned across the different pellets along 500 µm long patterns. The laser parameters are listed in Table 4-5. Blank values were acquired for 50 seconds followed by laser ablation for 200s, and the whole data acquisition consisted of 250 cycles. Ablated material was flushed with He (0.65 L min^{-1}) which later was mixed with Ar gas (0.874 L min^{-1} for 11.11.09 and 0.880 L min^{-1} for 11.11.10) carrying Tl tracer solution. For tracer solution, natural Tl solution (Merck, 1000 ppm and ^{205}Tl/^{203}Tl = 2.3871) was diluted with 2% nitric acid (HNO_3) to 100 ppb. Simultaneous nebulization of Tl tracer solution and aerosols from laser ablation were performed in order to correct for mass-discrimination of lead isotopes. The Neptune Faraday cup configuration is listed below:

Figure 4-6 Simplified sketch showing the two tracks of the lead isotope (2)- and heavy metal (2)- analysis, respectively.

Detector	L3	L2	L1	C	H1	H2	H3
Isotope	^{202}Hg	^{203}Tl	^{204}Pb	^{205}Tl	^{206}Pb	^{207}Pb	^{208}Pb

A sensitivity of 0.7 V was obtained for ^{205}Tl. Data were subsequently corrected for gas blank, Hg interference on ^{204}Pb, and mass discrimination of Pb isotopes. The effect of mass discrimination was corrected by using the exponential law and the measured Tl isotopes of the tracer solution. After laser ablation, the annual rings were counted in the microscope and resulted in ages of 43 and 42 years for tree #1 and #2, respectively.

	Lead isotope analysis	**Element analysis**
Frequency	20 Hz	20 Hz
Fluence	5J/ cm^2	2.6 J/cm^2
Ablation time	200 s	60 s
Washout time	60 s	45 s
Gas blank	50 s	34 s
Scan speed	10 µm/s	10 µm/s
Laser-beam spot diameter	100 µm	100 µm
Laser track length	500 µm	200 µm

Table 4-5 Laser parameters values used in the lead isotope and element analysis.

4.4 Element analysis

Parameter	Value	
Resolution	Low	%
Focus offset	30,0	%
UaUb	0,120	L/min
Cool gas	15,52	L/min
Aux gas	0,88	L/min
Sample gas	0,995	L/min
Additional 1	0,645	Watt
Plasma power	1300	V
Extraction	-2000,0	V
Focus	-864,0	V
X-Deflection	0,70	V
Y-Deflection	3,28	V
Shape	105,00	V
Rotation quadrupol 1	0,00	V
Rotation quadrupol 2	0,00	V
Focus quadrupol 1	0,00	V
Focus quadrupol 2	0,00	V
Matsuda-Plate	58,13	V
SEM-Deflection	-45,00	V
SEM	2205,0	V
Guard Electrode	YES	
Additional 2	0,000	L/min
Torch X-Pos	2,300	mm
Torch Y-Pos	0,900	mm
Torch Z-Pos	-4,800	mm
Peri. Pump Speed	0,00	rpm

Table 4-6 ICP-MS parameters for the element analysis.

Prior to analysis, tuning of the instrument by *in-situ* measurements of NIST-612 gave a sensitivity of analysis equal 4600 cps/ppm U. Several standards were investigated during the course of the analysis: NIST-612, NIST-610, BCR-2G, in-house wood standard and ERM-CD100. The aim of this analysis was to obtain element concentrations in the individual tree rings. However, for the in-house wood standard, only the lead concentration is known (Novak et al., 2010), and for the ERM-CD100 wood standard, only Ar, Cd, Cr, Cu, Hg and Pb are known (ERM-CD100 certification report). This limits the range of elements that can be determined in the tree rings. The following isotopes were analyzed to obtain the elemental contents in the tree rings: ^{12}C, ^{24}Mg, ^{28}Si, ^{29}Si, ^{43}Ca, ^{44}Ca, ^{51}V, ^{52}Cr, ^{53}Cr, ^{59}Cr, ^{60}Ni, ^{63}Cu, ^{66}Zn, ^{75}As, ^{79}Br, ^{111}Cd, ^{202}Hg, ^{208}Pb and ^{238}U. The laser and ICP-MS parameters for this analysis are listed in Table 4-5 and Table 4-6, respectively. For the internal standard ^{12}C was selected.

Programming of the laser was carried out the same way as for the lead isotope analysis with some different settings such as laser fluence, ablation time, washout time, gas blank and the laser track length (see Table 4-5).

5 Results

All results and the statistical tests encountered are listed in the appendix.

5.1 Data evaluation

5.1.1 Analysis of lead isotopes

5.1.1.1 Evaluation of instrument drift

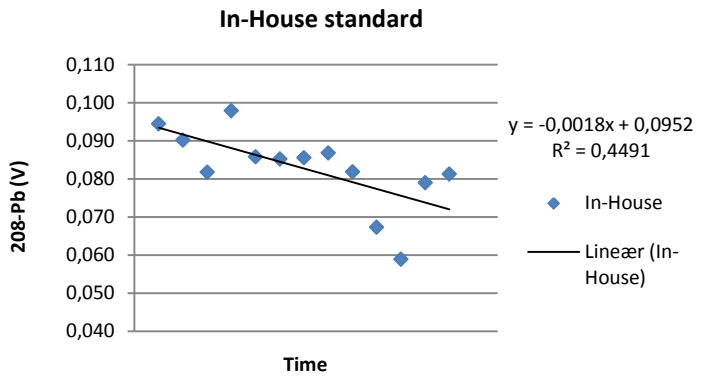

Figure 5-1 Measured ^{208}Pb signal (Volts) in the In-House standard during the course of analysis.

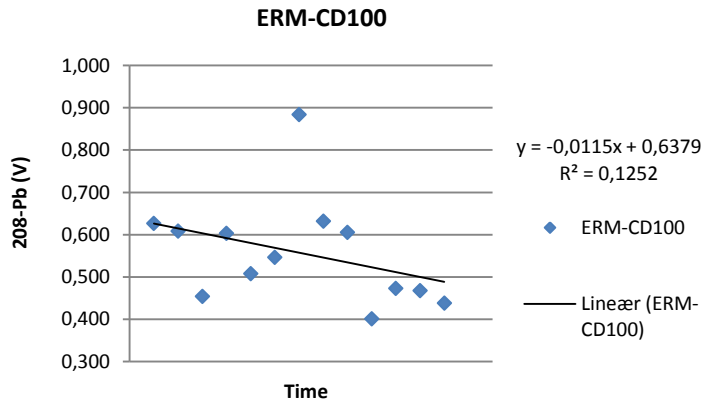

Figure 5-2 Measured ^{208}Pb signal (Volts) in the ERM-CD100 standard during the course of analysis.

The drift was evaluated by plotting the recorded ^{208}Pb signal (Volts) of the periodically analysed in-house wood and the ERM-CD100 wood standard. Figure 5-1 and Figure 5-2 demonstrates the ^{208}Pb signal (in volts) registered from the In-House and ERM-CD100 standards. The correlation factor of the two trend-lines of the In-House and ERM-CD100 are 0.4491 and 0.1252, respectively. The significance of the instrument drift was evaluated with the "Spearman's rank correlation test" (see appendix 9.3.1 for more information). This test allows evaluating the dependence on two variables, in this case time (x) and the ^{208}Pb signal (y), and ascribe the significance of correlation. For the In-House and ERM-CD100 standards r_s values of -0.7846 and -0.4725 were obtained. This shows a negative relationship between time and the registered ^{208}Pb signal indicating a drop in sensitivity during the analysis. The in-house and the ERM-CD100 wood standard demonstrate a significant drift of 95% ($t = 4.384$ with 12 degrees of freedom) and 90% ($t = 1.778$ with 11 degrees of

freedom) confidence level, respectively. However, since we are only seeking lead isotopic ratios, any drift correction may be omitted.

5.1.1.2 Pre-ablation – evidence of contamination

The effect of pre-ablation is illustrated in Figure 5-3. Here, ablation of both one standard (in-house wood standard) and one tree ring are shown for comparison. The first laser scans (50-100 cycles approx.) of all measurements were discarded due to the possibility of contamination. For the tree rings, this contamination is evident by the relatively high ^{208}Pb signal during the first scan. This contamination affects all tree rings, though to different degrees. For the standards, contamination is not particular pronounced. This is may be due to the different sample preparation procedures – the sample preparation of the tree rings involves more potential sources of contamination (e.g. the grinding and polishing procedure in section 4.1.1).

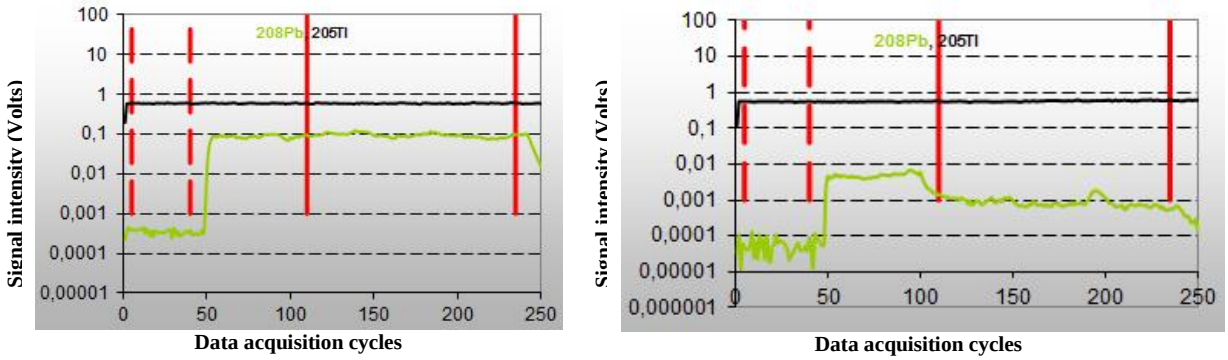

a **B**

Figure 5-3 The raw signal of ^{208}Pb for one measurement of the in-house standard (a) and the one tree ring formed in 2010 in tree #2 (b). The red stippled vertical lines indicate the interval used for background signal, and the solid red vertical line indicates the interval of the analyte signal. The plot also shows signal of ^{205}Tl from the tracer solution.

Figure 5-4 demonstrates a picture of a tree ring from tree #1 taken with an optical microscope. The ablation rasters from the lead isotopic- and heavy metals analysis indicate the area of the material analysed.

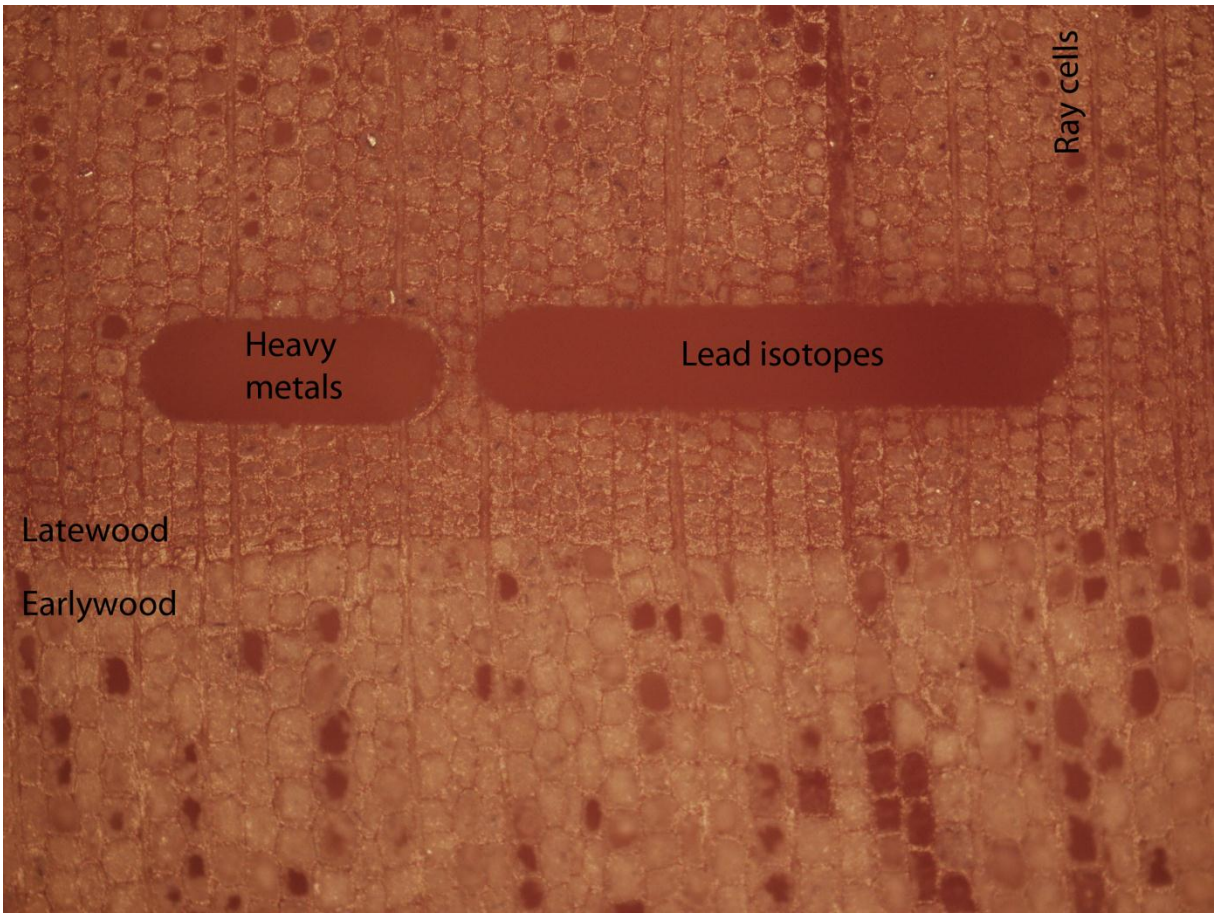

Figure 5-4 Microscope picture displaying the late- and earlywood of one tree ring in tree #1 along with the two ablation rasters in the latewood corresponding to the two analysis: the heavy metal analysis (200 µm in length) and the lead isotopic analysis (500 µm in length). The white small particles between the cells most likely represent relics from polishing. Also indicated are the ray cells.

5.1.1.3 Analyte signal vs. background signal

The lower limit of detection depends on numerous variables like laser energy, ablation pit volume, transport efficiency from sample chamber to the ICP-MS, the sensitivity of ICP-MS, polyatomic ion interferences, background intensity, along with other minor important parameters (Gunther et al., 1996). Since this analysis is a lead isotopic ratio analysis and not a concentration analysis, no internal standard was used. Factors affecting the intensity (measured in volts) of the ^{208}Pb signal, like variation in the amount of ablated material in standards and tree rings, are not significant when calculating the lead isotopic ratios. Figure 5-5 demonstrates the variation of the lower limit of detection ($\overline{x}_{BG} + 3\sigma$) for ^{208}Pb throughout the time of analysis. As it appears, the in-house wood standard shows consistently larger background signal than the other standards, blank (cellulose pellet) and tree rings. However, one measurement of NIST-610 has considerable high background signal. Background count

rates, or in this case measured in volts, may result from random ions, photons, random electronic noise generated in the detectors and poor flushing of the ablation chamber and the transport plastic tube connected to the ICP-MS. Poor flushing and the relative high lead content of the ERM-CD100 standard analysed prior to the in-house wood standard (see Figure 5-5), may be the reason for the consistently higher background registered for the in-house standard.

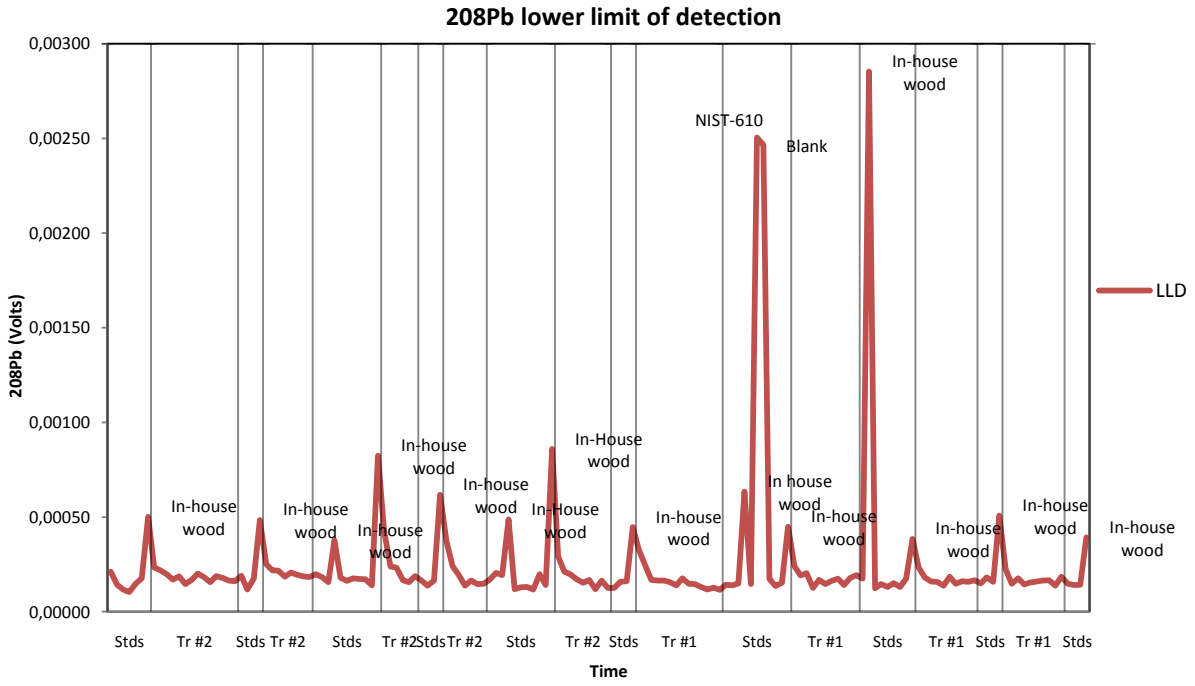

Figure 5-5 Lower limit of signal detection (LLD) from the lead isotopic LA-ICP-MS analysis of the tree rings, blank and standards. The black vertical grid lines function to separate the standard and tree ring analysis. Stds: Standards, Tr #1: Tree #1, Tr #2: Tree #2.

Figure 5-6 demonstrates the signal to background logarithmic ratio of ^{208}Pb for the various standards and the blank. The cellulose (blank) pellet show low signal to background ratios and one measurement even demonstrates larger background signal than sample signal (evident from the negative plot). This measurement is discarded, and based on the low signal to background ratio of the other measurements, it is reasonable to conclude that this pellet contains negligible amount of lead. Therefore it is not necessary to subtract the lead intensities measured for the cellulose blank, from the lead intensities for the cellulose+BCR-2 and cellulose+NIST-610 standards. Among the standards, the ERM-CD100 shows the overall highest signal to background ratios.

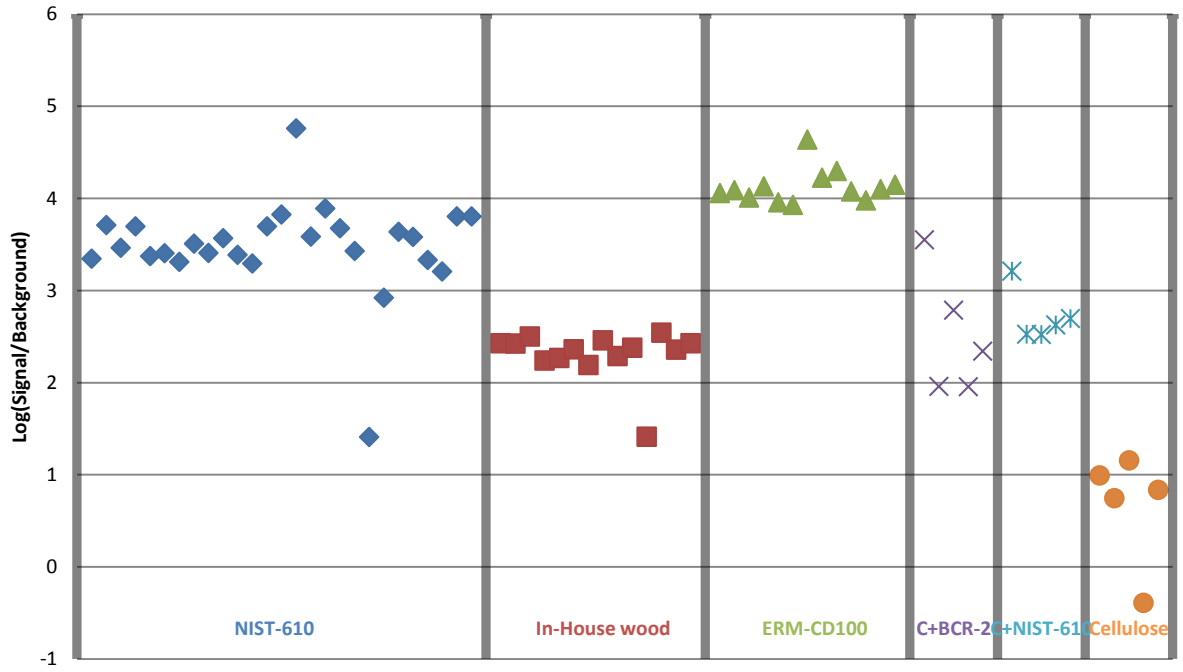

Figure 5-6 Plot of the signal to background ratio (SBR) for the various standards and the one blank.

Figure 5-7 and Figure 5-8 demonstrates the ^{208}Pb signal detected from the tree ring analysis along with the lower limit of signal detection. This is plotted in order to investigate if the signals recorded from the tree ring analysis are significantly different from the background signal. For tree #1 and #2, low ^{208}Pb signals are recorded from approx. year 2006 to the present. For tree #2, evident from the troughs in Figure 5-8, low signals are also recorded in 1984 and 1975. Some years overlap between the signal and the LLD. The low readings recorded in the outermost tree rings, and bark of the respective trees, have to be carefully interpreted. When interpreting lead isotopes, this problem should be addressed, before drawing any conclusion about the variation in the lead isotope ratios.

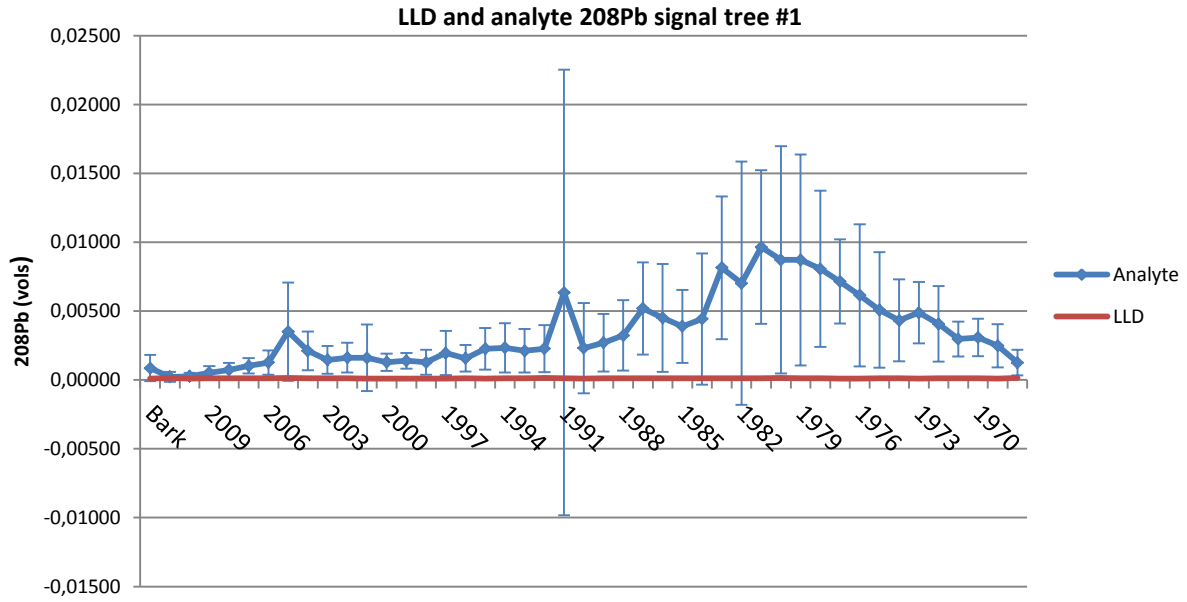

Figure 5-7 The ^{208}Pb signal in volts measured in the annual rings of tree #1 and the lower limit of signal detection.

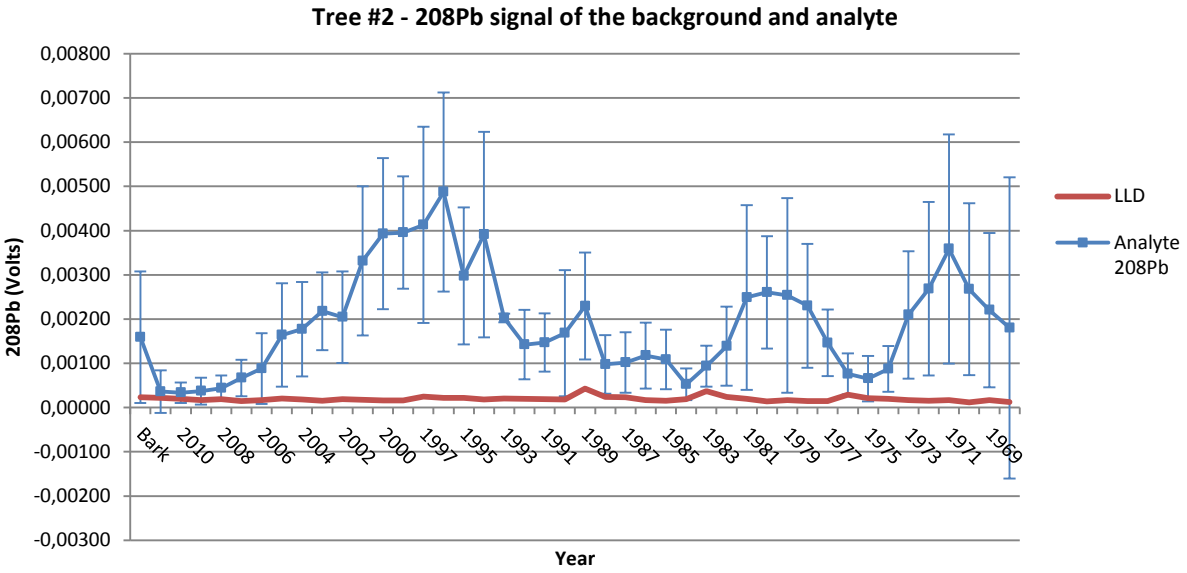

Figure 5-8 The ^{208}Pb signal in volts measured in the annual rings of tree #2 and the lower limit of signal detection.

5.1.1.4 Standard evaluation

5.1.1.4.1 In-House wood standard

Figure 5-9 demonstrates the obtained results in terms of the $^{207}Pb/^{206}Pb$ ratio for the in-house standard. According to the Cramer-von Mises test for distribution normality (see appendix 9.3.2 for test function and results), the data conform to a normal distribution with 95% confidence level. The red colored data point in Figure 5-9 appears to be an outlier due to its separation from the rest of the measurements. Since the data conforms to a normal distribution, this can be checked by calculating the three-standard deviations and if the prevailing measurement is outside the three-standard deviation, the measurement can be discarded on statistical grounds. After calculating the three-standard deviations, this measurement proves no to be significantly different from the rest of the measurements. Figure 5-10 compares the results of our measurements with the published measurements from Novak et al. (2010). Our measurements ($^{207}Pb/^{206}Pb$) were in agreement with the reported mean and

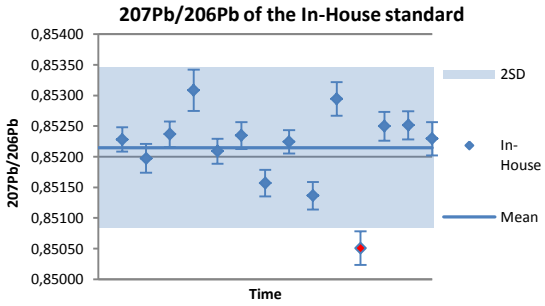

Figure 5-9 A plot of the measured $^{207}Pb/^{206}Pb$ ratio of the In-House standard, showing the mean (0.85215) and the two-standard deviation (0.00131). The data point colored in red was a potential outlier. See text for more information. n=14

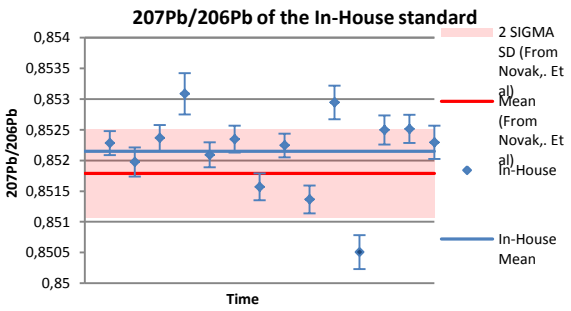

Figure 5-10 Comparison with published mean and two-standard deviation, 0.8518 ±0 .0007 from Novak et al. (2010). The in-house mean colored in blue is the mean as in Figure 5-9.

	$^{207}Pb/^{206}Pb$				
	n	**Mean**	**2SD**	**3SD**	**RSD**
Mean	14	0.85215	0.0013	0.0020	0.08%
Novak et al. (2010)	NA	0.85178	0.0007	0.0011	0.04%

Table 5-1 Results from the in-house wood standard analysis in terms of n-numbers of replicates, mean and standard deviation. For comparison, the published mean and standard deviation obtained from LA-ICP-MS analysis by Novak et al. (2010) of the same compound are listed.

standard deviation of Novak et al. (2010). Table 5-1 lists the mean and standard deviation of the in-house analysis, and the published measurements from Novak et al. (2010).

5.1.1.4.2 ERM-CD100

Figure 5-11 demonstrates the $^{207}Pb/^{206}Pb$ values obtained for the ERM-CD100 wood standard analysis along with the calculated mean value and two-standard deviations. Figure 5-12 shows the frequency distribution of the measurements. The measurements conform to normal distribution (Cramer-von Mises test) with 95% confidence level (see Table 9-6 in appendix 9.3.2 for results), and all measurements fall within the two-standard deviations. Table 5-2 lists the number of measurements (n), the calculated mean value, two-standard deviations and the relative standard deviations.

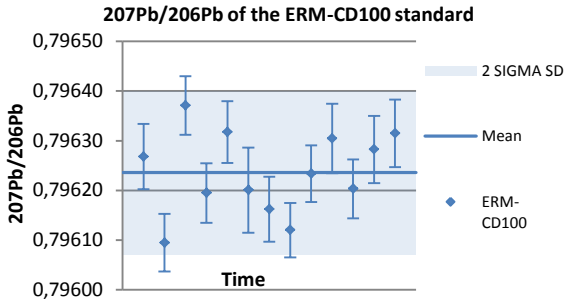

Figure 5-11 A plot of the measured $^{207}Pb/^{206}Pb$ ratio of the ERM-CD100 standard, showing the mean and the two-standard deviation (colored in transparent blue), 0.79623 ± 0.00017.

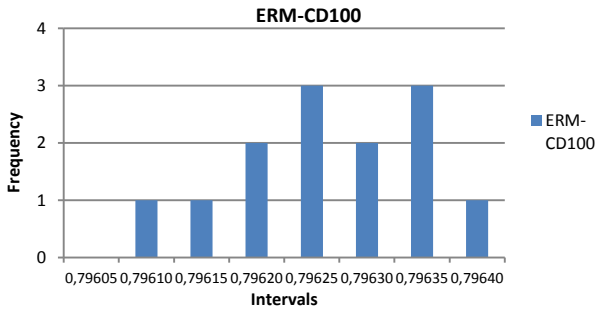

Figure 5-12 Frequency distribution of the ERM-CD100 measurements. The measurements are grouped in intervals of 0.00005.

	$^{207}Pb/^{206}Pb$			
	n	**Mean**	**2SD**	**RSD**
ERM-CD100	14	0.79623	0.00017	0.011%

Table 5-2 The calculated mean, two-standard deviation and relative standard deviation of the ERM-CD100 LA-ICP-MS analysis. n represents the number of replicate measurements.

5.1.1.4.3 NIST-610 standard

Figure 5-13 shows the $^{207}Pb/^{206}Pb$ values obtained for the NIST-610 LA-ICP-MS analysis, along with the mean value and the two-standard deviations. Performing the Cramer-von Mises test for distribution normality suggests the measurements are not normally distributed with 95% confidence level (see Table 9-6 in appendix 9.3.2 for results). Figure 5-15 demonstrates a frequency plot showing the distribution of the in-house data and data

from GEOREM. Most of the in-house measurements have values between 0.9095 and 0.9097. The data point marked red in Figure 5-13, may serve to distort the distribution curve towards a positively skewed distribution, thereby failing the normality test. When considering the measurement marked in red as an outlier, and performing the Cramer-von Mises test once again, the data conformed to a normal distribution with 95% confidence level. The new mean along with its new two-standard deviations are listed in Table 5-3.

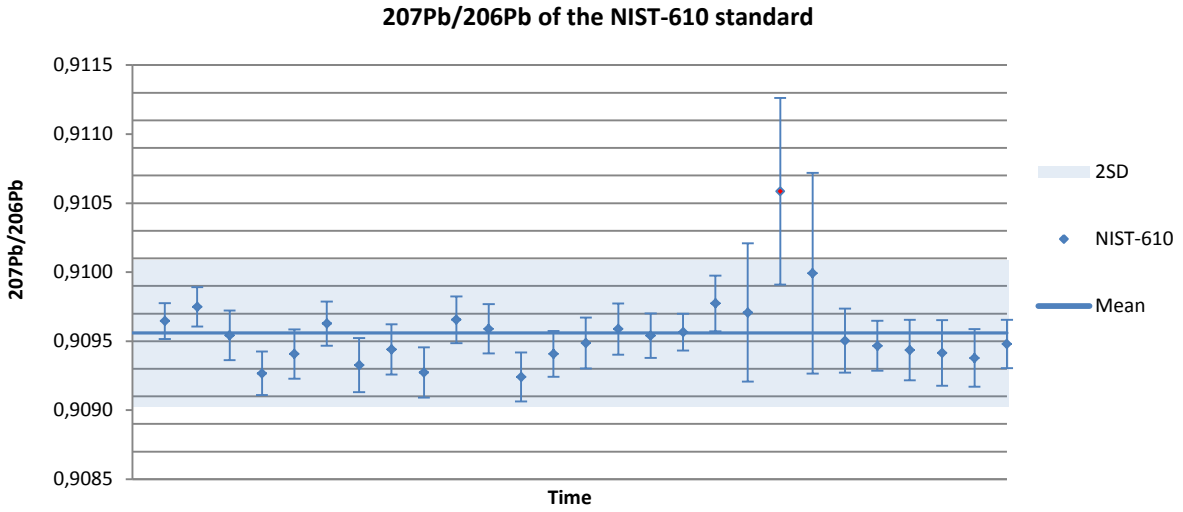

Figure 5-13 A plot of the measured $^{207}Pb/^{206}Pb$ ratio of the NIST-610 standard, showing the mean (0.9096) and the two-standard deviation (0.0005). The data point colored in red is considered as an outlier. The new mean and two-standard deviation are listed in Table 5-3. n=27

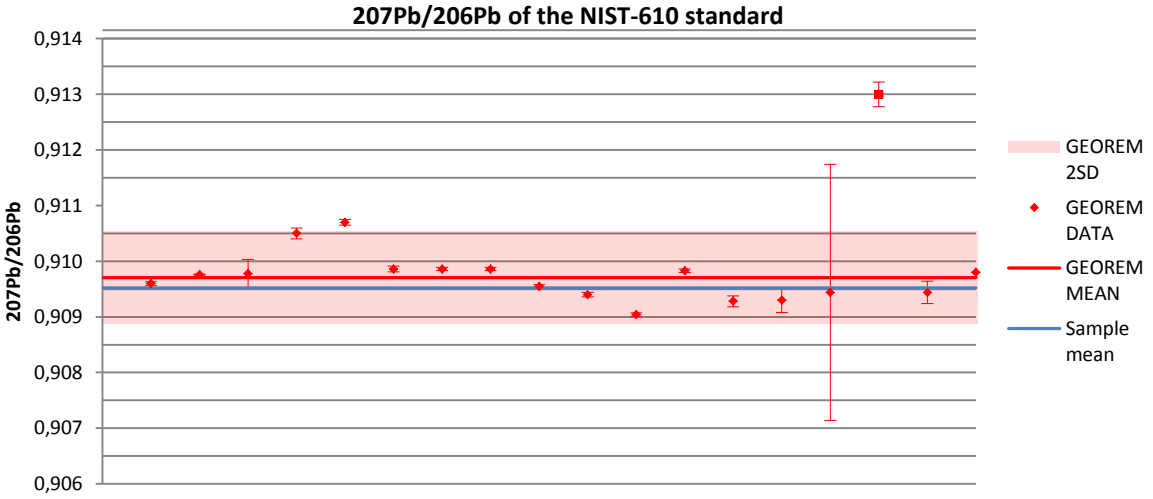

Figure 5-14 Comparison with published $^{207}Pb/^{206}Pb$ mean values at GEOREM. The mean value marked as a red square is considered as an outlier. Sample mean (blue colored): 0.9095 ± 0.0003. GEOREM mean: 0.9097 ± 0.0008.

The calculated mean and two-standard deviations of data from GEOREM are also listed. Figure 5-14 compares out results with that published at GEOREM. Figure 5-15 demonstrates

that most of the mean-values from GEOREM are lower than 0.9100, which is also the case for our measurements. This further supports discarding the outlier. Our calculated $^{207}Pb/^{206}Pb$ mean for NIST-610 were in agreement with published values at GEOREM.

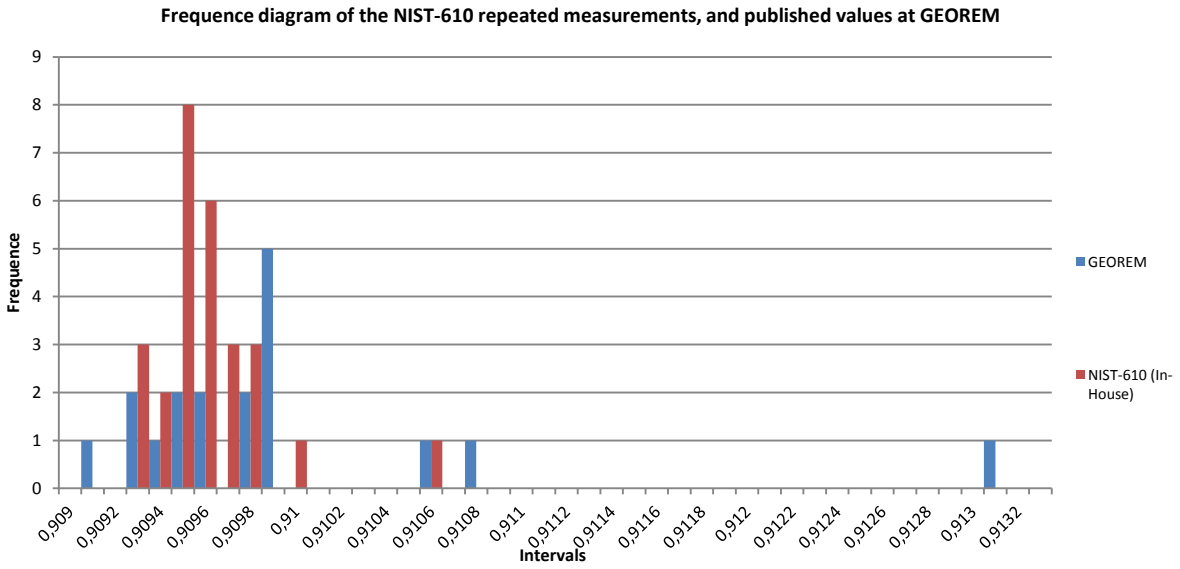

Figure 5-15 Diagram showing the frequency of occurrence of the different in-house measurements and measurements published at GEOREM. The values are grouped in intervals of 0.001.

	n	Variance	Mean	2SD	RSE
NIST-610	27	0.0000000660	0.9096	0.0005	0.029%
NIST-610 (Outlier removed)	26	0.0000000280	0.9095	0.0003	0.019%
GEOREM	18	0.0000007675	0.9099	0.0018	0.096%
GEOREM (outlier rejected)	17	0.0000001739	0.9097	0.0004	0.046%

Table 5-3 The variance, mean, two-standard deviation and relative standard deviation of the $^{207}Pb/^{206}Pb$ ratio of the analysis and the values published in GEOREM. n=number of replicates. For GEOREM n represents the number of published measurements used for calculation of the mean.

5.1.1.4.4 Cellulose+BCR-2 standard

Figure 5-16 demonstrates the $^{207}Pb/^{206}Pb$ ratios obtained from the cellulose+BCR-2 analysis. All measurements fall within the two-standard deviations. Applying the Cramer-von Mises test for distribution normality on the data, the measurements conformed to a normal distribution with 95% confidence level (see Table 9-6 in appendix 9.3.2 for results). However, as Figure 5-16 shows, only 5 mean values were obtained which is not ideal for assessment of distribution normality. Figure 5-17 compares the in-house measurements of the standard, and the published $^{207}Pb/^{206}Pb$ values of BCR-2 from GEOREM. They were in agreement.

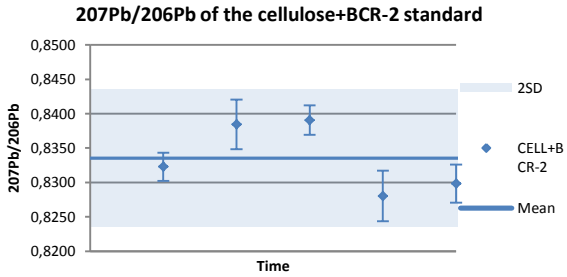

Figure 5-16 A plot of the measured $^{207}Pb/^{206}Pb$ ratio of the cellulose+BCR-2 standard, showing the mean (0.8535) and the two-standard deviations (0.0100).

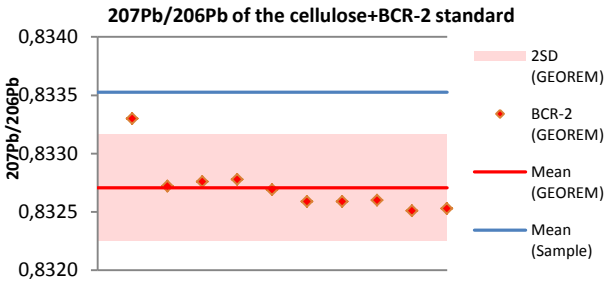

Figure 5-17 Comparison of our in-house cellulose+BCR-2 measurements with published (GEOREM) values of BCR-2. Not all standard deviations are listed for the means from GEOREM and are therefore omitted in this plot. See Table 5-4 for values.

	n	Mean	2SD	RSD
CELL+BCR-2	5	0.8335	0.01	0.6%
BCR-2 (GEOREM)	10	0.8327	0.0005	0.03%

Table 5-4 The mean value, two-standard deviations and the relative standard deviation of the cellulose+BCR-2 standard LA-ICP-MS analysis. For BCR-2 n represents the number of published measurements used.

5.1.1.4.5 Cellulose+NIST-612 standard

Figure 5-18 shows the results from the cellulose+NIST-612 LA-ICP-MS analysis for the $^{207}Pb/^{206}Pb$ ratios. According to the Cramer-von Mises test, the data conform to normal distribution with 95% confidence level (see Table 9-6 in appendix 9.3.2 for results). Figure 5-19 compares the calculated mean from Figure 5-18 with published GEOREM values. As it appears, the in-house data are systematically lower than the published GEOREM values (comparing the mean GEOREM value and the sample mean). Table 5-5 lists the results along with the mean, two-standard deviations and relative standard deviation of values published at GEOREM.

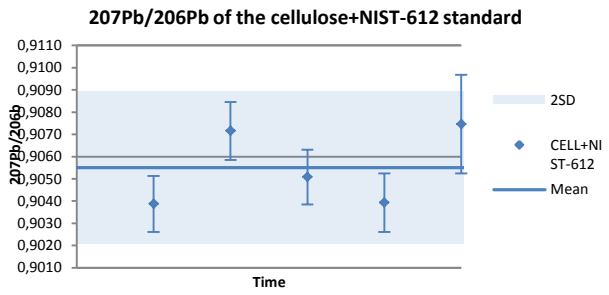

Figure 5-18 A plot of the measured $^{207}Pb/^{206}Pb$ ratio of the cellulose+NIST-612 standard, showing the mean (0.9055) and the two-standard deviations (0.0034).

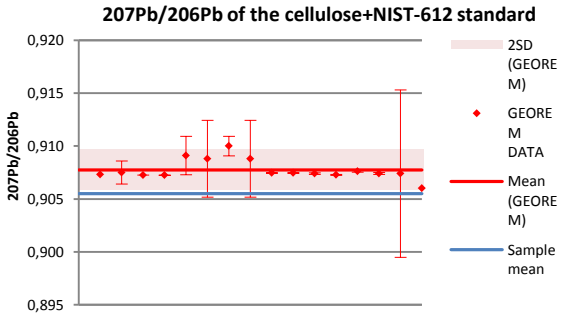

Figure 5-19 Comparison of our in-house cellulose+NIST-612 measurements with published (GEOREM) values of NIST-612. See Table 5-5 for values.

	n	Mean	2SD	RSD
CELL+NIST-612	5	0.9055	0.0034	0.19%
NIST-612	16	0.9077	0.0019	0.11%

Table 5-5 The mean value, two-standard deviations and the relative standard deviation of the cellulose+NIST-612 standard LA-ICP-MS analysis.

5.1.1.5 Precision and accuracy

As reproducibility is considered to be random in nature, the distribution is described by normal distribution. Precision may be defined as a measure of the reproducibility of replicate analysis, and in terms of normal distribution, the standard deviation provides a measure of the precision (Taylor, 2001). A large standard deviation indicates low precision and poor reproducibility. Comparison between the five different standards can be done using their relative standard deviations (RSDs). The ERM-CD100 standard has the lowest RSD followed by the NIST-610, in-house wood, cellulose+NIST-612 and the cellulose+BCR-2 standard (Table 5-6).

	$^{207}Pb/^{206}Pb$ of the LA-ICP-MS analysis of the various standards			**Reference values**	
	n	**Mean**	**RSD**	**$^{207}Pb/^{206}Pb$ (Mean ± 2SD)**	**Pb (µg/g) (Mean ± 2SD)**
In-House wood standard	14	0,8522	0,077%	0.8517 ± 0.0007	0,420 ± 0.08
ERM-CD100	13	0,7962	0,011%	NA	39 ± 8
NIST-610	26	0,9095	0,019%	0.9097 ± 0.0004	417 ± 58
CELL+BCR-2	5	0,8335	0,601%	0.8327 ± 0.0005	1,1 ± 0.4
CELL+NIST-612	5	0,9055	0,190%	0.9077 ± 0.0019	4,1 ± 0.6

Table 5-6 The mean and relative standard deviation of the $^{207}Pb/^{206}Pb$ ratio of the standards. The in-house wood, ERM-CD100, NIST-610, BCR-2 and NIST-612 reference values are from Novak et al. (2010) and certificate of ERM-CD100 for the first two, and GEOREM for the last three, respectively.

Accuracy provides a measure of how close the measurements of the standards are to the "true" value. GEOREM provides a list of published measurements of various standards from different laboratories, which will be an estimate of the "true" value. All the standards (except ERM-CD100 for which Pb isotopic ratios were not available) were in agreement with reference values (see Table 5-6). Figure 5-20 demonstrates a plot of the relative standard deviation of means (RSDOM) from the measurements of the various standards. As with external precision, ERM-CD100 shows the overall highest internal precision, followed by the NIST-610-, in-house wood-, cellulose+NIST-612- and cellulose+BCR-2 standards. The relatively poor precision of the cellulose+NIST-610 and cellulose+BCR-2 may be a result of these standards being heterogeneous. The in-house wood standard which even has the lowest lead content of all the standards has pronounced lower RSDOM of the individual measurements than that for cellulose+NIST610 and cellulose+BCR-2.

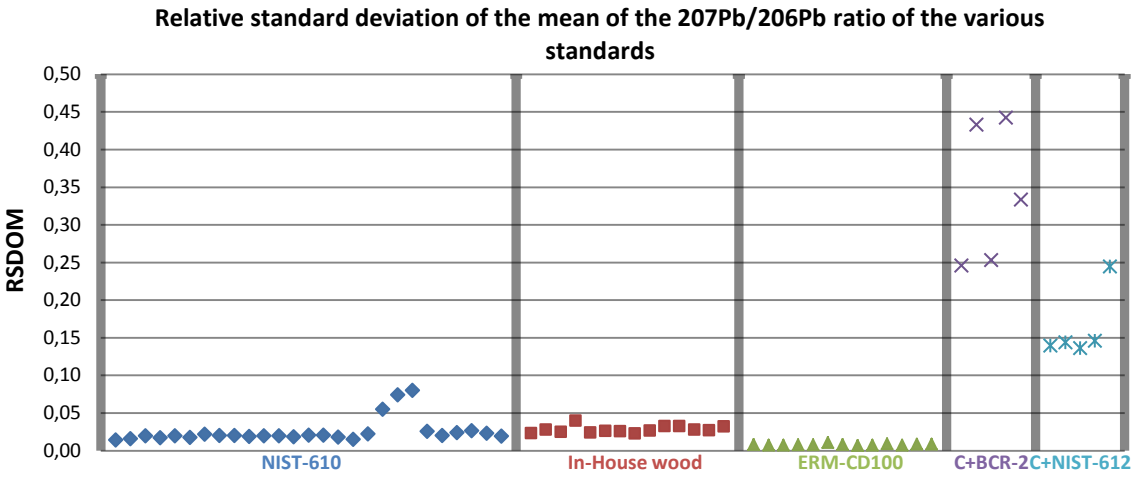

Figure 5-20 The relative standard deviation of the mean (RSDOM) of the $^{207}Pb/^{206}Pb$ ratio from the measurements of the various standards.

5.1.2 Analysis of elements

5.1.2.1 Standards

Determination of absolute concentrations by LA-ICP-MS requires an internal standard due to the complex interaction between the sample and laser (Dewaele et al., 2007), and because of the extensive variations in wood density (up to 85%) which affects the amount of material ablated and transported to the ICP-MS (Barrelet et al., 2006), the internal standard will account for the varying amount of ablated material (Dewaele et al., 2007). This standard should behave similarly during ablation of those elements whose concentration is sought (Jarvis and Williams, 1993) and should have similar properties such as mass, boiling point and ionization potential (Dewaele et al., 2007). However, for tree rings, the lack of appropriate matrix matched standards leads to problems in obtaining absolute element concentrations. Concerning the five standards prepared for this analysis, only the in-house wood- and the ERM-CD100 wood standard would be the most representative in terms of matrix. However, for the in-house wood standard the concentration of only one element (Pb) is known, and for the ERM-CD100 only certified concentrations of Ar, Cd, Cr, Cu, Hg and Pb exist. The heterogeneous nature of wood is also a problem in terms of reproducibility of analysis.

Some researchers use ^{12}C as an internal standard when assessing tree ring chemistry. Hoffmann et al. (1994), one of the pioneers, mixed cellulose powder with 5 mass % carbon powder, added multielement standard solution, and then pressed it into pellets. By using ^{12}C as an internal standard they reached precision better than 10% RSD. However, carbon content varies from the outer ring to the innermost ring of Norway spruces (Bertaud and Holmbom, 2004). Another problem is that the carbon content of the ERM-CD100 and the in-house wood standard is unknown. As a result carbon content may differ between the two wood standards, between tree rings and between tree rings and the standards. This makes the use of ^{12}C as an internal standard for LA-ICP-MS analysis of wood difficult. Therefore, only raw ratios without any corrections are presented in this study.

5.2 Result of the tree ring analysis

5.2.1 Lead

5.2.1.1 Isotopic ratios

Figure 5-21 displays the yearly variations in the $^{207}Pb/^{206}Pb$ ratio from 1968 to 2010 of the respective trees. Also shown, are the bark ratios which may be a measure of present day ratios. This figure reveals no specific trend but rather small variations between years. From 1968-1990 tree #2 demonstrates more pronounced year to year variation compared to tree #1. Tree #2 compared to tree #1 also have higher standard deviation of the means during this time

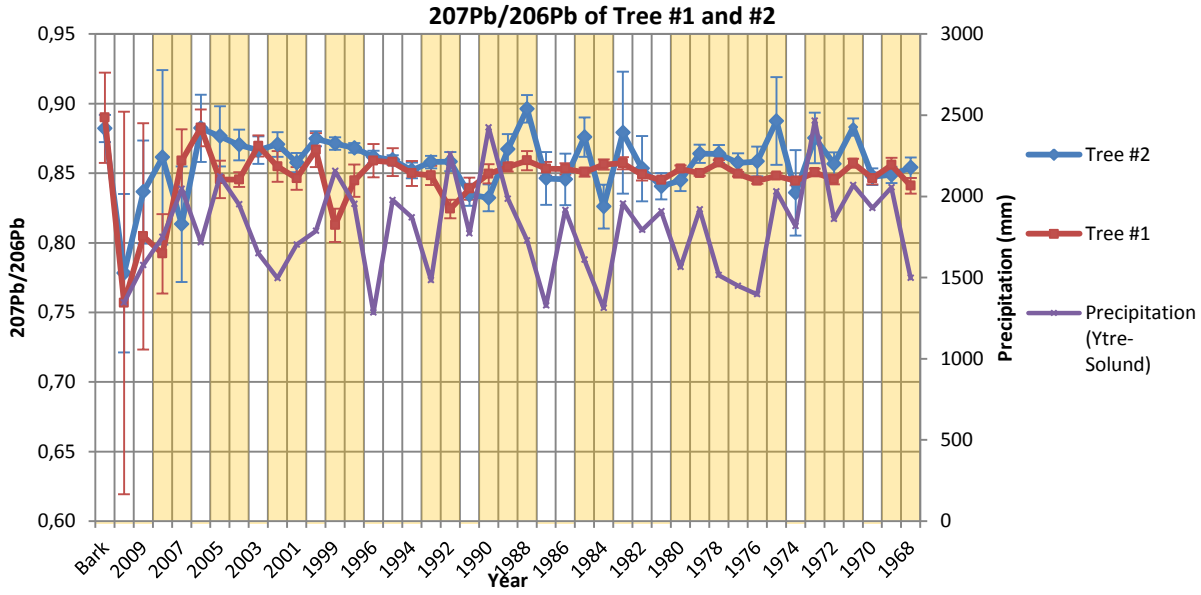

Figure 5-21 Yearly variation in the $^{207}Pb/^{206}Pb$ ratio of the individual trees. The orange-pink colored columns indicate years were there are significant differences in the lead isotopic ratio between the two trees.

interval. As shown in Figure 5-7 and Figure 5-8, tree #1 compared to tree #2 records systematically higher ^{208}Pb signals during this time interval. Then, from 1990 to 2006, there appears to be a moreover steady increase in the $^{207}Pb/^{206}Pb$ of tree #2. The $^{207}Pb/^{206}Pb$ ratio of tree #1 however, shows more pronounced year-to-year variation and larger standard deviations during this time interval. Then, for both trees from 2006 we witness a decline towards the present (2010), with some intermediate peaks, followed by an increase when encountering the bark. It should be noted that the outermost tree rings (2005-2010) demonstrate relatively large standard deviation of the mean. As evident from Figure 5-7 and

Figure 5-8, the most recent tree rings have very low recorded ^{208}Pb signal and for some the 3SD of the ^{208}Pb signal overlap with the LLD. This increases the uncertainty of the data.

Figure 5-22 demonstrates the $^{208}Pb/^{206}Pb$ ratio of the two trees from 1968-2010. The ratios recorded in tree #1 show no pronounced variation, while those of tree #2 show some pronounced peaks and deviations from those of tree #1. For both trees, the most pronounced variation is in the most recent years, from 2006-2010.

The $^{207}Pb/^{204}Pb$ ratios of the two trees are plotted in Figure 5-23. Tree #1 and #2 demonstrates pronounced different ratios from 1968 to 1989. The $^{207}Pb/^{204}Pb$ ratios of tree #2 show considerable decreases during this time period, while those of tree #1 show relatively small variations compared to those of tree #2. The considerable decreases coincide with the relatively low recorded ^{208}Pb signal for the same years (Figure 5-8). From the 1990s to 2010

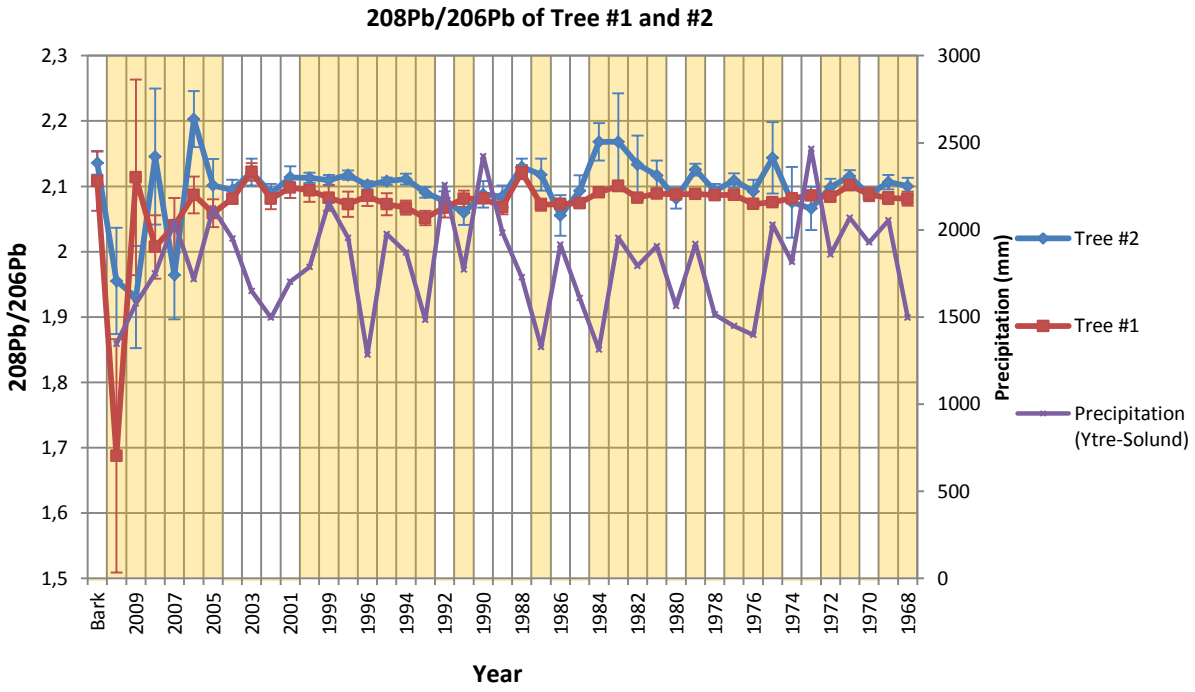

Figure 5-22 Yearly variation in the $^{208}Pb/^{206}Pb$ ratio of the individual trees. The orange-pink colored columns indicate years were there are significant differences in the lead isotopic ratio.

they show rather similar ratios.

In each of these plots, some years are marked with an orange transparent colour. This serves to indicate years which show statistically significant difference (95% confidence level) between lead isotopic ratios, and were calculated using first the Snedecor F-test for difference between variances followed by the student t-test for difference between means (see appendix 9.3.3 and 9.3.4 for test functions).

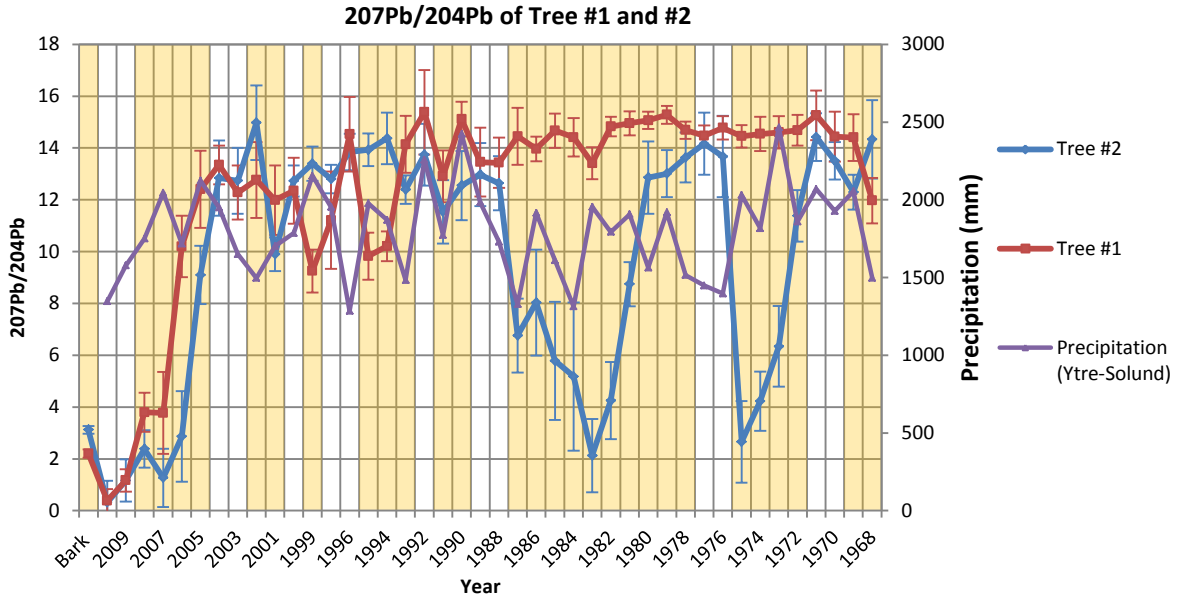

Figure 5-23 Yearly variation in the $^{207}Pb/^{204}Pb$ ratio of the two trees. The orange-pink colored columns indicate years were there are significant differences in the lead isotope ratio.

The $^{206}Pb/^{207}Pb$ ratios recorded by tree #1 and #2 conform to normal distribution (Cramer-von Mises test for distribution normality) with 95% confidence level, and yield means of 1.18±0.03 (1SD) and 1.17±0.03 (1SD), respectively.

Figure 5-24 demonstrates a scatter plot of the $^{206}Pb/^{207}Pb$ ratio vs. the $^{208}Pb/^{207}Pb$ ratio for the

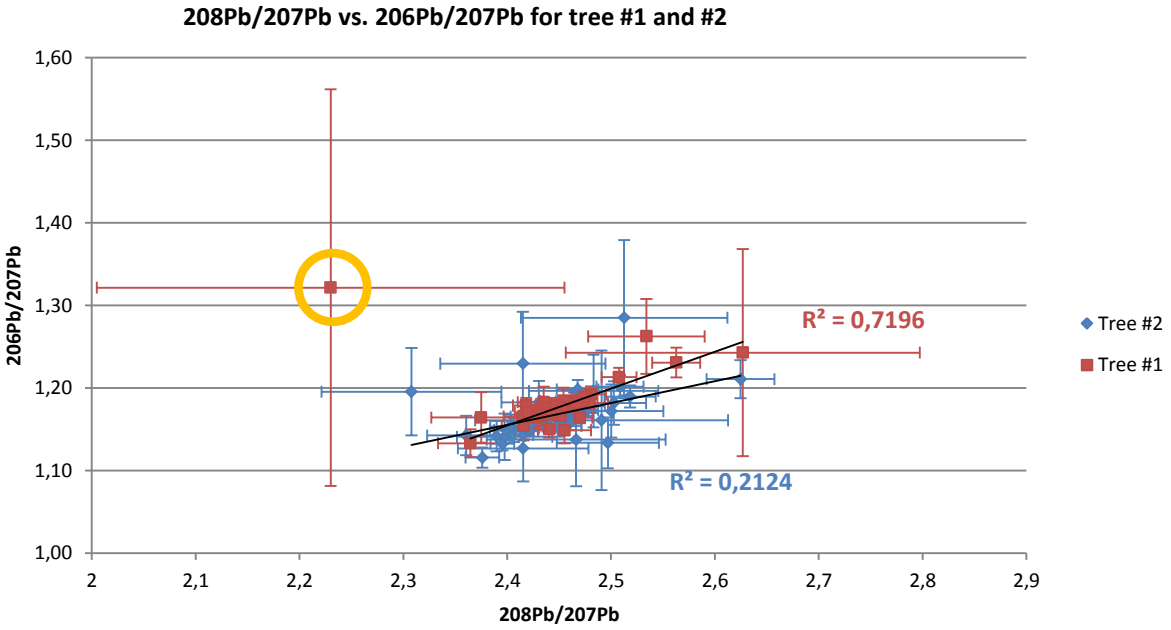

Figure 5-24 The measured $^{206}Pb/^{207}Pb$ and $^{208}Pb/^{207}Pb$ of the tree rings from the two studied trees. The measurement (year 2010) marked by a yellow circle are considered as an outlier when performing the linear regression for tree #1.

two trees. The isotopic composition of the annual rings of tree #2 shows more pronounced scatter than that of tree #1. Linear regression of the two series yields linear correlation factors of 0.7196 (when omitting the measurement marked with a yellow circle in Figure 5-24) and 0.2124 for tree #1 and #2, respectively. When plotting the lead isotopic composition of the tree rings, and grouping them in groups of approx. 10 tree rings per group, all groups seem to overlap, not showing any trend towards lower or higher isotopic values (Figure 5-25 and Figure 5-26). The only trend may be the tendency of increasing data scatter and standard deviation of the means towards the present. For both trees, the group enclosing tree rings from year 2000 to 2010 shows the largest scatter and standard deviation of the means, covering the other groups and extending further in directions.

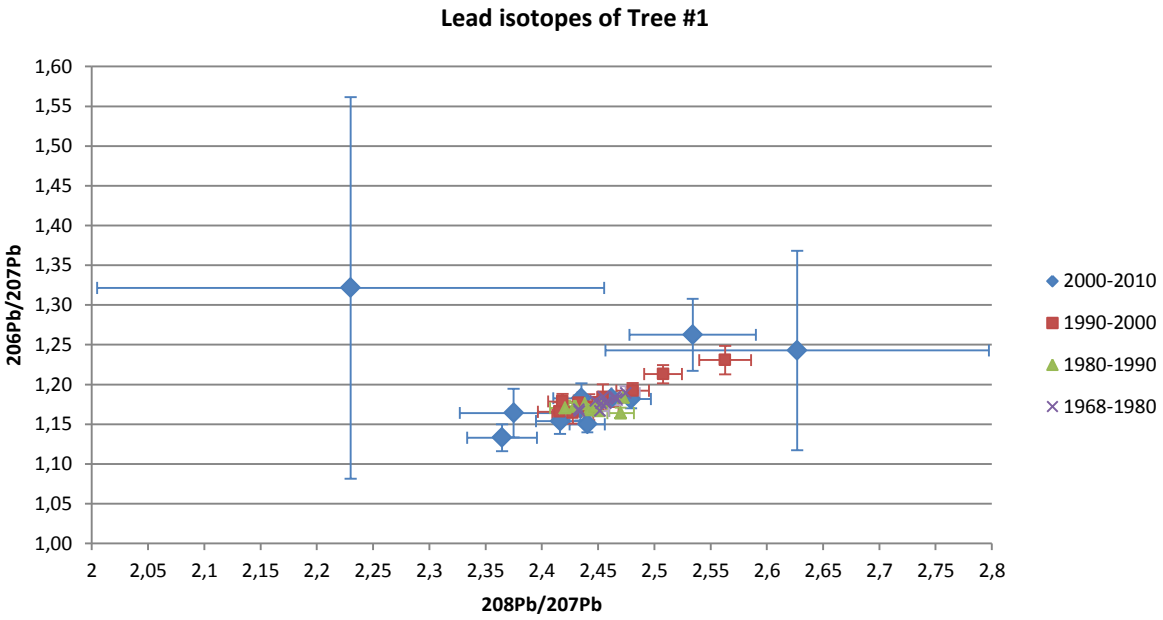

Figure 5-25 The measured $^{206}Pb/^{207}Pb$ and $^{208}Pb/^{207}Pb$ in tree-rings from tree #1. They are organized in terms of years in four different groups, 2000-2010, 1990-2000, 1980-1990 and 1968-1980.

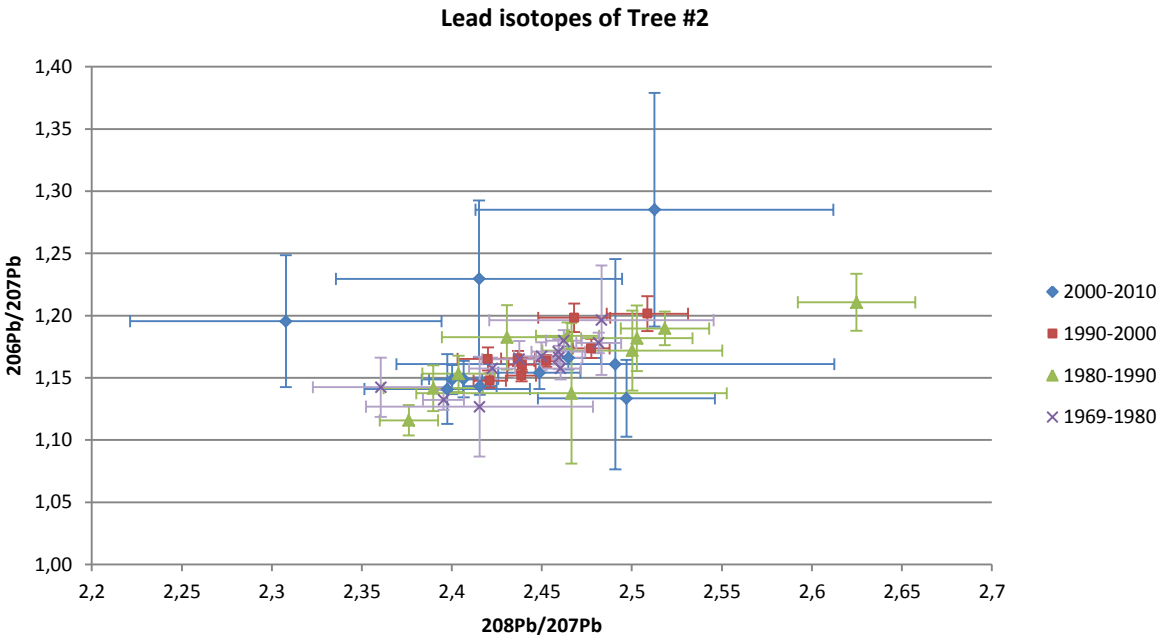

Figure 5-26 The measured $^{206}Pb/^{207}Pb$ and $^{208}Pb/^{207}Pb$ in tree-rings from tree #2. They are organized in terms of years in four different groups, 2000-2010, 1990-2000, 1980-1990 and pith-1980.

5.2.1.2 Pb normalized to ^{12}C

The $^{208}Pb/^{12}C$ ratios recorded in the annual rings of tree #1 show a steady increase from 1968-1979, followed by a steady decline towards the present (Figure 5-27). For tree #2, the $^{208}Pb/^{12}C$ ratio shows an overall decline from 1968-1975, followed by an increase towards 1976, then a decrease to 1982 followed by a steady increase to 1993, followed by a an overall decrease from 1993 to 2010 interrupted by some intermediate peaks. Also plotted in Figure 5-27a is the lead concentration in precipitation recorded at two stations, Birkenes and Kårvatn (locations are shown in Figure 3-8).

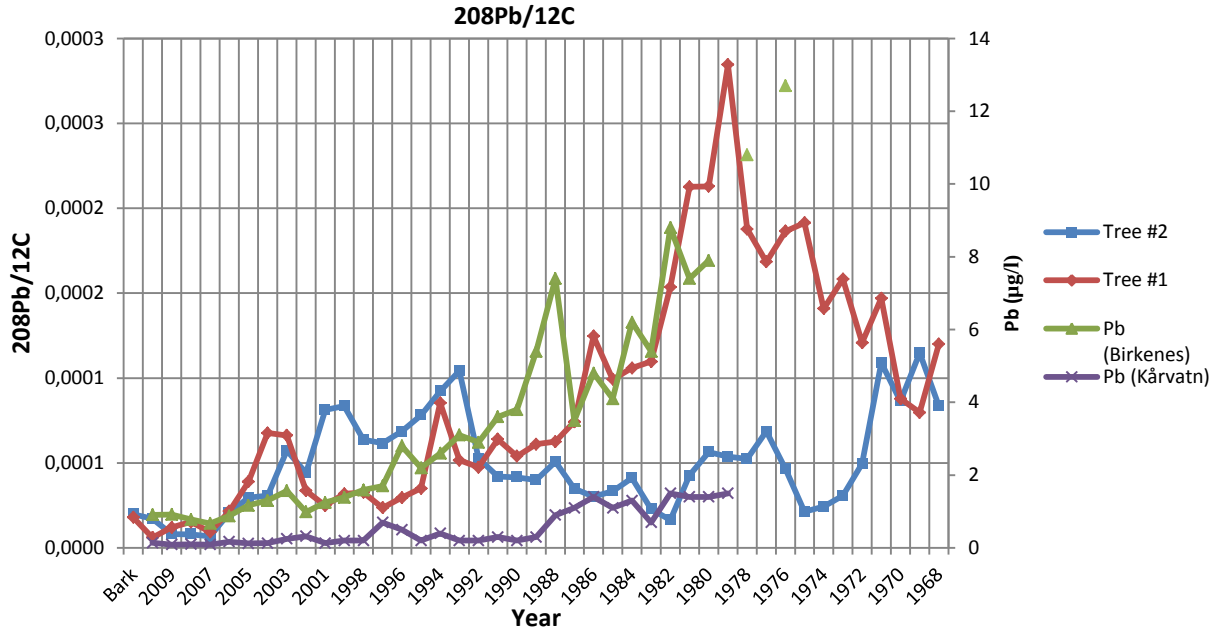

Figure 5-27 The raw signals (counts per second) of ^{208}Pb normalized to the raw ^{12}C signal (counts per second) of the corresponding tree rings. Lead concentration in precipitation is from two stations: Birkenes and Kårvatn (Schartau, 2011a). Background signals are subtracted. Data are not corrected for mass discrimination.

5.2.2 $^{63}Cu/^{12}C$ and $^{66}Zn/^{12}C$

Figure 5-28 illustrates two plots: raw counts per second of ^{63}Cu (a) and ^{66}Zn (b) normalized to the raw counts per second of ^{12}C. Tree #1 has two pronounced peaks, one in 1974 and on for the bark. However, these peaks are caused by individual measurement, and

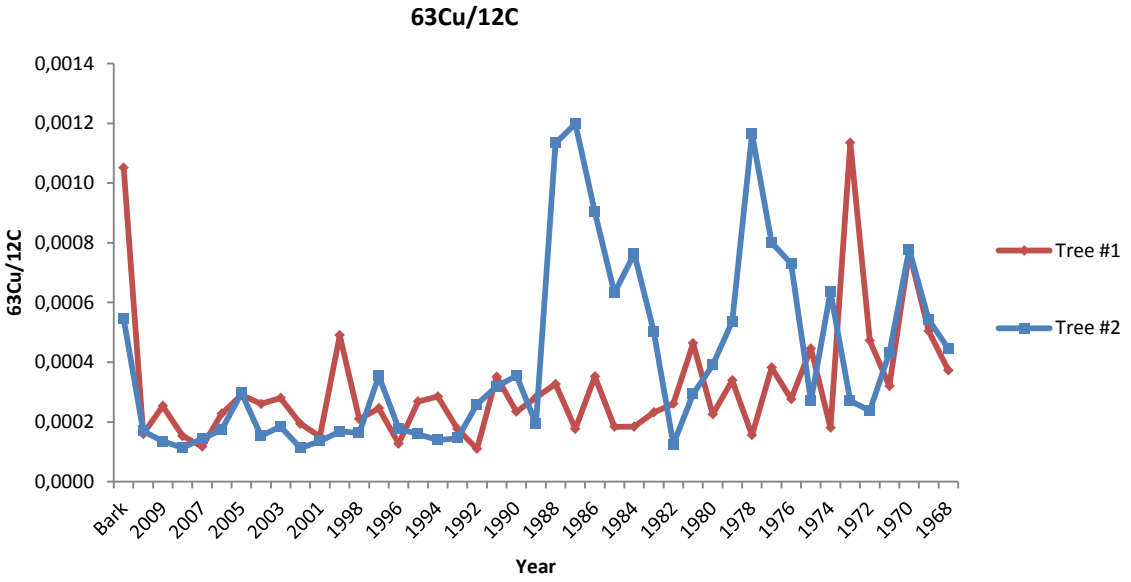

a

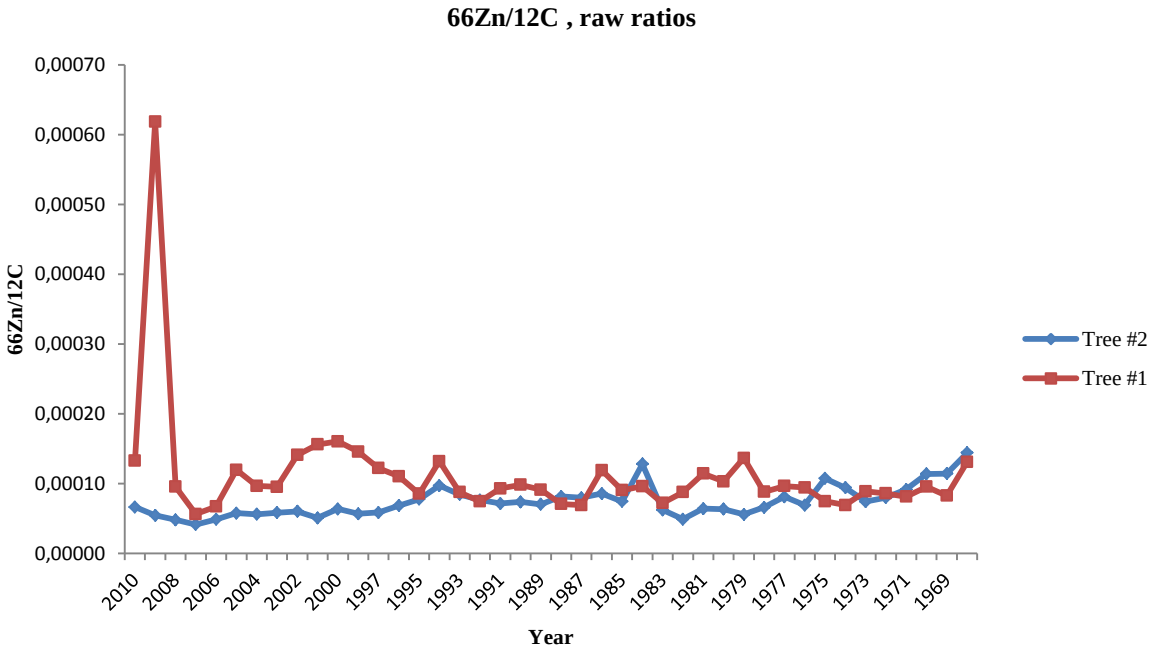

b

Figure 5-28 The raw signals (counts per second) of ^{63}Cu (a) and ^{66}Zn (b) are normalized to the raw ^{12}C signal (counts per second) of the corresponding tree rings. Background signals are subtracted from the analyte signals. Data are not corrected for any mass discrimination. For b, the $^{66}Zn/^{12}C$ ratio of the bark was considerable higher than the annual rings and is not shown. This was done in order to show the annual variation better.

taken into account the relatively large uncertainty of these data (raw data without reliable internal standard), the significance of these two abnormal measurements should be carefully evaluated. From 1975-2010 tree #1 demonstrates no systematically trend, only small year to year variation. For tree #2, the recorded $^{63}Cu/^{12}C$ ratios demonstrate two pronounced peaks (1978 and 1987). After the last peak and from 1989 to present, tree #2 only shows small year to year variation. Both trees show a pronounced increase in the bark.

For the $^{66}Zn/^{12}C$ ratios (Figure 5-28b), there is no clear distinction between the two trees, expect for some variations and a large increase when encountering the bark. However, from 1995-2003, tree #1 demonstrates relatively higher ratios.

Table 5-7 lists intra-tree correlation coefficients (see appendix 9.3.5 for test function) calculated between the various elements. Having 95% as minimum confidence limit (t_α=1.683), for tree #1, the following show significant correlation (one-tail hypothesis): $^{63}Cu/^{12}C$ and $^{66}Zn/^{12}C$, $^{66}Zn/^{12}C$ and $^{44}Ca/^{24}Mg$ and $^{208}Pb/^{12}C$ and $^{44}Ca/^{24}Mg$. For tree #2, significant correlations were only obtained between $^{63}Cu/^{12}C$ and $^{44}Ca/^{24}Mg$.

		Cu-Zn	**Cu-Pb**	**Cu-Ca/Mg**	**Zn-Pb**	**Zn-Ca/Mg**	**Pb-Ca/Mg**
Tree #1	Correlation coefficient	0.4887	0.1795	0.1849	-0.2248	-0.3778	0.6416
	t-value	3.5863	1.1681	1.2050	1.4770	2.6130	5.3561
Tree #2	Correlation coefficient	0.1143	0.0336	0.3980	-0.1128	-0.1423	0.1857
	t-value	0.7368	0.2155	2.7779	0.7266	0.9208	1.2101

Table 5-7 Intra-tree correlations between elements (all normalized to carbon). Correlations were done for tree rings formed from 1968-2010 (except 1999) and bark. Degrees of freedom=n-2=43-2=41.

5.2.3 The $^{44}Ca/^{24}Mg$ ratio

Figure 5-29 shows ^{44}Ca normalized to ^{24}Mg. From 1968 to the present, both trees demonstrate a steadily declining $^{44}Ca/^{24}Mg$ ratio. Linear regressions of tree #1 and #2 yield correlation factors of 0.6406 and 0.4165, respectively. Also plotted in this diagram is the pH values of precipitation measured at Haukeland weather-station.

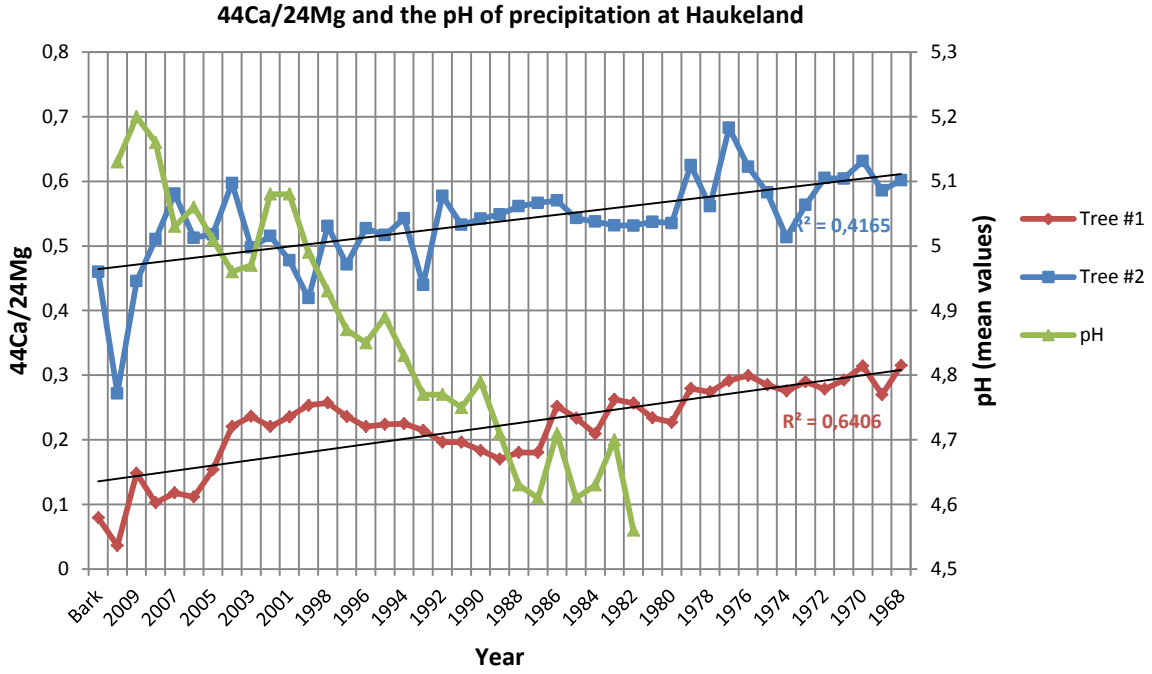

Figure 5-29 Raw signals (counts per second) of ^{44}C are normalized to the raw ^{24}Mg signal (counts per second) of the corresponding tree rings. The pH of annual precipitation from 1982-2010 was measured at Haukeland (for location see Figure 3-8). Background signals are subtracted from the analyte signals. Data are not corrected for any mass discrimination.

5.2.4 Inter-tree correlations

Correlation coefficients between the two trees for the various lead isotopic ratios are listed in Table 5-8. All ratios show positive correlation except the $^{208}Pb/^{207}Pb$ ratio and all ratios show significant correlation with minimum 95% confidence level (Table 5-8).

	Correlation between tree #1 and #2		**Confidence level**
	Coefficient	**t-value**	
$^{207}Pb/^{206}Pb$	0.5232	3.9308	99.98%
$^{208}Pb/^{206}Pb$	0.4483	3.2110	99.75%
$^{208}Pb/^{207}Pb$	-0.2927	1.9603	95%
$^{207}Pb/^{204}Pb$	0.5370	4.0764	99.98%

Table 5-8 The correlation coefficients of various lead isotope ratios between tree #1 and #2, for the time period 1969-2010 (except year 1998), with DF=n-2=43-2=41. The significance of correlation is evaluated by testing a one-tail hypothesis.

Table 5-9 lists the inter tree correlation coefficients of tree #1 and #2 obtained for $^{208}Pb/^{12}C$, $^{66}Zn/^{12}C$, $^{63}Cu/^{12}C$, and $^{44}Ca/^{24}Mg$. High t-values were obtained for the $^{66}Zn/^{12}C$ and the $^{44}Ca/^{24}Mg$ ratios.

	Correlations coefficient	**t-value**
$^{208}Pb/^{12}C$	0.0668	0.4284
$^{66}Zn/^{12}C$	0.9265	15.77
$^{63}Cu/^{12}C$	0.0877	0.5637
$^{44}Ca/^{24}Mg$	0.6127	4.9456

Table 5-9 Inter tree correlation coefficients of tree #1 and #2. DF=n-2=43-2=41. The significance of correlation is evaluated by testing a one-tail hypothesis.

6 Discussion

6.1 Intra tree and inter tree variations

The two studied trees demonstrate no systematically trend in the lead isotopic ratio from the innermost to the outermost tree ring and bark (Figure 5-21 and Figure 5-22). The bark value may be representative of recent or present air lead isotopic composition, but should be carefully interpreted due to its different anatomy and Pb uptake mechanism than the tree rings. Lead accumulation in bark is characterized by direct deposition from the atmosphere, while that of the tree rings are mostly characterized by uptake through the root system (see section 3.3.4). The two studied trees show relatively similar yearly increases and decreases of the annual recorded Pb isotopic ratios. This is evident by the significant correlation coefficients listed in Table 5-8. The correlation coefficients show values between -0.29 ($^{208}Pb/^{206}Pb$) and 0.54 ($^{207}Pb/^{204}Pb$), which suggest that the yearly increases and decreases are not exactly the same. In terms of absolute isotope ratios, the two trees record significantly different isotope ratios in some of the annual tree rings (these years are indicated by orange colour in Figure 5-21 and Figure 5-22). This may shed light on whether the lead content in the two trees dates back to the same pollution sources or natural variations. The annually recorded $^{207}Pb/^{204}Pb$ ratio of the two trees show relatively similar trends (0.54 in correlation coefficient), but in terms of absolute ratios they differ considerably between 1968 and 1989 (Figure 5-23). Tree #1 demonstrates a relatively stable $^{207}Pb/^{204}Pb$ ratio, while tree #1 shows two considerable decreases and increases. Since ^{204}Pb lead is the least natural occurring Pb isotope, only accounting for 1% of the naturally occurring Pb, and since there is no pronounced observed change in the $^{207}Pb/^{206}Pb$ ratio, there is reason to question the reliability of the relatively low observed $^{207}Pb/^{204}Pb$ ratio. It is also worth mentioning the relatively low ^{208}Pb signal recorded during the same time period. A possible explanation could be Hg interferences on ^{204}Pb, which will create the relatively low observed $^{207}Pb/^{204}Pb$ ratio. Annual rings of tree #1 and #2 formed after 1989 show rather similar ratios, before a steep decline is witnessed for both trees from 2005 to the present.

Since no absolute concentrations were obtained, the annual variation in $^{208}Pb/^{12}C$ may be a weak measure of the annual variation in Pb concentration. For the recorded variation in $^{208}Pb/^{12}C$, tree #1 shows increasing $^{208}Pb/^{12}C$ from 1968 to 1979 followed by a steady decline towards the outermost tree ring formed in 2010 (Figure 5-27). Therefore, in terms of concentration, Pb reaches a peak value in 1979. To what degree the observed trend is natural

or a consequence of increasing amount of bioavailable lead is difficult to assess. The recorded $^{208}Pb/^{12}C$ ratio of tree #2 from 1968-1992 is consistently lower than that of tree #1, but shows some intermediate peaks. These intermediate peaks are consistent with the temporal peaks of the $^{207}Pb^{204}Pb$ ratio (Figure 5-23). The low correlation coefficient obtained between the recorded $^{208}Pb/^{12}C$ of tree #1 and #2 of 0.0877 and the consistently lower $^{208}Pb/^{12}C$ ratio of tree #2 from 1968-1992, suggests different amounts of Pb available for root uptake throughout this period. The annual variations in the $^{63}Cu/^{12}C$, $^{66}Zn/^{12}C$ ratio, $^{208}Pb/^{12}C$ and $^{44}Ca/^{12}C$ were compared to check whether intra tree annual variations in the different elemental ratios are similar. Relatively low correlation coefficients were obtained for both trees, but tree #2 showed even smaller correlation coefficient than tree #1 (Table 5-7). Tree #1 showed a relative high correlation coefficient for the $^{44}Ca/^{24}Mg$ ratio. The intra ring correlations of the $^{208}Pb/^{12}C$ with the $^{63}Cu/^{12}C$ and $^{66}Zn/^{12}C$ ratios were calculated to investigate if Pb, Zn and Cu show a similar accumulation trend.

The $^{63}Cu/^{12}C$ ratio of tree #1 and #2 (Figure 5-28a) do not demonstrates any overall trend from the innermost to the outermost tree ring. Tree #1 only shows peaks (one in 1974 and one for the bark) characterized by individual measurements which is highly questionable. Tree #2 shows two pronounced peaks which was not observed for tree #1. These two peaks demonstrate relatively equal intensities and duration. The inter tree correlation of the annual variation of the $^{63}Cu/^{12}C$ ratio (Figure 5-28a) yielded a very low positive correlation coefficient (Table 5-9). This means that the annual uptake and deposition of Cu within the tree rings are considerably different at the two sites. According to Steinnes (2001) Cu originates from local point sources within Norway compared to the long range transportation and Pb and Zn.

For the two trees no specific overall trend from the inner to the outermost annual ring towards higher or lower $^{66}Zn/^{12}C$ values were observed. Inter tree correlation of the annual $^{66}Zn/^{12}C$ ratio yielded a very high correlation coefficient of 0.93, the highest obtained for the inter trees correlations. This significant correlation indicates similar variations in root uptake, and similar deposition patterns within the boles.

However, causes of annual variation when no pronounced trend is observed are hard to assess. Natural trends of individual elements may exist, i.e. one element may increase from the outer ring toward the pith, while another may show the opposite, some may increase and peak at the heartwood/sapwood boundary and vice versa, and some may not show any trends at all (Chun and Huang, 1992, Okada et al., 1993). As mentioned in chapter 3.3.3, Longuetaud et al. (2006) calculated a heartwood initiation age of 17 years when investigating 4 Norway

spruce (*Picea abies*) stands, and Zimmermann et al. (1971) noted that irreversible embolism in all tracheids of an annual ring had occurred when reached the age of 40 years. Hagemeyer and Schafer (1995) measured highest Zn concentration in the cambial zone and stem center of beech trees, while that of lead showed low concentration in the cambial zone and highest just inside the sapwood-heatwood transition.

6.2 Relationship with data recorded by weather-stations

6.2.1 Annual precipitation registered at Ytre-Solund weather station

Annual amount precipitation from 1968-2010 registered at Ytre-Solund weather station (for location see Figure 3-1) are correlated with the recorded Pb isotopic ratios and the $^{63}Cu/^{12}C$, $^{66}Zn/^{12}C$ and $^{44}Ca/^{24}Mg$ ratios of the annually tree rings. This may be indicative of the influence of rainfall on the deposition and uptake of the various elements. Water content in soils affect the nutrient solubility (Pantera et al., 2007), and the changes in the annual precipitation may be a measure of this. The results from this correlation are listed in Table 6-1. Having a minimum confidence limit of 90% (t_α=1.3031), only the $^{207}Pb/^{206}Pb$ recorded by tree #2, the $^{63}Cu/^{12}C$ recorded by both trees and the $^{44}Ca/^{24}Mg$ ratio recorded by tree #2 were significant (see appendix 9.3.5 for test function).

The correlation coefficients of $^{63}Cu/^{12}C$ recorded by the trees were opposite to each other: negative correlation for tree #2 and positive for tree #1. For the $^{44}Ca/^{24}Mg$ ratio only tree #2 reveals significant correlation. The significant correlations may provide some explanation of the variation observed.

	Tree #1		**Tree #2**	
	CC	t-value	CC	t-value
$^{207}Pb/^{206}Pb$	0.0807	0.5119	0.2363	1.5378
$^{208}Pb/^{206}Pb$	0.1990	1.2846	0.0205	0.1298
$^{207}Pb/^{204}Pb$	0.1240	0.7906	0.0447	0.2832
$^{208}Pb/^{12}C$	0.0511	0.3237	-0.0340	0.2150
$^{63}Cu/^{12}C$	0.4368	3.0710	-0.2504	1.6359
$^{66}Zn/^{12}C$	-0.1510	1.0249	-0.0543	0.3439
$^{44}Ca/^{24}Mg$	0.11057	0.7036	0.2605	1.7069

Table 6-1 Correlation coefficients (CC) between element and element ratios recorded in the two trees and the registered precipitation at Ytre-Solund weather station from 1968-2010. Degrees of freedom=n-2=42-2=40.

6.2.2 The pH of precipitation at Haukeland

The annual pH of precipitation collected at Haukeland from 1982-2010 (for location see Figure 3-8) are correlated with the $^{208}Pb/^{12}C$, $^{63}Cu/^{12}C$, $^{66}Zn/^{12}C$ and $^{44}Ca/^{24}Mg$ ratios of the annual formed tree rings between 1982 and 2010. The results from these correlations are listed in Table 6-2.

	Tree #1		**Tree #2**	
	CC	t-value	CC	t-value
$^{208}Pb/^{12}C$	-0.7985	6.7627	-0.1822	0.9448
$^{63}Cu/^{12}C$	-0.1610	0.8316	-0.6189	4.0178
$^{66}Zn/^{12}C$	0.4113	2.3009	-0.5989	3.8135
$^{44}Ca/^{24}Mg$	-0.5182	3.0892	-0.4110	2.2990

Table 6-2 Correlation coefficients (CC) between element ratios recorded in the two trees and the registered pH of precipitation at Haukeland. Degrees of freedom=n-2=28-2=40. The correlation coefficients were obtained for the time period 1982-2010.

Having a minimum confidence limit of 90% (t_α=1.3149), most of the element ratios demonstrate significant correlations with the pH of precipitation, with the highest coefficient recorded for the $^{208}Pb/^{12}C$ ratio (Table 6-2). Inter tree differences in correlation coefficients are also evident here. For example, the recorded $^{208}Pb/^{12}C$ ratios of tree #1 compared to tree #2, demonstrate a relatively high correlation of -0.7985 compared to -0.1822 obtained for tree #2.

A study performed by Sauve et al. (2000) collected data from various papers and computed the reported metal partitioning coefficients in soils of Cu, Pb and Zn as a function of soil solution pH. Linear correlation factors of 0.288, 0.473 and 0.557 were achieved, respectively, but it was found that pH only accounted for 30-60% of the total variation in partitioning coefficients of the different metals. The significant correlations obtained in Table 6-2 indicate a relationship between the pH of precipitation from 1982-2010 and the incorporated elements in the tree rings.

The trends towards lower $^{44}Ca/^{24}Mg$ ratios registered for the two trees (Figure 5-29), and the significant negative correlations (Table 6-2) with the pH of precipitation indicates a significant relationship between the $^{44}Ca/^{24}Mg$ ratio recorded by the two trees and the pH of precipitation at Haukeland. This relationship is also evident from published literature. For example, Chen et al. (2010) used xylem Ca/Mg of *Abies fabri* to reconstruct the historical changes of soil pH in Emei Mountain, and found significant correlation between recent xylem Ca/Mg and the measured soil pH (correlation coefficient of -0.84). Therefore, the plot in Figure 5-29 suggests that the increasing pH of precipitation correlates with the corresponding

soil pH which further affects and controls the root uptake ratio of Ca/Mg. The significant inter tree correlation of the $^{44}Ca/^{24}Mg$ ratio (see Table 5-9) suggests that the two trees show the same trend from 1968 to the present. However, the $^{44}Ca/^{24}Mg$ ratios of tree #2 are consistently higher than that of tree #1. These inter site differences are hard to address, because the chemistry of the local soils are not known. The two trees do however show the same trend with a correlation coefficient of 0.6127 (see Table 5-9). Therefore, it seems likely that the two trees record past environmental changes in terms of soil acidity.

6.2.3 Wind directions

As evident from the wind-roses in Figure 3-1 south to south-eastern winds, followed by north and western winds are the dominating wind directions throughout the lifespan covered by the two trees. The north-northwest location of tree #1 and the relatively shorter distance from the refinery – 10.1 km vs. 17.8 km for tree #1- suggests that tree #1 should contain the highest amount of potential pollutants. For lead, this is clearly the case between 1970 and 1991, where tree #1 demonstrates considerably higher $^{208}Pb/^{12}C$ (Figure 5-27). For the other elements, only $^{63}Cu/^{12}C$ show considerable different evolution from 1968-2010.

6.2.4 Composition of precipitation

Only Pb and Zn concentration of precipitation were available. Data obtained from Kårvatn and Birkenes stations (for location see Figure 3-8) were correlated with the $^{208}Pb/^{12}C$ and $^{66}Zn/^{12}C$ ratios of the annual tree rings.

Correlation of the recorded $^{208}Pb/^{12}C$ ratio of tree #1 with the concentration recorded at the two stations was significant (see Table 6-3). For tree #2, correlation coefficients were rather small and yielded a t-value of 0.1380. As Figure 5-27 shows, continuous lead precipitation data only exist from 1980 to 2010 for the Birkenes station, and for the Kårvatn station, from 1979-2010. For this reason, it is not possible to check whether the peak recorded by tree #1 coincide with the peak concentration in precipitation. However, according to measurements made in 1976 and 1978 at Birkenes, the peak concentration in tree #1 could be delayed relative to the precipitation. This may indicate a time lag between lead deposition and the following uptake. The problem of time lag is also addressed by Momoshima and Bondietti (1990) and Savard et al. (2006). Momoshima and Bondietti (1990) attributed the registered time lag to slow movement of metals in soil, followed by slow movement up the tree bole. This was also discussed in Hagemeyer (1993), where it was attributed to metal adsorption on inorganic and organic matter. Savard et al. (2006) combined measurements of both natural

and anthropogenic geochemical tracers in tree-rings of spruce trees (*Picea mariana*), and found that abrupt changes in the $\delta^{13}C$ ratio marked the onset of smelter operations in 1928 in Rouyn-Noranda, Canada. However, delays of 8 to 20 years were registered for the Ca, Cd, and Pb concentrations as well as for $^{206}Pb/^{207}Pb$ and $^{208}Pb/^{206}Pb$ ratios. This clearly demonstrates the different uptake mechanism: the carbon being taken up during photosynthesis while the macro- and micro nutrients and heavy metals being taken up by the roots. In contrast, carbon is incorporated by photosynthesis in the leaves and therefore records changes in the atmosphere much faster than elements typically incorporated by roots.

For the $^{63}Zn/^{12}C$ ratio, the correlation coefficients were relatively small except for the $^{63}Zn/^{12}C$ ratios (see Table 6-3) between tree #2 and the Zn data from Birkenes station. However, the Birkenes station is located in the southern part of Norway (Figure 3-8) and may not be representative of Zn in precipitation at Mongstad.

		Tree #1		**Tree #2**	
		CC	t-value	CC	t-value
Kårvatn	$^{208}Pb/^{12}C$ - Pb	0.8344	8.1859	-0.0261	0.1380
	$^{66}Zn/^{12}C$ - Zn	-0.1335	0.7255	0.2644	1.4764
Birkenes	$^{208}Pb/^{12}C$ - Pb	0.8398	8.1859	-0.0814	0.4398
	$^{66}Zn/^{12}C$ – Zn	-0.2172	1.1776	0.5327	3.3005

Table 6-3 Correlation with measured Pb and Zn concentration in precipitation at Kårvatn station and Birkenes station. Kårvatn and Birkenes stations had concentration measurements from 1979 and 1980, respectively. Kårvatn: DF= n-2=31-2=29. Birkenes: Degrees of freedom=30-2=28.

6.3 Comparison with other environmental archives

6.3.1 Environmental archives in the UK

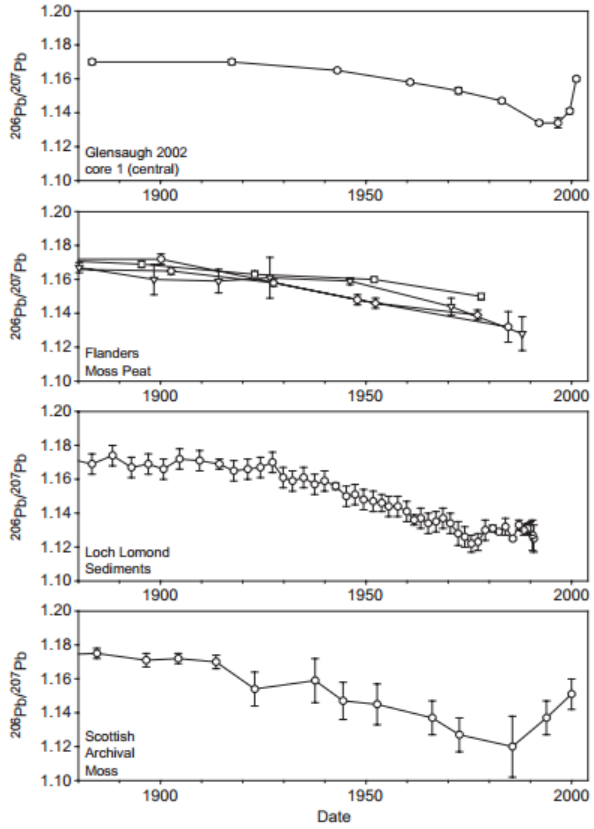

Figure 6-1 $^{206}Pb/^{207}Pb$ from Pb in peat at Thorter, Glensaugh (Farmer et al., 2005), Flanders moss peat cores (Farmer et al., 1997), anthropogenic Pb of a sediment core located in the southern basin of Loch Lomond (Farmer et al., 1996, Eades et al., 2002) and Pb in Scottish *Shapgnum* moss samples (Farmer et al., 2002). All diagrams from Farmer et al. (2005).

Figure 6-1 provides four diagrams showing the $^{206}Pb/^{207}Pb$ evolution since the 1880s as recorded by peat cores, sediment cores and moss samples in Scotland (see figure text for more information). Comparing the Scottish lead evolution with that recorded by the trees in Hordaland, Norway (Figure 5-21), suggests quite different evolutions. However, it should be noted that Figure 5-21 shows the $^{207}Pb/^{206}Pb$ ratios which is the inverse of the $^{206}Pb/^{207}Pb$ ratio plotted in Figure 6-1. All the diagrams demonstrate a systematically declining $^{206}Pb/^{207}Pb$ ratio from the 1930s to approx. 1960 and 1970. The $^{206}Pb/^{207}Pb$ ratios recorded by the Scottish Shagnum moss samples (lowest diagram in Figure 6-1), show a steady increase in the $^{206}Pb/^{207}Pb$ ratio from between 1980 and 1990 to the present (2000). This is also the case for the uppermost diagram, which demonstrates an increase from the mid 1990s to the present. The decline from the 1930s is attributed to the use of leaded gasoline and the following increase corresponds to the phasing out of leaded gasoline (Farmer et al., 2005). Farmer et al. (2000) collected and measured the $^{206}Pb/^{207}Pb$ ratio of petrol used in Edinburgh from 1989-1998, and calculated a mean of 1.076 ± 0.0011 (1SD).

The evolution of the $^{206}Pb/^{207}Pb$ ratio for the period 1985-2000 of the Scottish mosses (Figure 6-1) is not observed for the $^{207}Pb/^{206}Pb$ ratio of the two trees in Figure 5-21, which demonstrate a relatively flat evolution with some year to year fluctuations. For the $^{206}Pb/^{207}Pb$ ratios recorded in peat in Thorter, Glensaugh, a pronounced increase from 1995 to 2000 is

observed. Tree #1 and #2 demonstrate $^{206}Pb/^{207}Pb$ ratios ranging between 1.13 (2006) and 1.32 (2010), and 1.12 (1988) and 1.29 (2010), respectively. Even though the highest recorded lead isotopic ratio was found for the outermost tree ring, corresponding to year 2010, there is no overall trend from the tree rings formed in 1968 towards the outermost tree rings. However, from 2005 to 2010 an overall increase in the $^{206}Pb/^{207}Pb$ ratio can be documented. These measurements show relatively large standard deviation of the mean, and are therefore quite uncertain.

In the end it we can conclude that the trees do not show the same trend as observed for peat cores, sediment cores and moss samples from the UK.

6.3.2 Lead in Norwegian peat bogs and mosses

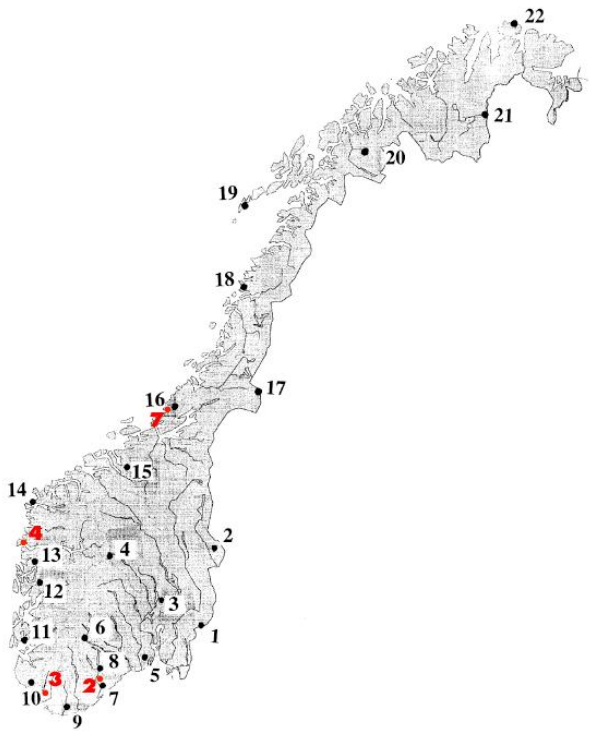

Figure 6-2 Map of Norway showing samples of peat bogs (red) and mosses (blacks). Only moss data from locality 11, 12, 13, 14 were compiled and plotted in Figure 6-3. Map from Steinnes et al. (2005).

For location of the peat bogs and mosses used for the following discussion see Figure 6-2. Data from Figure 5-24 are re-plotted in Figure 6-3 together with Norwegian peat bog data, moss data and ice-core data from Greenland. The relative large scatter in tree ring data compared to the Norwegian moss data (Steinnes et al., 2005) and peat bog data (Dunlap et al., 1999) is noticeable. The mosses were collected in 1977, 1985, 1990, 1995, and 2000. When comparing these values with other published results, it should be noted, as mentioned by Steinnes et al. (2005), that these values represent the lead incorporated during the period of growth during the three preceding years. Therefore, Steinnes et al. (2005), suggest that the years 1975, 1983, 1988, 1993 and 1998, rather be used when comparison are to be made. The peat bog data show Pb isotopes recorded from <1691-1991 AD. Linear regression of the moss- and peat bog data yield a linear correlation factor of 0.98. In comparison, a linear correlation factor of 0.385 was achieved for the two trees (Figure 6-3).

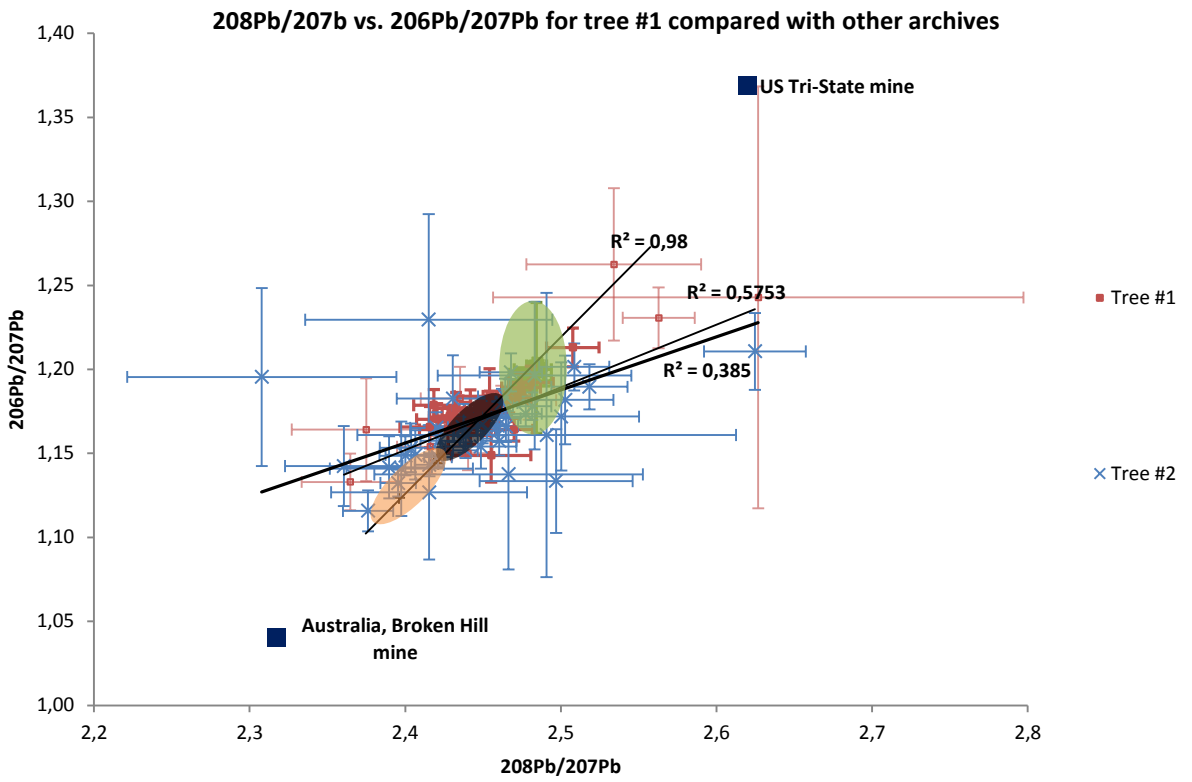

Figure 6-3 Lead isotopic composition of mosses (orange in color) and peat bogs (black in color) of Norway. The moss data correspond to 5 locations in the south-western part of Norway marked as number 10, 11, 12, 13 and 14 in Figure 6-2, and are grouped together in years: 2000, 1995, 1990, 1985 and 1977. Data from the Greenlandic ice core (green filled circle) is from Rosman et al. (1997) and demonstrates lead isotopic ratios from 7313 BC to 1523 AD. Peat bog data correspond to 4 locations marked in red as number 2, 3, 4 and 7 in Figure 6-2, and represent Pb recorded from <1691-1991 AD. Moss data from Steinnes et al. (2005) and peat bog data from Dunlap et al. (1999). For a closer look at the peat bog data and mosses data see Figure 6-4.

However, when discarding the most recently formed tree rings (2000-2010), a linear correlation factor of 0.5783 was obtained. Even better linear correlation factor (0.7196) was achieved when only using data from tree #1, which is closer to that of the peat bogs and mosses. Most of the recorded lead isotopic ratios of both trees plot towards higher ratios than mosses which represent approximately the same time period (1975-2000) as well as geographically area of interest (see location in Figure 6-2). Most of the recorded Pb isotopic data in rings of tree #1 overlap with data recorded by peat bogs. The lead isotopes recorded by tree #2 show a much larger scatter and are hard to confine within a certain area. Also, both the peat bogs and mosses demonstrate evolution trends during their respective time intervals. The peat bog data show a general decline in lead isotopic ratios towards the most recent time (1961-1991). However, as pointed out by Dunlap et al. (1999), overlap between the two groups older than 1950 occur, but do not occur between the youngest age groups (1921 to

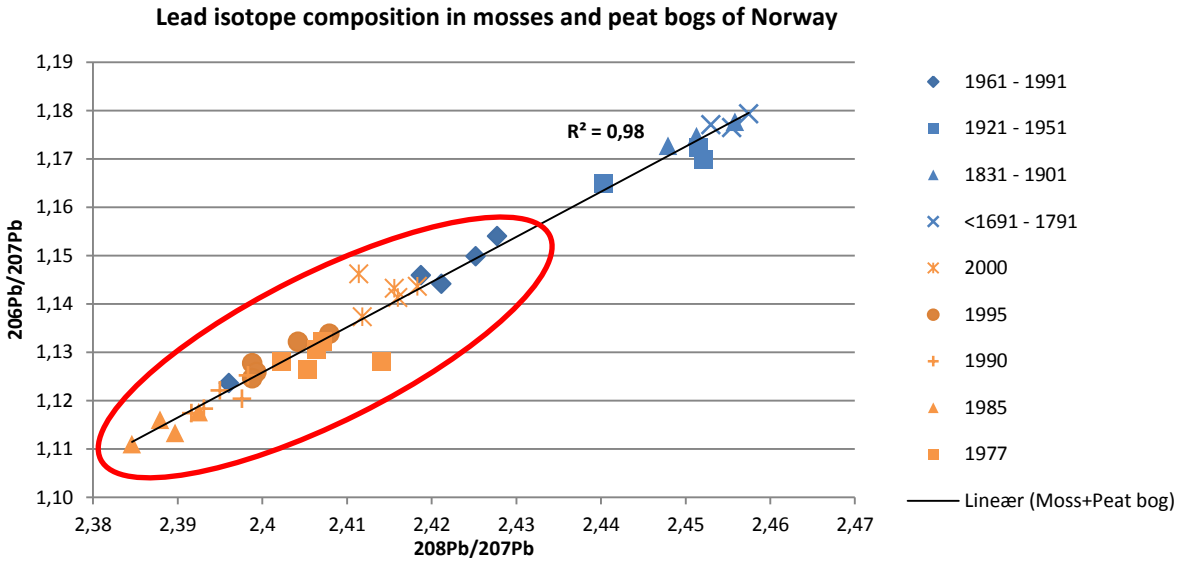

Figure 6-4 Moss and peat bog data from Steinnes et al. (2005) and Dunlap et al. (1999), respectively. The red circle serves to indicate data corresponding to the time interval covered by the two trees collected for this study.

1951, and 1961 to 1991). Generally, the $^{206}Pb/^{207}Pb$ and $^{208}Pb/^{207}Pb$ ratios of the mosses appear to decrease from 1977 to 1985 followed by a steady increase towards year 2000, exceeding 1977 ratios (1977 ratios overlap with 1995 values). This is in consistency with the general trend observed elsewhere in the country, but the southwestern coast of Norway demonstrates consistently lower $^{206}Pb/^{207}Pb$ ratios through time (Steinnes et al., 2005). This trend is absent for the two trees, and is evident in Figure 5-25 and Figure 5-26 where all age groups overlap. Based on the UK airborne lead and the predominantly south-south westerly winds, Steinnes et al. (2005) conclude that the moss data follow the UK trend quite closely. Also shown in Figure 6-3 are lead isotopes in a Greenlandic ice-core (7313 BC to 1523 AD). Dunlap et al. (1999) attribute the Pb isotopic ratios recorded from 7313 to 366 BC by the ice core, as representing Holocene background values. The lead isotopic composition of the tree rings also overlap data recorded by the ice-core. This highlights the large variation in lead isotopic ratios recorded by the tree rings, and may suggest that the tree rings record normal background values. Considering lead concentrations, the decline registered from 1979 in tree #1 (Figure 5-27) corresponds to the decrease in lead concentration in mosses for the same area (Figure 6-5). This declining lead concentration is also registered by the peat bog in Figure 6-6. However, tree #2 does not follow this trend.

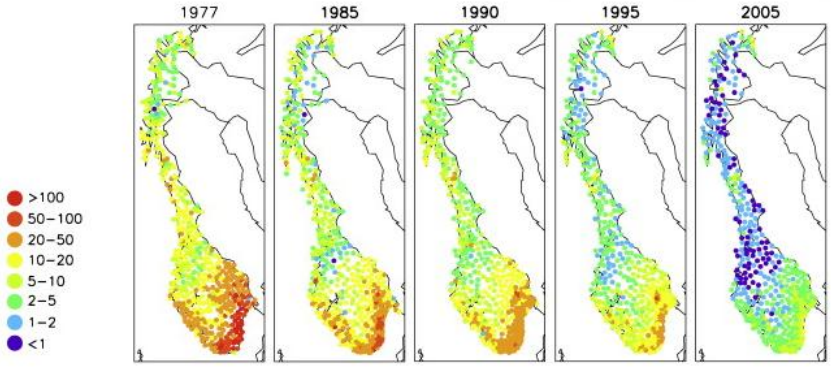

Figure 6-5 These five different figures show lead concentrations in moss samples measured in 1977, 1985, 1990, 1995, and 2005, respectively. Clearly, these five different years, reveal a decrease in lead concentration from 1977 to 2005. From Steinnes et al. (2011).

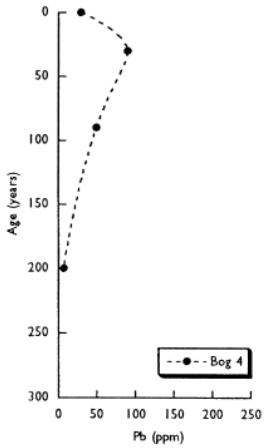

Figure 6-6 Peat bog #4 lead data. For location see Figure 6-2. From Dunlap et al. (1999).

The paper by Bindler et al. (2004) compared $^{206}Pb/\ ^{207}Pb$ ratios measured in Scots pine (*Pinus Sylvestri*s L.) and Norway spruce (*Picea abies*), with their respective soils ratios, and with existing measurements derived from peat bogs and lake sediments. This revealed poor agreement with peat bogs and lake sediments; peat-bogs and lake sediment were showing a changing $^{206}Pb/\ ^{207}Pb$ ratio through time, while the tree rings do not show such trend. The measured signal at each site was in between that of the humus layer (approx. 1.15) layer and the C-horizon (1.37 – 1.63). Bindler et al. (2004) conclude that the record of lead isotopes in tree rings is a mixture of natural geogenic lead derived from the mineral horizon, and anthropogenic lead derived either directly from the atmosphere or the organic layer by root uptake.

6.3.3 Aerosols

Lead isotopic ratios of tree rings formed from 1990-2000 are plotted together with worldwide measured aerosols between 1994 and 1999 (Bollhofer and Rosman, 2001a) in Figure 6-7. Some tree ring values do overlap the western and European aerosols, but this is also the case for aerosols collected in North America, Asia and North Africa/Near East aerosols. The trend of the tree ring data recorded from 1990-2000 deviates from that of the

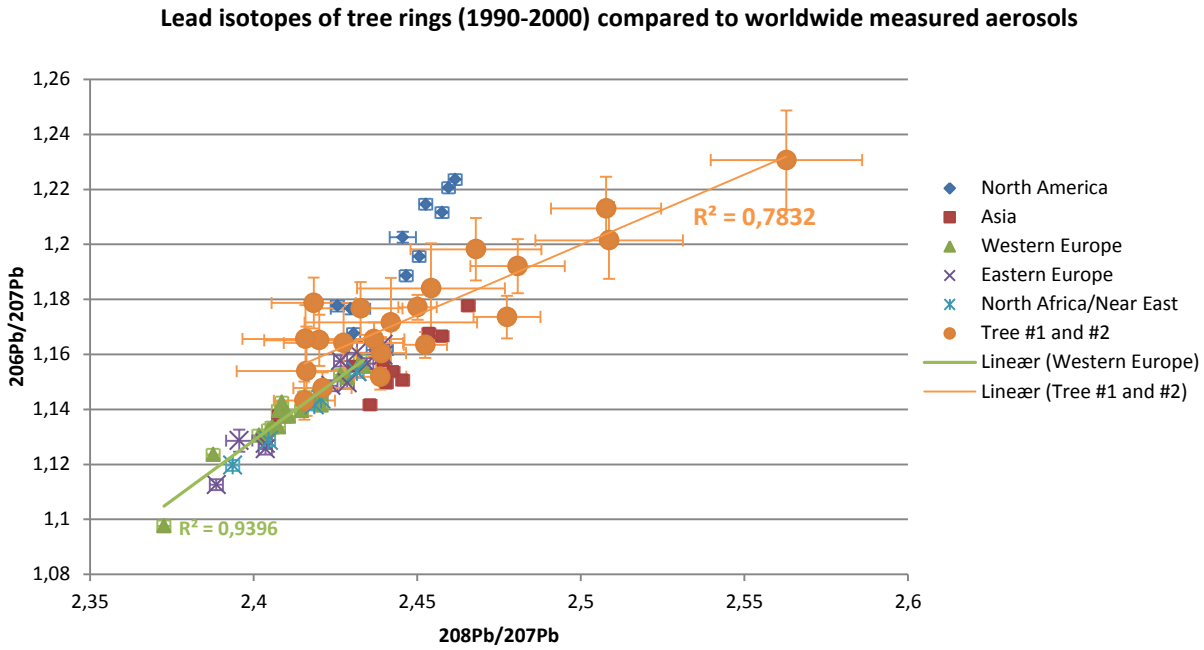

Figure 6-7 Lead isotope ratios for tree rings (both trees) formed from 1990-2000, plotted together with the lead isotope composition (mean ± 2SD) of aerosol collected from various sites in the northern hemisphere between 1994 and 1999. Aerosol data are from Bollhofer and Rosman (2001a).

western and European aerosols. However, considering trends, the tree ring record is more closely related to the western European trend than for example the North American trend. Tree ring values plot towards higher $^{206}Pb/^{207}Pb$ and $^{208}Pb/^{207}Pb$ ratios than those of the western and eastern European trend. On the contrary, the lead isotopes of mosses collected at the southwestern coast of Norway representing the same time period (1990, 1995 and 2000) overlap with these data and show linear correlation factors of 0.9522 and 0.9363 for the western and eastern European aerosols, respectively. This may suggest that the mosses are more influenced by the European atmospheric lead composition, or that they better record variation in the atmospheric lead composition. Another factor may be that the trees are located closer to Mongstad refinery.

6.4 Pollutants and emission rates

6.4.1 Pb isotopic composition of coal, lead ores and gasoline

Figure 6-8 demonstrates the lead isotopic composition of tree rings formed from 1968-2000 in relation to the published lead isotopic values of coals and ores used for lead extraction, and petrol in various countries. The tree ring values overlap with the UK coal and the continental European coal of Germany and Poland. The lead isotopic signatures of the UK coal are

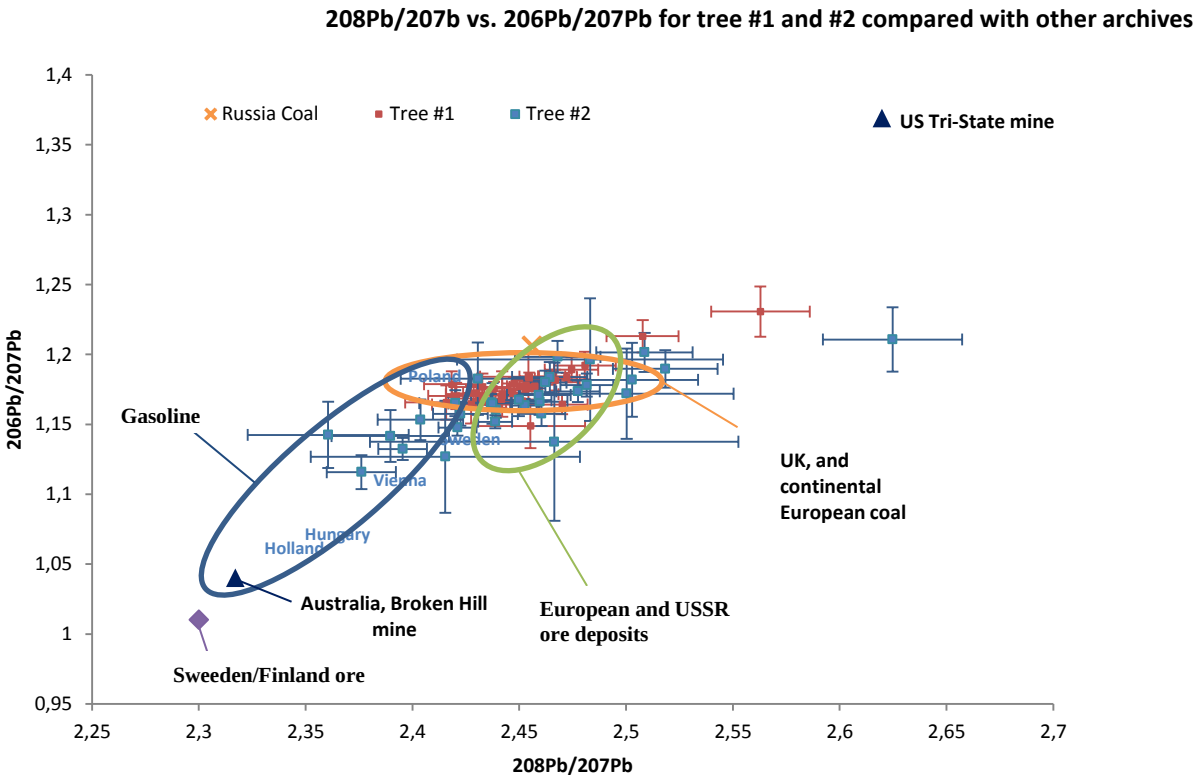

Figure 6-8 Plot of tree rings formed from 1968-2000 along with coal isotope composition of UK coal, European Coal (Poland and Germany) and Russian coal (Farmer et al., 1999). Also shown is the lead isotope composition of gasoline (defined by the blue ellipse) from Sweden (1988), Poland (1988), Vienna (1990), Hungary (1990) and Holland (1990), from Hopper et al. (1991). The green ellipse encompasses the lead composition of major ore-deposits from Germany/Austria, Italy, Greece, Spain, Eastern Europe, Poland, North Africa and USSR (Hopper et al., 1991). US Tri-State mine and the Broken Hill mine located in Australia are also plotted (Cumming and Richards, 1975, Sturges and Barrie, 1987).

plotted for the following countries: England and Wales, Scotland and Ireland. Data were obtained from more than 60 coal samples, mostly from the principal coalfields of the respective countries (Farmer et al., 1999). Farmer et al. (1999) concluded that despite the dramatic decrease in coal-combustion emissions after the mid 1950s, emissions from coal

combustion still have an impact at a time when the uses of unleaded petrol is prevalent and continues to increase. Most of the tree rings from tree #1 that formed between 1968 and 2000 plot in the area defined by the UK and continental European coal. The large scattered data from tree rings of tree #2 do not plot in any specific area.

Pb used for antiknock in western European gasoline is characterized by a low $^{206}Pb/^{207}Pb$ ratio of approx. 1.03-1.04 (the composition of Pb in Broken Hill mine), while the central and eastern European gasoline show a slightly higher ratio of approx. 1.11-1.13 (Weiss et al., 1999). The Pb isotopic signature of the UK gasoline is defined by the Pb composition of Broken Hill mine (Farmer et al., 1999) , and Norway gasoline demonstrate a $^{206}Pb/^{207}Pb$ ratio between 1.07-1.10 (Aberg et al., 2004). Proposing that emissions originating from Eastern Europe compared to the UK may have a small effect on Pb concentration and composition in the western parts of Norway, we would expect lower recorded $^{206}Pb/^{207}Pb$ ratio if vehicle emissions in the UK were the dominating source of pollution. Tree #1 and #2

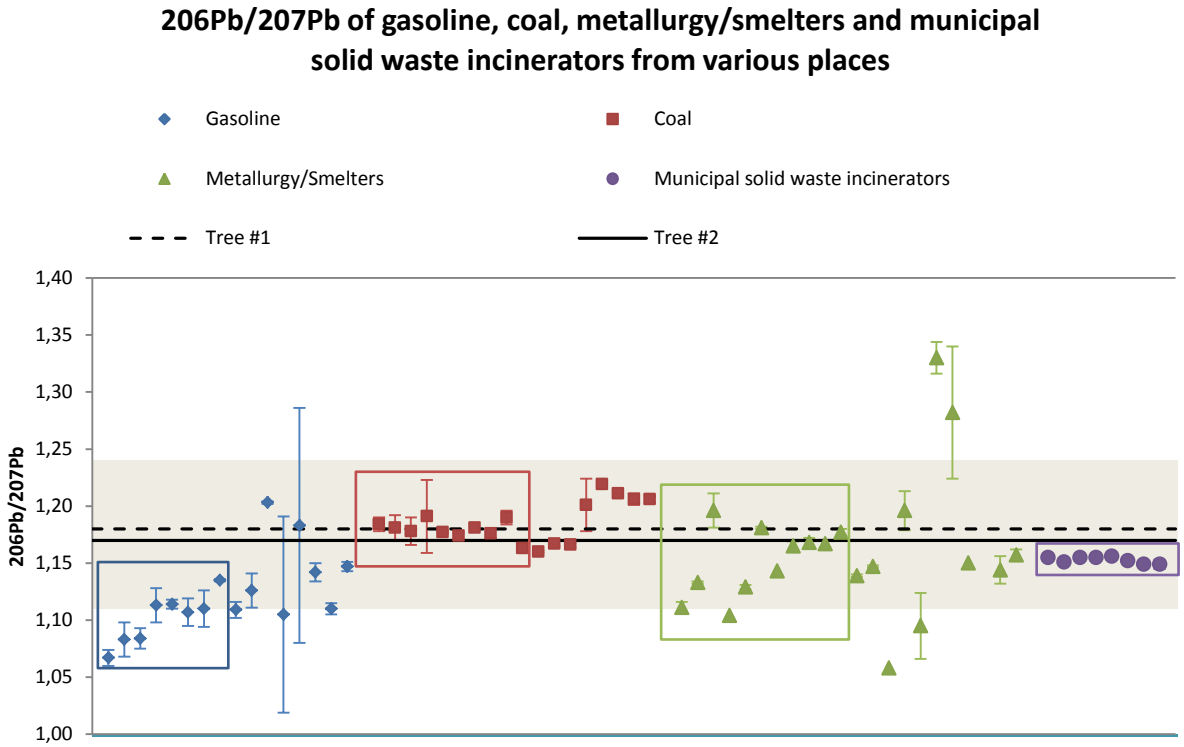

Figure 6-9 Data compiled by Komarek et al. (2008) plotted with the calculated means of tree #1 (black stippled line) and #2 (black solid line). The grey area encompasses the two standard deviations of the calculated means of tree #1 and #2. For convenience, the references for the individual data points are not included. These can be found in table #2 in the paper by Komarek et al. (2008). Data from Komarek et al. (2008) are plotted with 1 standard deviation if available. The squares indicate data compiled for Europe. Data outside the squares include data from Israel, North America, Russia, Asia, and Australia. The European data for gasoline contain data from the UK, France, Switzerland and the Chech Republic. For coal, European data are represented by the UK (England, Wales and Scotland), Ireland, Spain, Poland, Germany, Switzerland, Belgium and the Chech Republic. For metallurgy/smelters, France, Switzerland and the Chech Republic represent the European data. Finally, for the municipal solid waste incinerators, Switzerland and France represent the European data.

record $^{206}Pb/^{207}Pb$ ratios ranging between 1.13 (2006) and 1.32 (2010) 1.12 (1988) and 1.2850 (2010), respectively. If vehicle emissions were the dominating source of Pb incorporated by the two trees, they would have recorded lower $^{206}Pb/^{207}Pb$ ratios, since both western European and Norwegian gasoline are characterized by low $^{206}Pb/^{207}Pb$ ratios. The fact that tree #1 is located along "Fylkesvei 4" and tree #2 along "Fylkesvei 570", should result in higher lead content in tree #2 compared to tree #1 if local vehicle lead emissions were the main lead contributor to the environment. This is, however, not the case, which suggests that the lead content and composition may originate from other lead sources. Also, the $^{206}Pb/^{207}Pb$ ratio recorded by the tree rings should be lower considering a Norwegian gasoline $^{206}Pb/^{207}Pb$ ratio in between 1.07-1.10.

In Figure 6-9, the calculated $^{206}Pb/^{207}Pb$ mean ratios recorded for tree #1 and #2 are plotted together with the $^{206}Pb/^{207}Pb$ ratios of various sources compiled by Komarek et al. (2008). The lead isotopic composition of European coals plot quite close to the mean values of tree #1 (1.18±0.03 (1SD)) and #2 (1.17±0.03 (1SD)) compared to the other sources. For gasoline, the two highest recorded $^{206}Pb/^{207}Pb$ ratios were for Mexico and the US (highest). The $^{206}Pb/^{207}Pb$ ratios of European gasoline show relatively lower values than the

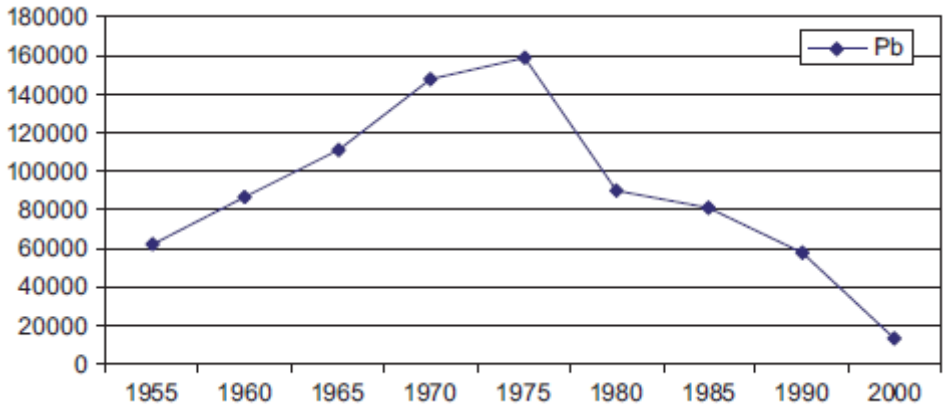

Figure 6-10 European lead emission to the atmosphere as prepared by Pacyna et al. (2007) on the basis of emission factors and data regarding production and consumption of industrial goods and of raw materials, respectively.

trees. The contribution to the atmospheric lead from the other two sources, metallurgy/smelters and municipal solid waste incinerators, may be overshadowed by lead originating from gasoline and coal. This might suggest that Pb emissions as a result of coal burning may be a possible explanation for the subsequent Pb composition of the trees. However, after the 1950s, the UK coal consumption decreased considerable (Farmer et al., 1999). Another factor is that the European lead emission increased from 1955 to 1975 (Figure 6-10), followed by declining trend towards year 2000 (Pacyna and Pacyna, 2000) . During this

time, vehicle emissions have been the most important source of atmospheric lead (49.5-76.1%), followed by the non-ferrous metal manufacturing and the iron and steel production (Pacyna and Pacyna, 2000). The Pb emission from the iron and steel production may represent the composition of coal due to the use of coal and coke as fuels. Therefore, industry using coal may have been a contributor to the observed Pb composition of the tree rings.

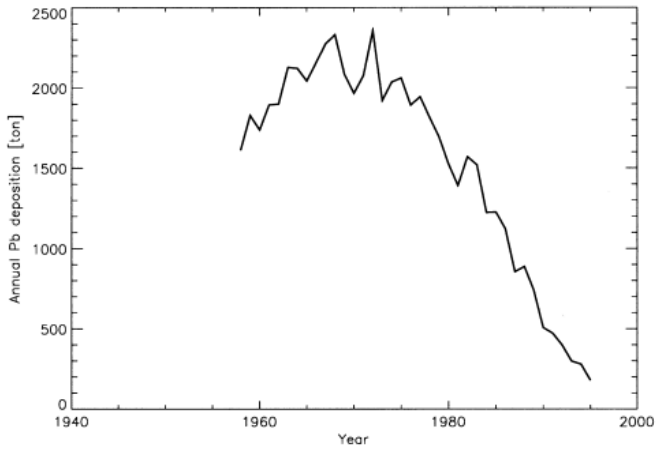

Figure 6-11 Simulated lead deposition over the North Sea. Diagram from von Storch et al. (2003).

von Storch et al. (2003) reconstructed lead pollution in Europe since 1958 with the help of a regional climate model, NCEP re-analysis. Simulation of total annual lead deposition to the North Sea revealed an extended peak covering the 1965-1975 period followed by a steady decrease towards 1995. von Storch et al. (2003) correlates this with UK lead emissions and states that UK is the main contributor of lead to the North Sea. This peak value is also consistent with the peak estimated for European lead emission by Pacyna et al. (2007). When comparing the estimated European emissions from Pacyna et al. (2007) and the simulated lead deposition over the North Sea (von Storch et al., 2003) with the registered $^{208}Pb/^{12}C$ of tree #1 (Figure 5-27), they show similar evolution. The peak value of $^{208}Pb/^{12}C$ of tree #1 is,however, recorded some time later than that of Figure 6-10 and Figure 6-11. A possible delay in relation to Pb content in precipitation was also discussed earlier in chapter 6.2.4. In terms of these comparisons, it seems likely that tree #1 records changes in Pb content of the atmosphere.

If UK is the main contributor of Pb deposition over the North Sea (von Storch et al., 2003), and because most of the annually recorded Pb isotope ratios of tree #1 are constrained within the values defined by the UK and EU coal, it is likely that tree #1 records Pb mainly derived from coal. Watmough et al. (1999a) also report that typical UK industrial and urban emissions have $^{206}Pb/^{207}Pb$ ratio between 1.17 and 1.19 which is in the range recorded by the annual tree rings of tree #1 and #2, though tree #1 demonstrate a better consistency with these values.

6.4.2 Mongstad refinery

No change in the lead isotopic composition was registered on the start-up of Mongstad refinery in 1975 (Figure 5-21 and Figure 5-22) and no pronounced deviations were observed at the several events listed in Figure 3-3. For the recorded $^{208}Pb/^{12}C$ ratios of tree #1 and #2, the onset of production and events at Mongstad did not seem to have any influence. For tree #1, the $^{208}Pb/^{12}C$ was already increasing when production started in 1975. Tree #2 does record an increase from 1975 to 1977, but then a decline is observed. The recorded $^{63}Cu/^{12}C$ ratio of the two trees does not coincide with the onset of production or any of the events. However, tree #2 demonstrates a pronounced peak in 1978 which may be a response of the Mongstad start up, but the production enlargement in 1987 and 1989 does not correspond to any increase in the $^{63}Cu/^{12}C$ or $^{66}Zn/^{12}C$ ratios. The $^{44}Ca/^{24}Mg$ ratio shows an overall declining trend from 1968 to 2010 but show no deviation associated with the onset of pollution from Mongstad refinery or the events.

Table 6-4 demonstrates some significant correlation coefficients between SO_2 released from the Mongstad refinery and the various elements recorded by the tree rings of tree #1. Tree #2, however, shows rather poor correlation coefficients. The SO_2 released to the atmosphere may subsequently affect the soil pH thereby affecting the uptake of Pb and the other elements (Pearson et al., 2005).

		$^{208}Pb/^{12}C$		**$^{63}Cu/^{12}C$**		**$^{66}Zn/^{12}C$**		**Ca/Mg**	
		CC	t-value	CC	t-value	CC	t-value	CC	t-value
SO_2	Tree #1	0.5166	2.0899	0.4029	1.5249	-0.4376	1.6862	0.3001	1.1767
	Tree #2	0.2874	1.0396	-0.0121	0.0421	0.0319	0.1059	0.1833	0.6978

Table 6-4 Correlation coefficients (CC) between various elements as recorded by the tree-rings from 1994-2010 and amount of released SO_2 from Mongstad refinery. Degrees of freedom=n-2=14-2=12.

The highest correlation coefficients were obtained for Tree #1 which is located closest to the Mongstad refinery. This demonstrates a relationship between the annual recorded $^{208}Pb/^{12}C$, $^{63}Cu/^{12}C$, $^{66}Zn/^{12}C$ and $^{44}Ca/^{24}Mg$ ratios and the annual emissions of SO_2. The $^{208}Pb/^{12}C$, $^{63}Cu/^{12}C$ and $^{44}Ca/^{24}Mg$ of tree #1 all show significant (90% confidence level) correlation coefficients. The significant correlations suggest that the emission of SO_2 may influence the soil properties, i.e. changing the bioavailability of the elements involved.

Officially reported Pb emission from the Mongstad refinery are not available which makes it difficult to differentiate between the effect from increased Pb uptake during periods of low soil pH and Pb pollution from the Mongstad refinery. The relatively high positive correlation coefficients of 0.8344 and 0.8398 obtained for tree #1 between $^{208}Pb/^{12}C$ and the

Pb concentration of precipitation measured at Kårvatn and Birkenes, respectively, suggest that the lead content of precipitation is the more controlling factor in the observed annual variation.

According to Aarnes and Bøhler (1992), sulphate content in local precipitation is not associated with emission from Mongstad refinery, and is most probable overshadowed by long range transported pollution (Traaen, 1992). Local contribution of pollution from the Mongstad refinery was estimated to be 6% (Traaen, 1992). Research performed by Larsen (2000), investigated the heavy metal (Pb, Ni and Zn) accumulation trend in one lake (Svartatjønn) located northeast from the Mongstad refinery and east for tree #1 and found that the sediments did not indicate any higher heavy metal deposition after the onset of production at Mongstad in 1975. However, an increase in spheroidal carbonaceous particles (SCP) showed an increase after 1975 and in 1987 when the production capacity was expanded.

6.5 Anthropogenic vs. geochemical background

Reimann et al. (2008) address the problem of natural contribution of Pb to the atmosphere. Lead originating from soil erosion, volcanic emissions, forest fire debris, biogenic emission and oceanic emission may contribute to the overall lead composition of the atmosphere (Rasmussen, 1998). Reimann et al. (2008) studied the lead istopic composition of samples of bedrock, complete soil profiles of forest soils and various biological materials collected along a 120 km long transect running NE-SE through Oslo. When plotting the $^{206}Pb/^{207}Pb$ vs. $^{208}Pb/^{207}Pb$ for these samples, the bedrock lead istopic ratios were found to cover the whole range of the lead isotopic ratios found for the other samples (Reimann et al., 2008).

In this study, no soil samples and no bedrock samples were analyzed. Also, a literature search on whole rock lead composition of the western gneiss region did not reveal any Pb isotopic data from the study area. However, feldspars in Precambrian granitic gneisses of the Rombak window (1860-1760 Ma.) located in Nordland, Norway (Nøttvedt et al., 2007), of similar age as the gneisses of the Western Gneiss region, demonstrate $^{206}Pb/^{207}Pb$ ratios of 1.01-1.03 (Romer, 1991). This may be indicative of the whole rock lead composition at the two tree sites. Such low $^{206}Pb/^{207}Pb$ ratios were not observed in the tree rings, suggesting little influence by bedrock lead composition.

Regarding the soil lead isotopic composition, Steinnes et al. (2005) refers to an unpublished study by Steinnes et al., that the $^{206}Pb/^{207}Pb$ ratios of the C-horizon from different parts of Norway (not specified which places), vary between 1.20-1.73. The calculated mean of the annually recorded $^{206}Pb/^{207}Pb$ ratio from 1968-2010 for tree #1 and #2, yielded 1.18±0.03 and 1.17±0.03, respectively. Only 5 and 4 annual rings of tree #1 and #2, respectively, recorded $^{206}Pb/^{207}Pb$ ratios above 1.20.

Soil and bedrock samples from the two sites need to be investigated before any conclusion can be drawn. Therefore, the influence of natural soil Pb, Zn and Cu content is currently hard to assess.

7 Summary and conclusions

The five different standards analysed during the lead isotopic analysis: in-house wood standard, ERM-CD100, NIST-610, cellulose mixed with BCR-2 and cellulose mixed with NIST-612, gave relative standard deviations for the $^{207}Pb/^{206}Pb$ ratio of 0.077%, 0.011%, 0.019%, 0.601% and 0.190%, respectively.

Tree #1 and #2 recorded $^{206}Pb/^{207}Pb$ ratios between 1.13 and 1.32, and 1.12 and 1.29, respectively. From the innermost to the outermost tree rings of tree #1 and #2, the $^{207}Pb/^{206}Pb$ and $^{208}Pb/^{206}Pb$ ratios did not show any significant trend towards higher or lower values. The isotopic composition (the $^{206}Pb/^{207}Pb$ ratio vs. the $^{208}Pb/^{206}Pb$ ratio) of the annual rings of tree #1 and #2 plotted along linear trendlines with linear correlation factors of 0.7196 and 0.2124, respectively, but did not show any trend towards higher or lower ratios from 1968 to 2010. The only trends observed for lead isotopes from 1968-2010 were the trend of increasing data scatter and standard deviation of the means. For the recorded $^{208}Pb/^{12}C$ ratio, the most interesting result was found for tree #1 which showed a steady increase from 1968 to 1979, followed by a steady decline towards 2010. The $^{66}Zn/^{12}C$ and the $^{63}Cu/^{12}C$ ratios of the two trees show some variation but no the specific overall trend from the outermost to the innermost tree rings. The $^{63}Cu/^{12}C$ of tree #2 show two pronounced peaks, one in 1978 and one in 1987, but could not be related to any specific event.

The onset of production at Mongstad refinery in 1975 and the subsequent expansion in the refinery production and occasional accidents in the factory did not have any significant impact on the lead isotope composition of the tree rings, nor significantly influenced the $^{208}Pb/^{12}C$, $^{63}Cu/^{12}C$, $^{66}Zn/^{12}C$ or the $^{44}Ca/^{24}Mg$ elemental ratios. However, the Mongstad refinery may have an indirect impact on the $^{208}Pb/^{12}C$, $^{63}Cu/^{12}C$, $^{66}Zn/^{12}C$ and the $^{44}Ca/^{24}Mg$ ratios in terms of SO_2 emissions which may affect the soil pH. This is highlighted by the significant correlations within 90% confidence level for the various ratios of tree #1 with the annual SO_2 emissions reported from 1994-2010. In accordance with the prevailing wind directions and the closer proximity of tree #1 to the refinery, it may suggest a higher input of SO_2 at this site. On the other hand, according to Traaen (1992), pollution from the Mongstad refinery is probably overshadowed by the long range pollution. The absence of any higher metal deposition in Svartatjønn lake after the onset of production at the refinery in 1975 (Larsen, 2000) also suggests that heavy metal pollution associated with the Mongstad refinery in this area may be minor. Since the Pb isotopic composition of the North Sea oil could not be identified, it was difficult to assess whether the lead in tree rings originates from the refinery,

foreign sources (industrial emissions and vehicle emission), local transport or natural soil and bedrock. However, the relatively higher recorded $^{206}Pb/^{207}Pb$ ratio of the tree rings (mean values of 1.18±0.03 and 1.17±0.03 for tree #1 and #2, respectively) compared to the Norwegian gasoline between 1.07-1.10 (Aberg et al., 2004), suggest that local vehicle emissions had a minor to no impact on the lead composition of the trees. Most of the annual rings of tree #1 plotted into the lead isotope composition defined by UK and European (only Germany and Poland) coal, which may suggest that tree #1 is affected by industrial coal burning.

The observed recorded $^{208}Pb/^{12}C$ ratio in tree #1 may correspond to the estimated amount of emitted European Pb to the atmosphere (Pacyna et al., 2007) and the estimated lead deposition over the North Sea (von Storch et al., 2003). However, the calculated peaks from von Storch et al. (2003) and Pacyna et al. (2007) do not overlap or coincide with the peak recorded by tree #1. Tree #1 shows a maximum $^{208}Pb/^{12}C$ ratio in 1979 at a time when the Pb of von Storch et al. (2003) and Pacyna et al. (2007) have already started to decrease. If the peak recorded by tree #1 corresponds to these peaks, it can be explained by metal retention in the soil.

The reliability of these trees in tracing past and present pollution sources may be addressed as these annual rings plot toward higher Pb isotope ratios ($^{206}Pb/^{207}Pb$ vs. $^{208}Pb/^{207}Pb$) than moss isotopes recorded for the same time period and area, into the fields confined by Norwegian peat bogs (<1691-1991) and a Greenlandic ice core (7313 BC to 1523 AD). The most significant correlation coefficients with weather station data were obtained between the annually recorded $^{208}Pb/^{12}C$ ratio of tree #1 and the lead content and pH of precipitation, with coefficients of 0.86 and -0.79. This may suggest that tree #1 records variation in lead content and responds to changes in pH of precipitation. Tree #1 compared to tree #2 seems to have higher Pb content, but to fingerprint the source of Pb is still difficult. This could be improved by isotopic analysis of local soil and bedrock and a chemical and isotopic analysis of Pb in oil that is being refined at the Mongstad refinery.

8 References

AARNES, M. J. & BØHLER, T. 1992. Nedbørkvalitet ved Mongstad September 1989-August 1990. *NILU OR,* 56/92**,** 22.

ABERG, G., ABRAHAMSEN, G., STEINNES, E. & HJELMSETH, H. 2004. Utilization of bark pockets as time capsules of atmospheric-lead pollution in Norway. *Atmospheric Environment,* 38**,** 6231-6237.

ABERG, G., PACYNA, J. M., STRAY, H. & SKJELKVALE, B. L. 1999. The origin of atmospheric lead in Oslo, Norway, studied with the use of isotopic ratios. *Atmospheric Environment,* 33**,** 3335-3344.

ADRIANO, D. C. 1986. *Trace elements in the terrestrial environment,* New York, Springer-Verlag.

ALLOWAY, B. J. 1995. *Heavy metals in soils,* London, Blackie Academic & Professional.

BARRELET, T., ULRICH, A., RENNENBERG, H. & KRAHENBUHL, U. 2006. Seasonal profiles of sulphur, phosphorus, and potassium in Norway spruce wood. *Plant Biology,* 8**,** 462-469.

BERG, T., ROYSET, O. & STEINNES, E. 1994. Trace-Elements in Atmospheric Precipitation at Norwegian Background Stations (1989-1990) Measured by Icp-Ms. *Atmospheric Environment,* 28**,** 3519-3536.

BERGGREN, D., BERGKVIST, B., FALKENGRENGRERUP, U., FOLKESON, L. & TYLER, G. 1990. Metal Solubility and Pathways in Acidified Forest Ecosystems of South Sweden. *Science of the Total Environment,* 96**,** 103-114.

BERTAUD, F. & HOLMBOM, B. 2004. Chemical composition of earlywood and latewood in Norway spruce heartwood, sapwood and transition zone wood. *Wood Science and Technology,* 38**,** 245-256.

BINDLER, R., RENBERG, I., KLAMINDER, J. & EMTERYD, O. 2004. Tree rings as Pb pollution archives? A comparison of Pb-206/Pb-207 isotope ratios in pine and other environmental media. *Science of the Total Environment,* 319**,** 173-183.

BJØRNEVOLL, O. & MONGSTAD ADMINISTRASJON 2004. *Historien om Mongstadbasen,* [Mongstad], Mongstad administrasjon.

BOLLHOFER, A. & ROSMAN, K. J. R. 2001a. Isotopic source signatures for atmospheric lead: The Northern Hemisphere. *Geochimica Et Cosmochimica Acta,* 65**,** 1727-1740.

BOLLHOFER, A. & ROSMAN, K. J. R. 2001b. Lead isotopic ratios in European atmospheric aerosols. *Physics and Chemistry of the Earth Part B-Hydrology Oceans and Atmosphere,* 26**,** 835-838.

BREKKE, K. & SVENDSEN, R. H. 2008. Mongstad-brann under kontroll. *NRK*.

CERMAK, J., CIENCIALA, E., KUCERA, J. & HALLGREN, J. E. 1992. Radial-Velocity Profiles of Water-Flow in Trunks of Norway Spruce and Oak and the Response of Spruce to Severing. *Tree Physiology,* 10**,** 367-380.

CHEN, L., WU, F. H., LIU, T. W., CHEN, J. A., LI, Z. J., PEI, Z. M. & ZHENG, H. L. 2010. Soil acidity reconstruction based on tree ring information of a dominant species Abies fabri in the subalpine forest ecosystems in southwest China. *Environmental Pollution,* 158**,** 3219-3224.

CHUN, L. A. & HUANG, H. Y. 1992. Tree-Ring Element Analysis of Korean Pine (Pinus-Koraiensis Sieb Et Zucc) and Mongolian Oak (Quercus-Mongolica Fisch Ex Turcz) from Changbai Mountain, North-East China. *Trees-Structure and Function,* 6**,** 103-108.

CUMMING, G. L. & RICHARDS, J. R. 1975. Ore Lead Isotope Ratios in a Continuously Changing Earth. *Earth and Planetary Science Letters,* 28**,** 155-171.

CUTTER, B. E. & GUYETTE, R. P. 1993. Anatomical, Chemical, and Ecological Factors Affecting Tree Species Choice in Dendrochemistry Studies. *Journal of Environmental Quality,* 22**,** 611-619.

DEWAELE, S., MUCHEZ, P. & HERTOGEN, J. 2007. Production of a matrix-matched standard for quantitative analysis of iron sulphides by laser ablation inductively coupled plasma-mass spectrometry by welding: A pilot study. *Geologica Belgica,* 10**,** 109-119.

DONNELLY, J. R., SHANE, J. B. & SCHABERG, P. G. 1990. Lead Mobility within the Xylem of Red Spruce Seedlings - Implications for the Development of Pollution Histories. *Journal of Environmental Quality,* 19**,** 268-271.

DUNLAP, C. E., STEINNES, E. & FLEGAL, A. R. 1999. A synthesis of lead isotopes in two millennia of European air. *Earth and Planetary Science Letters,* 167**,** 81-88.

DUNN, C. E. 2007. *Biogeochemistry in mineral exploration,* Amsterdam, Elsevier.

DUNSTAN, L. P., GRAMLICH, J. W., BARNES, I. L. & PURDY, W. C. 1980. Absolute Isotopic Abundance and the Atomic Weight of a Reference Sample of Thallium. *Journal of Research of the National Bureau of Standards,* 85**,** 1-10.

DURRANT, S. F. 1999. Laser ablation inductively coupled plasma mass spectrometry: achievements, problems, prospects. *Journal of Analytical Atomic Spectrometry,* 14**,** 1385-1403.

EADES, L. J., FARMER, J. G., MACKENZIE, A. B., KIRIKA, A. & BAILEY-WATTS, A. E. 2002. Stable lead isotopic characterisation of the historical record of environmental lead contamination in dated freshwater lake sediment cores from northern and central Scotland. *Science of the Total Environment,* 292**,** 55-67.

ELLMORE, G. S. & EWERS, F. W. 1986. Fluid-Flow in the Outermost Xylem Increment of a Ring-Porous Tree, Ulmus-Americana. *American Journal of Botany,* 73**,** 1771-1774.

ESAU, K. 1977. *Anatomy of seed plants,* New York [etc.] ,, Wiley.

FARJON, A. 2010. *A handbook of the world's conifers,* Leiden, Brill.

FARMER, J. G., EADES, L. J., ATKINS, H. & CHAMBERLAIN, D. F. 2002. Historical trends in the lead isotopic composition of archival Sphagnum mosses from Scotland (1838-2000). *Environmental Science & Technology,* 36**,** 152-157.

FARMER, J. G., EADES, L. J. & GRAHAM, M. C. 1999. The lead content and isotopic composition of British coals and their implications for past and present releases of lead to the UK environment. *Environmental Geochemistry and Health,* 21**,** 257-272.

FARMER, J. G., EADES, L. J., GRAHAM, M. C. & BACON, J. R. 2000. The changing nature of the Pb-206/Pb-207 isotopic ratio of lead in rainwater, atmospheric particulates, pine needles and leaded petrol in Scotland, 1982-1998. *Journal of Environmental Monitoring,* 2**,** 49-57.

FARMER, J. G., EADES, L. J., MACKENZIE, A. B., KIRIKA, A. & BAILEYWATTS, T. E. 1996. Stable lead isotope record of lead pollution in Loch Lomond sediments since 1630 AD. *Environmental Science & Technology,* 30**,** 3080-3083.

FARMER, J. G., GRAHAM, M. C., BACON, J. R., DUNN, S. M., VINOGRADOFF, S. I. & MACKENZIE, A. B. 2005. Isotopic characterisation of the historical lead deposition record at Glensaugh, an organic-rich, upland catchment in rural NE Scotland. *Science of the Total Environment,* 346**,** 121-137.

FARMER, J. G., MACKENZIE, A. B., SUGDEN, C. L., EDGAR, P. J. & EADES, L. J. 1997. A comparison of the historical lead pollution records in peat and freshwater lake sediments from central Scotland. *Water Air and Soil Pollution,* 100**,** 253-270.

FINNIGAN-NEPTUNE-MANUAL 2004. Finnigan Neptune: Hardware Manual.

FRAMSTAD, A. P. 2010. Hundrevis evakuert etter vulkanutbrudd på Island. *Verdens Gang*.

GARTNER, B. L. 1995. *Plant stems : physiology and functional morphology,* San Diego ; London, Academic Press.

GUNTHER, D., LONGERICH, H. P., JACKSON, S. E. & FORSYTHE, L. 1996. Effect of sampler orifice diameter on dry plasma inductively coupled plasma mass spectrometry (ICP MS) backgrounds, sensitivities, and limits of detection using laser ablation sample introduction. *Fresenius Journal of Analytical Chemistry,* 355**,** 771-773.

HAGEMEGER, J. 1995. Radial Distributions of Cd in Stems of Oak Trees (Quercus-Robur L) Re-Analyzed after 10 Years. *Trees-Structure and Function,* 9**,** 200-203.

HAGEMEYER, J. 1993. Monitoring trace metal pollution with tree rings: A critical reassessment. *B. Markert,* Plants as Biomonitors. Indicators for Heavy Metals in the Terrestrial Environment**,** 541-563.

HAGEMEYER, J. & LOHRIE, K. 1995. Distribution of Cd and Zn in Annual Xylem Rings of Young Spruce Trees [Picea-Abies (L) Karst] Grown in Contaminated Soil. *Trees-Structure and Function,* 9**,** 195-199.

HAGEMEYER, J., LULFSMANN, A., PERK, M. & BRECKLE, S. W. 1992. Are There Seasonal-Variations of Trace-Element Concentrations (Cd, Pb, Zn) in Wood of Fagus Trees in Germany. *Vegetatio,* 101**,** 55-63.

HAGEMEYER, J. & SCHAFER, H. 1995. Seasonal-Variations in Concentrations and Radial-Distribution Patterns of Cd, Pb and Zn in Stem Wood of Beech Trees (Fagus-Sylvatica L). *Science of the Total Environment,* 166**,** 77-87.

HAGEMEYER, J. & WEINAND, T. 1996. Radial distributions of Pb in stems of young Norway spruce trees grown in Pb-contaminated soil. *Tree Physiology,* 16**,** 591-594.

HINE, R. 2008a. *A dictionary of biology,* Oxford, Oxford University Press.

HINE, R. S. 2008b. *A Dictionary of biology,* Oxford, University Press.

HOADLEY, R. B. 2000. *Understanding wood : a craftsman's guide to wood technology,* Newtown, Conn, Taunton Press.

HOFFMANN, E., LUDKE, C., SCHOLZE, H. & STEPHANOWITZ, H. 1994. Analytical Investigations of Tree-Rings by Laser-Ablation Icp-Ms. *Fresenius Journal of Analytical Chemistry,* 350**,** 253-259.

HOPPER, J. F., ROSS, H. B., STURGES, W. T. & BARRIE, L. A. 1991. Regional Source Discrimination of Atmospheric Aerosols in Europe Using the Isotopic Composition of Lead. *Tellus Series B-Chemical and Physical Meteorology,* 43**,** 45-60.

HUTCHINSON, T. C. & WHITBY, L. M. 1977. Effects of Acid Rainfall and Heavy-Metal Particulates on a Boreal Forest Ecosystem near Sudbury Smelting Region of Canada. *Water Air and Soil Pollution,* 7**,** 421-438.

JACKSON, S. E. The application of Nd : YAG lasers in LA-ICP-MS.

JARVIS, K. E. & WILLIAMS, J. G. 1993. Laser-Ablation Inductively-Coupled Plasma-Mass Spectrometry (La-Icp-Ms) - a Rapid Technique for the Direct, Quantitative-Determination of Major, Trace and Rare-Earth Elements in Geological Samples. *Chemical Geology,* 106**,** 251-262.

KAHLE, H. 1993. Response of Roots of Trees to Heavy-Metals. *Environmental and Experimental Botany,* 33**,** 99-119.

KOECHNER, W. & BASS, M. 2003. *Solid-state lasers: a graduate text,* New York, Springer.

KOLSTAD, K. 1999. *Mongstad : frå utkantbygd til industristad,* Oslo, Samlaget.

KOMAREK, M., ETTLER, V., CHRASTNY, V. & MIHALJEVIC, M. 2008. Lead isotopes in environmental sciences: A review. *Environment International,* 34**,** 562-577.

KONHAUSER, K. 2007. *Introduction to geomicrobiology,* Malden, MA, Blackwell Pub.

KOVALEVSKI, A. L. 1987. *Biogeochemical exploration for mineral deposits, second ed.*, VNU Science Press, Utrecht, The Netherlands.

LARSEN, J. 2000. Recent changes in diatom-inferred pH, heavy metals, and spheroidal carbonaceous particles in lake sediments near an oil refinery at Mongstad, Western Norway. *Journal of Paleolimnology,* 23**,** 343-363.

LEGGE, A. H., KAUFMANN, H. C. & WINCHESTER, J. W. 1984. Tree-Ring Analysis by Pixe for a Historical Record of Soil Chemistry Response to Acidic Air-Pollution. *Nuclear Instruments & Methods in Physics Research Section B-Beam Interactions with Materials and Atoms,* 3**,** 507-510.

LEPP, N. W. 1975. Potential of Tree-Ring Analysis for Monitoring Heavy-Metal Pollution Patterns. *Environmental Pollution,* 9**,** 49-61.

LEPP, N. W. & DOLLARD, G. J. 1974a. Studies on Behavior of Lead in Wood - Binding of Free and Complexed Pb-210 to Xylem Tissue. *Oecologia,* 16**,** 369-373.

LEPP, N. W. & DOLLARD, G. J. 1974b. Studies on Lateral Movement of Pb-210 in Woody Stems - Patterns Observed in Dormant and Non-Dormant Stems. *Oecologia,* 16**,** 179-184.

LIN, Z. Q., BARTHAKUR, N. N., SCHUEPP, P. H. & KENNEDY, G. G. 1995. Uptake and translocation of Mn-54 and Zn-65 applied on foliage and bark surfaces of balsam fir [Abies balsamea (L) Mill] seedlings. *Environmental and Experimental Botany,* 35**,** 475-&.

LONGUETAUD, F., MOTHE, F., LEBAN, J. M. & MAKELA, A. 2006. Picea abies sapwood width: Variations within and between trees. *Scandinavian Journal of Forest Research,* 21**,** 41-53.

MCBRIDE, M., SAUVE, S. & HENDERSHOT, W. 1997. Solubility control of Cu, Zn, Cd and Pb in contaminated soils. *European Journal of Soil Science,* 48**,** 337-346.

METEROLOGISK-INSTITUTT. 2012. Available: http://sharki.oslo.dnmi.no/portal/page?_pageid=73,39035,73_39049&_dad=portal&_schema=PORTAL [Accessed 30.03.2012 2012].

MIHALJEVIC, M., ZUNA, M., ETTLER, V., CHRASTNY, V., SEBEK, O., STRNAD, L. & KYNCL, T. 2008. A comparison of tree rings and peat deposit geochemical archives in the vicinity of a lead smelter. *Water Air and Soil Pollution,* 188**,** 311-321.

MOMOSHIMA, N. & BONDIETTI, E. A. 1990. Cation Binding in Wood - Applications to Understanding Historical Changes in Divalent-Cation Availability to Red Spruce. *Canadian Journal of Forest Research-Revue Canadienne De Recherche Forestiere,* 20**,** 1840-1849.

MOTTO, H. L., DAINES, R. H., CHILKO, D. M. & MOTTO, C. K. 1970. Lead in Soils and Plants - Its Relationship to Traffic Volume and Prximity to Highways. *Environmental Science & Technology,* 4**,** 231-&.

NABAIS, C., FREITAS, H. & HAGEMEYER, J. 1999. Dendroanalysis: a tool for biomonitoring environmental pollution? *Science of the Total Environment,* 232**,** 33-37.

NEMEC, W. 2011. *Geostatistics: Lecture notes,* Deparment of Earth Science, University of Bergen.

NORWEGIAN-INSTITUTE-OF-FORESTS-AND-LANSCAPE. 2007. *Nedlasting av kartdata - jordsmonn* [Online]. Available: http://www.skogoglandskap.no/kart/artikler/2007/nedlasting_jordsmonn [Accessed 02.05 2012].

NOVAK, M., MIKOVA, J., KRACHLER, M., KOSLER, J., ERBANOVA, L., PRECHOVA, E., JACKOVA, I. & FOTTOVA, D. 2010. Radial distribution of lead and lead isotopes in stem wood of Norway spruce: A reliable archive of pollution trends in Central Europe. *Geochimica Et Cosmochimica Acta,* 74**,** 4207-4218.

NRIAGU, J. O. 1990. The Rise and Fall of Leaded Gasoline. *Science of the Total Environment,* 92**,** 13-28.

NTB. 2004. Mongstad-brann kostet nær 100 millioner. *Dagens Næringsliv*.

NØTTVEDT, A., BRYHNI, I., RAMBERG, I. B. & NORSK GEOLOGISK FORENING 2007. *Landet blir til : Norges geologi*, Trondheim, Norsk geologisk forening.

OKADA, N., KATAYAMA, Y., NOBUCHI, T., ISHIMARU, Y. & AOKI, A. 1993. Trace-Elements in the Stems of Trees .6. Comparisons of Radial Distributions among Hardwood Stems. *Mokuzai Gakkaishi,* 39**,** 1119-1127.

PACYNA, E. G., PACYNA, J. M., FUDALA, J., STRZELECKA-JASTRZAB, E., HLAWICZKA, S., PANASIUK, D., NITTER, S., PREGGER, T., PFEIFFER, H. & FRIEDRICH, R. 2007. Current and future emissions of selected heavy metals to the atmosphere from anthropogenic sources in Europe. *Atmospheric Environment,* 41**,** 8557-8566.

PACYNA, J. M. & PACYNA, E. G. 2000. Atmospheric emissions of anthropogenic lead in Europe: Improvements, updates, historical data and projections. .

PANTERA, A., PAPADOPOULOS, A. M. & ORFANOUDAKIS, M. 2007. Trace element accumulation in tree rings of Pinus halepensis during the last 140 years. *Global Nest Journal,* 9**,** 286-292.

PEARSON, C., MANNING, S. W., COLEMAN, M. & JARVIS, K. 2005. Can tree-ring chemistry reveal absolute dates for past volcanic eruptions? *Journal of Archaeological Science,* 32**,** 1265-1274.

POTTS, P. J. 1987. *A handbook of silicate rock analysis,* Glasgow, Blackie.

RASMUSSEN, P. E. 1998. Long-range atmospheric transport of trace metals: the need for geoscience perspectives. *Environmental Geology,* 33**,** 96-108.

REIMANN, C., FLEM, B., ARNOLDUSSEN, A., ENGLMAIER, P., FINNE, T. E., KOLLER, F. & NORDGULEN, O. 2008. The biosphere: A homogeniser of Pb-isotope signals. *Applied Geochemistry,* 23**,** 705-722.

ROMER, R. L. 1991. The Late Archean to Early Proterozoic Lead Isotopic Evolution of the Northern Baltic Shield of Norway, Sweden and Finland. *Precambrian Research,* 49**,** 73-95.

ROSMAN, K. J. R., CHISHOLM, W., HONG, S. M., CANDELONE, J. P. & BOUTRON, C. F. 1997. Lead from Carthaginian and Roman Spanish mines isotopically identified in Greenland ice dated from 600 BC to 300 AD. *Environmental Science & Technology,* 31**,** 3413-3416.

SAUTER, J. J. & VANCLEVE, B. 1992. Seasonal-Variation of Amino-Acids in the Xylem Sap of Populus X Canadensis and Its Relation to Protein Body Mobilization. *Trees-Structure and Function,* 7**,** 26-32.

SAUVE, S., HENDERSHOT, W. & ALLEN, H. E. 2000. Solid-solution partitioning of metals in contaminated soils: Dependence on pH, total metal burden, and organic matter. *Environmental Science & Technology,* 34**,** 1125-1131.

SAVARD, M. M., BEGIN, C., PARENT, M., MARION, J. & SMIRNOFF, A. 2006. Dendrogeochemical distinction between geogenic and anthropogenic emissions of metals and gases near a copper smelter. *Geochemistry-Exploration Environment Analysis,* 6**,** 237-247.

SCHARTAU, A. K. 2011a. *Overvåking av langtransportert forurenset luft og nedbør : årsrapport - effekter 2010,* Oslo ,, Norsk institutt for vannforskning.

SCHARTAU, A. K. 2011b. *Overvåking av langtransporterte forurensninger 2010 : sammendragsrapport,* Oslo ,, Norsk institutt for vannforskning.

SLETTA, K. 2009. Millionkrangel etter Vest-Tank-eksplosjonen. *Bergens Avisa*.

SLINN, W. G. N. 1977. Some Approximations for Wet and Dry Removal of Particles and Gases from Atmosphere. *Water Air and Soil Pollution,* 7**,** 513-543.

SMITH, D. & FLEGAL, A. R. 1995. Lead in the Biosphere - Recent Trends. *Ambio,* 24**,** 21-23.

STATISTISK SENTRALBYRÅ 2002. *Energistatistikk,* Oslo, Statistisk sentralbyrå.

STEINNES, E. 2001. Metal Contamination of the Natural Environment in Norway from Long Range Atmospheric Transport. *Water, Air, & Soil Pollution: Focus,* 1**,** 449-460.

STEINNES, E., ABERG, G. & HJELMSETH, H. 2005. Atmospheric deposition of lead in Norway: spatial and temporal variation in isotopic composition. *Science of the Total Environment,* 336**,** 105-117.

STEINNES, E., BERG, T. & UGGERUD, H. T. 2011. Three decades of atmospheric metal deposition in Norway as evident from analysis of moss samples. *Science of the Total Environment,* 412**,** 351-358.

STEWART, C. M. 1966. Excretion and Heartwood Formation in Living Trees. *Science,* 153**,** 1068-&.

STURGES, W. T. & BARRIE, L. A. 1987. Lead-206/207 Isotope Ratios in the Atmosphere of North-America as Tracers of United-States and Canadian Emissions. *Nature,* 329**,** 144-146.

TAIZ, L. & ZEIGER, E. 2007. *Plant Physiology : das Original mit Übersetzungshilfen,* Spektrum Akad.Verlag.

TAYLOR, H. E. 2001. *Inductively coupled plasma-mass spectrometry : practices and techniques,* San Diego, Calif., Academic Press.

TOMMASINI, S., DAVIES, G. R. & ELLIOTT, T. 2000. Lead isotope composition of tree rings as bio-geochemical tracers of heavy metal pollution: a reconnaissance study from Firenze, Italy. *Applied Geochemistry,* 15**,** 891-900.

TRAAEN, T. 1992. Overvåking av innsjøer rundt Mongstad, 1991. *NIVA-rapport,* 2760**,** 29pp.

VANBEL, A. J. E. 1990. Xylem-Phloem Exchange Via the Rays - the Undervalued Route of Transport. *Journal of Experimental Botany,* 41**,** 631-644.

VANHAECKE, F. & MOENS, L. 1999. Recent trends in trace element determination and speciation using inductively coupled plasma mass spectrometry. *Fresenius Journal of Analytical Chemistry,* 364**,** 440-451.

VON STORCH, H., COSTA-CABRAL, M., HAGNER, C., FESER, F., PACYNA, J., PACYNA, E. & KOLB, S. 2003. Four decades of gasoline lead emissions and control policies in Europe: a retrospective assessment. *Science of the Total Environment,* 311**,** 151-176.

WATMOUGH, S. A. 1999. Monitoring historical changes in soil and atmospheric trace metal levels by dendrochemical analysis. *Environmental Pollution,* 106**,** 391-403.

WATMOUGH, S. A., HUGHES, R. J. & HUTCHINSON, T. C. 1999a. Pb-206/Pb-207 ratios in tree rings as monitors of environmental change. *Environmental Science & Technology,* 33**,** 670-673.

WATMOUGH, S. A. & HUTCHINSON, T. C. 1996. Analysis of tree rings using inductively coupled plasma mass spectrometry to record fluctuations in a metal pollution episode. *Environmental Pollution,* 93**,** 93-102.

WATMOUGH, S. A., HUTCHINSON, T. C. & EVANS, R. D. 1999b. The distribution of Zn-67 and Pb-207 applied to white spruce foliage at ambient concentrations under different pH regimes. *Environmental and Experimental Botany,* 41**,** 83-92.

WATMOUGH, S. A., HUTCHINSON, T. C. & SAGER, E. P. S. 1998. Changes in tree ring chemistry in sugar maple (Acer saccharum) along an urban-rural gradient in southern Ontario. *Environmental Pollution,* 101**,** 381-390.

WEISS, D., SHOTYK, W., APPLEBY, P. G., KRAMERS, I. D. & CHEBURKIN, A. K. 1999. Atmospheric Ph deposition since the industrial revolution recorded by five

Swiss peat profiles: Enrichment factors, fluxes, isotopic composition, and sources. *Environmental Science & Technology,* 33**,** 1340-1352.
WHITE, W. M. 1998. Geochemistry. John-Hopkins University Press.
ZIMMERMANN, M. H., BROWN, C. L. & TYREE, M. T. 1971. *Trees : structure and function,* Berlin, Springer.

9 Appendix

This appendix contains results of the chemical and isotopic analysis of the tree rings and various statistical tests used throughout the text.

9.1 Lead isotopic analysis

		206Pb/204Pb		207Pb/204Pb		208Pb/204Pb		207Pb/206Pb		208Pb/206Pb	
		Mean	StdMean	Mean	StdMean	Mean	StdMean	Mean	StdMean	Mean	StdMean
Cell+BCR-2	1	16,3712	0,4843	13,7117	0,4091	34,2857	1,0369	0,8323	0,0020	2,0591	0,0042
	2	16,7588	0,7603	14,1670	0,6265	35,3552	1,6399	0,8384	0,0036	2,0576	0,0055
	3	18,4374	0,4489	15,5520	0,3847	38,5243	0,9777	0,8391	0,0021	2,0564	0,0040
	4	17,0916	0,6075	14,2670	0,5182	35,5398	1,2873	0,8280	0,0037	2,0534	0,0058
	5	18,2317	0,5205	15,3611	0,4618	37,9414	1,1178	0,8298	0,0028	2,0581	0,0049
Cell+NIST-612	1	17,0682	0,2585	15,5028	0,2372	37,4524	0,5600	0,9039	0,0013	2,1574	0,0019
	2	17,7243	0,3232	16,2106	0,2941	38,9348	0,7138	0,9071	0,0013	2,1645	0,0030
	3	17,0915	0,2523	15,5949	0,2284	37,3975	0,5396	0,9051	0,0012	2,1623	0,0017
	4	16,9416	0,2463	15,3842	0,2249	37,0456	0,5423	0,9039	0,0013	2,1614	0,0022
	5	16,8684	0,3022	15,4437	0,2888	36,9208	0,6742	0,9075	0,0022	2,1634	0,0030
ERM-CD100 wood standard	1	19,7082	0,0189	15,7948	0,0146	39,1175	0,0380	0,7963	0,0001	1,9589	0,0001
	2	19,7363	0,0202	15,8118	0,0163	39,1499	0,0411	0,7961	0,0001	1,9585	0,0001
	3	19,6965	0,0236	15,7887	0,0190	39,0855	0,0483	0,7964	0,0001	1,9592	0,0001
	4	19,6976	0,0143	15,7890	0,0115	39,0888	0,0288	0,7962	0,0001	1,9590	0,0001
	5	19,7482	0,0181	15,8283	0,0144	39,1961	0,0362	0,7963	0,0001	1,9590	0,0001
	6	19,6424	0,0243	15,7365	0,0196	38,9422	0,0481	0,7962	0,0001	1,9590	0,0002
	7	19,7739	0,0127	15,8344	0,0095	39,1772	0,0240	0,7962	0,0001	1,9589	0,0001
	8	19,6990	0,0188	15,7747	0,0150	39,0308	0,0374	0,7961	0,0001	1,9589	0,0001
	9	19,7348	0,0154	15,7994	0,0133	39,1006	0,0318	0,7962	0,0001	1,9590	0,0001
	10	19,8187	0,0195	15,8916	0,0155	39,3705	0,0383	0,7963	0,0001	1,9594	0,0002
	11	19,7477	0,0183	15,8259	0,0155	39,1976	0,0372	0,7962	0,0001	1,9590	0,0002
	12	19,8250	0,0154	15,8944	0,0123	39,3698	0,0302	0,7963	0,0001	1,9593	0,0001
	13	19,7824	0,0190	15,8557	0,0164	39,2816	0,0381	0,7963	0,0001	1,9593	0,0001

In-House wood standard	1	18,3806	0,0442	15,7516	0,0381	38,8684	0,0917	0,8523	0,0002	2,0887	0,0004
	2	18,5201	0,0511	15,8805	0,0437	39,1800	0,1081	0,8520	0,0002	2,0887	0,0003
	3	18,3834	0,0607	15,7591	0,0525	38,8997	0,1254	0,8524	0,0002	2,0888	0,0004
	4	18,4755	0,0610	15,8690	0,0522	39,1588	0,1341	0,8531	0,0003	2,0903	0,0007
	5	18,5069	0,0523	15,8720	0,0442	39,1419	0,1091	0,8521	0,0002	2,0882	0,0003
	6	18,5269	0,0525	15,8753	0,0461	39,1763	0,1109	0,8523	0,0002	2,0893	0,0004
	7	18,4866	0,0440	15,8357	0,0392	39,0559	0,0939	0,8516	0,0002	2,0886	0,0004
	8	18,3742	0,0486	15,7375	0,0418	38,8043	0,1016	0,8522	0,0002	2,0886	0,0004
	9	18,4833	0,0472	15,8193	0,0411	39,0320	0,0991	0,8514	0,0002	2,0879	0,0004
	10	18,4694	0,0530	15,8579	0,0444	39,1193	0,1145	0,8529	0,0003	2,0903	0,0005
	11	18,4397	0,0788	15,7954	0,0681	39,0396	0,1638	0,8505	0,0003	2,0875	0,0006
	12	18,4467	0,0564	15,8340	0,0493	39,0495	0,1193	0,8525	0,0002	2,0896	0,0004
	13	18,3616	0,0444	15,7742	0,0375	38,9254	0,0940	0,8525	0,0002	2,0898	0,0004
	14	18,5569	0,0698	15,9123	0,0576	39,2770	0,1441	0,8523	0,0003	2,0889	0,0005
NIST-610	1	17,2125	0,0209	15,7473	0,0185	37,7583	0,0437	0,9096	0,0001	2,1673	0,0002
	2	17,2317	0,0230	15,7742	0,0208	37,8252	0,0490	0,9097	0,0001	2,1680	0,0003
	3	17,2519	0,0279	15,7929	0,0264	37,8642	0,0620	0,9095	0,0002	2,1669	0,0003
	4	17,2143	0,0243	15,7550	0,0233	37,7794	0,0595	0,9093	0,0002	2,1667	0,0003
	5	17,2446	0,0299	15,7884	0,0263	37,8559	0,0659	0,9094	0,0002	2,1674	0,0003
	6	17,2688	0,0245	15,8111	0,0223	37,9213	0,0519	0,9096	0,0002	2,1675	0,0004
	7	17,2709	0,0253	15,8062	0,0237	37,9253	0,0556	0,9093	0,0002	2,1670	0,0003
	8	17,2558	0,0309	15,8124	0,0298	37,9109	0,0683	0,9094	0,0002	2,1668	0,0003
	9	17,2225	0,0217	15,7644	0,0202	37,8289	0,0481	0,9093	0,0002	2,1670	0,0003
	10	17,3004	0,0303	15,8565	0,0258	38,0147	0,0645	0,9097	0,0002	2,1679	0,0003
	11	17,3210	0,0310	15,8422	0,0286	38,0164	0,0705	0,9096	0,0002	2,1677	0,0003
	12	17,2741	0,0316	15,8123	0,0291	37,9245	0,0681	0,9092	0,0002	2,1674	0,0004
	13	17,2242	0,0231	15,7475	0,0201	37,7611	0,0496	0,9094	0,0002	2,1678	0,0003
	14	17,1897	0,0287	15,7223	0,0254	37,6974	0,0617	0,9095	0,0002	2,1676	0,0003

15	17,2304	0,0301	15,7640	0,0269	37,7781	0,0652	0,9096	0,0002	2,1681	0,0003
16	17,1729	0,0243	15,6987	0,0208	37,6336	0,0493	0,9095	0,0002	2,1682	0,0003
17	17,1974	0,0287	15,7329	0,0266	37,6911	0,0631	0,9096	0,0001	2,1673	0,0003
18	17,2233	0,0278	15,7597	0,0254	37,7595	0,0591	0,9098	0,0002	2,1673	0,0004
19	17,2577	0,0526	15,8127	0,0505	37,9470	0,1158	0,9097	0,0005	2,1682	0,0007
20	17,2745	0,1008	15,7679	0,1002	37,8806	0,2393	0,9106	0,0007	2,1681	0,0010
21	17,3318	0,0997	15,8973	0,0913	38,0835	0,2201	0,9100	0,0007	2,1679	0,0013
22	17,2435	0,0339	15,7892	0,0314	37,8615	0,0749	0,9095	0,0002	2,1672	0,0004
23	17,2156	0,0274	15,7670	0,0256	37,8369	0,0589	0,9095	0,0002	2,1679	0,0003
24	17,3249	0,0344	15,8595	0,0311	38,0578	0,0753	0,9094	0,0002	2,1685	0,0004
25	17,2436	0,0321	15,7749	0,0290	37,8583	0,0707	0,9094	0,0002	2,1678	0,0004
26	17,2412	0,0194	15,7915	0,0184	37,8792	0,0450	0,9094	0,0002	2,1668	0,0004
27	17,2821	0,0214	15,8256	0,0193	37,9710	0,0460	0,9095	0,0002	2,1678	0,0003

Table 9-1 Results from the continuously measured standards. StdMean: Standard devitation of the mean.

	206Pb/204Pb			207Pb/204Pb			208Pb/204Pb			207Pb/206Pb			208Pb/206Pb			206Pb/207Pb		208Pb/207b	
	Mean	**StdMean**	**n**	**Mean**	**StdMean**	**n**	**Mean**	**StdMean**	**n**	**Mean**	**StdMean**	**n**	**Mean**	**StdMean**	**n**	**Mean**	**Stdmean**	**Mean**	**Stdmean**
Bark	2,420	0,187	103	2,203	0,163	104	5,426	0,415	106	0,890	0,032	109	2,108	0,045	98	1,124	0,041	2,369	0,056
2010	0,194	0,453	95	0,386	0,442	97	0,022	0,837	98	0,757	0,137	90	1,687	0,178	91	1,322	0,240	2,230	0,225
2009	1,474	0,413	95	1,169	0,436	93	4,064	1,246	98	0,805	0,081	96	2,114	0,150	99	1,243	0,126	2,627	0,170
2008	4,329	0,910	86	3,797	0,755	88	9,496	1,912	86	0,792	0,028	103	2,007	0,048	101	1,263	0,045	2,534	0,056
2007	6,039	1,580	92	3,773	1,585	97	11,583	3,608	94	0,859	0,023	100	2,040	0,042	107	1,164	0,031	2,375	0,048
2006	11,422	1,331	96	10,196	1,184	96	24,111	2,798	95	0,883	0,013	102	2,087	0,028	109	1,133	0,017	2,365	0,031
2005	15,213	1,615	85	12,401	1,491	87	31,819	3,422	85	0,846	0,013	107	2,059	0,021	105	1,183	0,019	2,435	0,025
2004	16,002	0,933	98	13,346	0,747	95	33,087	1,838	95	0,845	0,005	115	2,081	0,008	110	1,183	0,007	2,462	0,009
2003	13,417	1,085	87	12,278	1,043	91	29,293	2,455	88	0,870	0,008	104	2,122	0,014	109	1,150	0,010	2,440	0,016
2002	15,363	1,986	98	12,766	1,464	94	31,885	3,664	95	0,855	0,011	106	2,081	0,016	95	1,170	0,015	2,434	0,019
2001	13,542	1,410	81	11,988	1,341	84	29,048	3,082	82	0,846	0,008	100	2,098	0,016	106	1,182	0,011	2,479	0,018
2000	13,925	1,388	90	12,347	1,274	91	29,971	3,069	91	0,867	0,012	114	2,094	0,018	102	1,154	0,016	2,416	0,021
1999	11,402	1,089	90	9,250	0,829	88	24,206	2,290	91	0,813	0,012	108	2,082	0,020	110	1,231	0,018	2,563	0,023
1998	13,459	1,925	92	11,211	1,879	95	27,619	4,235	93	0,845	0,012	105	2,073	0,019	113	1,184	0,016	2,454	0,023
1997	11,003	1,170	81	9,584	0,990	82	23,823	2,489	82	0,854	0,012	102	2,084	0,024	113	1,172	0,016	2,442	0,026
1996	17,029	1,716	93	14,527	1,441	92	35,557	3,547	92	0,859	0,010	106	2,085	0,015	112	1,164	0,013	2,427	0,018
1995	11,182	1,007	92	9,826	0,908	93	23,633	2,172	92	0,858	0,009	103	2,073	0,017	104	1,166	0,012	2,416	0,019
1994	12,006	0,682	98	10,209	0,573	97	25,303	1,448	98	0,850	0,007	113	2,067	0,011	108	1,177	0,010	2,433	0,013
1993	16,250	1,213	92	14,137	1,098	94	33,679	2,529	92	0,848	0,007	113	2,052	0,011	111	1,179	0,009	2,418	0,013
1992	18,181	1,889	91	15,378	1,631	92	38,859	4,149	92	0,824	0,008	108	2,067	0,015	110	1,213	0,012	2,508	0,017
1991	15,042	1,188	95	12,908	0,999	96	32,132	2,536	96	0,839	0,007	108	2,081	0,013	110	1,192	0,010	2,481	0,014
1990	17,618	0,827	106	15,114	0,668	103	37,094	1,659	103	0,850	0,003	91	2,081	0,005	89	1,177	0,005	2,450	0,006
1989	15,734	1,576	99	13,451	1,327	99	33,535	3,431	100	0,854	0,007	105	2,068	0,011	96	1,170	0,009	2,420	0,013
1988	15,245	1,080	92	13,430	0,973	94	33,586	2,446	95	0,859	0,005	101	2,122	0,011	109	1,164	0,007	2,470	0,012
1987	16,478	1,215	97	14,448	1,102	99	35,249	2,702	99	0,853	0,004	107	2,072	0,009	110	1,172	0,006	2,429	0,010
1986	16,263	0,572	104	13,965	0,476	103	34,497	1,227	106	0,853	0,003	107	2,073	0,005	104	1,172	0,004	2,430	0,006

1985	17,071	0,752	100	14,667	0,667	101	35,868	1,561	98	0,851	0,004	106	2,074	0,006	103	1,175	0,005	2,438	0,007
1984	16,861	0,838	100	14,412	0,743	101	35,478	1,752	99	0,856	0,004	111	2,091	0,007	107	1,168	0,006	2,442	0,008
1983	15,425	0,693	99	13,411	0,622	100	33,212	1,548	101	0,857	0,004	115	2,101	0,008	110	1,167	0,006	2,451	0,009
1982	17,329	0,443	109	14,827	0,375	109	36,598	0,940	109	0,849	0,002	107	2,082	0,004	115	1,178	0,003	2,453	0,004
1981	17,676	0,536	102	14,954	0,466	102	37,228	1,176	104	0,845	0,002	103	2,089	0,004	102	1,183	0,003	2,472	0,005
1980	17,576	0,388	107	15,065	0,332	106	37,022	0,836	107	0,853	0,002	110	2,087	0,003	113	1,172	0,002	2,447	0,004
1979	17,886	0,406	107	15,278	0,349	106	37,943	0,882	108	0,850	0,002	107	2,088	0,003	100	1,176	0,003	2,457	0,004
1978	16,975	0,402	105	14,687	0,336	104	36,022	0,836	104	0,857	0,002	106	2,087	0,003	105	1,166	0,002	2,433	0,004
1977	16,856	0,457	112	14,472	0,396	113	35,821	0,979	113	0,849	0,002	119	2,087	0,003	105	1,177	0,003	2,457	0,004
1976	17,261	0,525	106	14,777	0,456	108	36,349	1,111	107	0,844	0,002	99	2,073	0,004	113	1,184	0,003	2,455	0,005
1975	17,176	0,552	107	14,453	0,435	103	35,995	1,136	106	0,848	0,003	119	2,076	0,004	107	1,179	0,004	2,447	0,005
1974	17,085	0,791	104	14,539	0,662	104	36,145	1,666	105	0,844	0,003	109	2,082	0,006	110	1,184	0,004	2,465	0,006
1973	17,057	0,733	99	14,602	0,622	99	36,193	1,566	99	0,851	0,004	104	2,086	0,006	106	1,176	0,005	2,453	0,007
1972	16,961	0,658	102	14,684	0,592	106	36,273	1,438	105	0,846	0,003	113	2,084	0,007	112	1,183	0,005	2,465	0,007
1971	17,386	1,066	103	15,261	0,957	105	37,574	2,339	105	0,857	0,004	108	2,102	0,007	106	1,167	0,006	2,452	0,008
1970	16,880	1,109	105	14,437	0,968	105	35,757	2,372	105	0,846	0,005	113	2,088	0,010	113	1,182	0,007	2,467	0,011
1969	17,081	1,124	105	14,403	0,900	102	35,361	2,235	102	0,856	0,006	115	2,082	0,009	112	1,169	0,008	2,433	0,011
1968	14,321	1,078	99	11,971	0,878	98	29,703	2,195	98	0,841	0,006	106	2,081	0,011	102	1,189	0,009	2,474	0,012
1967	10,001	2,030	93	9,011	1,724	92	22,581	4,257	92	0,870	0,012	103	2,137	0,023	110	1,149	0,016	2,455	0,026

Table 9-2 Results from the LA-ICP-MS analysis of the annual tree rings of tree #1. StdMean: Standard deviation of the mean. n represents the number of measurements used for calculation of the mean.

	206Pb/204Pb			207Pb/204Pb			208Pb/204Pb			207Pb/206Pb			208Pb/206Pb			206Pb/207Pb		208Pb/207Pb	
	Mean	**StdMean**	**n**	**Mean**	**StdMean**	**n**	**Mean**	**StdMean**	**n**	**Mean**	**StdMean**	**n**	**Mean**	**StdMean**	**n**	**Mean**	**Stdmean**	**Mean**	**Stdmean**
Bark	3,510	0,167	105	3,119	0,150	106	7,499	0,353	105	0,882	0,010	99	2,136	0,018	103	1,134	0,013	2,421	0,021
2010	0,630	0,941	77	0,319	0,841	78	1,080	1,956	76	0,778	0,057	76	1,955	0,082	76	1,285	0,094	2,513	0,099
2009	1,646	1,040	94	1,164	0,818	91	3,070	2,204	92	0,836	0,037	90	1,930	0,078	99	1,195	0,053	2,308	0,087
2008	2,672	0,856	94	2,379	0,723	93	6,297	1,752	92	0,861	0,063	112	2,146	0,104	107	1,161	0,085	2,491	0,122
2007	0,918	1,357	99	1,269	1,127	96	3,826	2,818	98	0,813	0,042	105	1,964	0,068	109	1,230	0,063	2,415	0,079
2006	4,310	1,856	95	2,863	1,748	96	8,405	4,087	93	0,882	0,024	107	2,203	0,043	104	1,133	0,031	2,497	0,049
2005	8,814	0,994	81	9,099	1,122	88	20,076	2,756	88	0,876	0,022	108	2,101	0,041	113	1,141	0,028	2,397	0,046
2004	14,267	1,504	89	12,842	1,451	91	30,451	3,205	89	0,870	0,011	105	2,094	0,016	103	1,149	0,015	2,407	0,019
2003	15,297	1,659	85	12,738	1,273	82	31,073	2,997	82	0,867	0,010	106	2,122	0,021	110	1,154	0,013	2,449	0,023
2002	17,010	1,602	91	14,980	1,440	91	33,919	2,952	86	0,871	0,009	113	2,090	0,014	117	1,149	0,012	2,400	0,017
2001	11,605	0,785	96	9,892	0,648	94	25,044	1,689	97	0,858	0,007	101	2,114	0,017	113	1,166	0,009	2,465	0,018
2000	14,634	0,696	100	12,728	0,603	99	31,192	1,496	99	0,875	0,005	113	2,113	0,008	99	1,143	0,007	2,416	0,009
1999	15,283	0,738	101	13,395	0,661	102	32,138	1,511	99	0,871	0,004	110	2,109	0,008	112	1,148	0,006	2,421	0,009
1998	14,565	0,610	99	12,801	0,546	101	31,786	1,390	103	0,868	0,003	103	2,117	0,007	115	1,152	0,005	2,439	0,008
1996	16,132	0,846	101	13,847	0,706	100	34,032	1,763	100	0,862	0,004	112	2,102	0,006	101	1,160	0,006	2,439	0,008
1995	15,828	0,676	103	13,930	0,627	106	33,917	1,454	104	0,860	0,003	112	2,108	0,006	115	1,163	0,005	2,452	0,007
1994	16,869	1,165	101	14,372	0,998	100	35,124	2,355	99	0,852	0,006	110	2,111	0,008	100	1,174	0,008	2,477	0,010
1993	14,265	0,641	100	12,389	0,549	98	29,972	1,350	99	0,858	0,005	116	2,091	0,008	113	1,166	0,006	2,437	0,009
1992	15,614	1,351	94	13,742	1,191	95	33,996	3,091	96	0,858	0,007	102	2,077	0,015	113	1,165	0,009	2,420	0,017
1991	13,028	1,314	82	11,537	1,225	85	28,111	2,922	84	0,835	0,008	96	2,060	0,018	109	1,198	0,011	2,468	0,020
1990	14,959	1,588	89	12,549	1,330	89	31,893	3,378	90	0,832	0,010	107	2,088	0,020	117	1,201	0,014	2,509	0,023
1989	14,902	1,432	89	12,973	1,220	89	30,843	2,867	87	0,867	0,011	114	2,084	0,017	110	1,153	0,015	2,404	0,020
1988	13,573	1,047	88	12,635	1,043	91	29,154	2,241	88	0,896	0,010	121	2,130	0,013	105	1,116	0,012	2,376	0,016
1987	7,527	1,628	94	6,763	1,428	94	16,203	3,481	94	0,846	0,019	112	2,118	0,025	99	1,182	0,026	2,503	0,031
1986	9,308	2,494	93	8,032	2,048	91	19,936	5,179	91	0,846	0,018	110	2,055	0,031	105	1,183	0,026	2,431	0,036
1985	6,002	2,584	90	5,784	2,281	89	12,453	5,673	91	0,876	0,014	106	2,093	0,024	107	1,142	0,019	2,390	0,028

1984	6,485	3,427	97	5,177	2,866	96	16,016	7,110	95	0,826	0,016	108	2,168	0,029	110	1,211	0,023	2,625	0,033
1983	3,642	1,556	103	2,126	1,414	105	6,385	3,455	102	0,879	0,044	113	2,168	0,074	110	1,138	0,057	2,466	0,086
1982	5,083	1,625	93	4,251	1,490	95	11,121	3,566	93	0,853	0,023	107	2,133	0,044	112	1,172	0,032	2,500	0,050
1981	10,637	1,087	88	8,743	0,856	86	22,770	2,248	87	0,841	0,010	100	2,117	0,023	104	1,190	0,013	2,518	0,025
1980	14,845	1,555	48	12,860	1,397	49	31,422	3,199	48	0,845	0,008	57	2,082	0,016	59	1,184	0,011	2,464	0,018
1979	15,190	1,109	93	13,009	0,905	92	32,217	2,278	92	0,864	0,007	113	2,126	0,009	107	1,157	0,009	2,460	0,011
1978	15,419	1,105	99	13,632	0,961	100	33,391	2,444	101	0,864	0,006	110	2,093	0,011	112	1,158	0,009	2,422	0,013
1977	16,105	1,298	91	14,160	1,199	93	35,304	2,954	93	0,857	0,007	107	2,109	0,011	102	1,166	0,009	2,460	0,013
1976	15,772	1,819	84	13,670	1,570	83	33,460	3,965	84	0,858	0,011	103	2,092	0,018	111	1,165	0,015	2,437	0,021
1975	3,632	1,624	92	2,659	1,575	98	7,658	3,418	93	0,887	0,032	111	2,144	0,054	115	1,127	0,040	2,415	0,063
1974	5,460	1,369	92	4,226	1,140	92	9,842	2,986	95	0,836	0,031	110	2,076	0,054	117	1,196	0,044	2,483	0,062
1973	7,700	1,740	96	6,342	1,560	96	15,638	3,789	97	0,875	0,018	107	2,066	0,033	102	1,142	0,024	2,361	0,038
1972	13,030	1,119	97	11,381	0,996	98	27,586	2,378	97	0,857	0,008	115	2,099	0,013	110	1,167	0,011	2,450	0,015
1971	15,993	0,979	98	14,421	0,925	100	34,576	2,120	99	0,883	0,006	107	2,115	0,010	103	1,132	0,008	2,395	0,011
1970	15,707	0,814	101	13,504	0,720	102	33,179	1,707	101	0,848	0,006	120	2,087	0,008	108	1,180	0,008	2,462	0,010
1969	14,801	0,869	102	12,298	0,673	97	30,915	1,755	99	0,849	0,006	110	2,106	0,011	107	1,178	0,008	2,482	0,012
1968	16,669	1,756	90	14,334	1,512	90	35,549	3,724	90	0,854	0,007	115	2,100	0,013	109	1,171	0,010	2,459	0,015
Pith	11,689	1,051	100	10,036	0,855	99	25,415	2,205	100	0,851	0,010	94	2,124	0,014	88	1,175	0,014	2,494	0,017

Table 9-3 Results from the LA-ICP-MS analysis of the annual tree rings of tree #2. StdMean: Standard deviation of the mean. n represents the number of measurements used for calculation of the mean.

9.2 Element analysis

	Tree #1				Tree #2			
	$^{44}Ca/^{24}Mg$	$^{208}Pb/^{12}C$	$^{66}Zn/^{12}C$	$^{63}Cu/^{12}C$	$^{44}Ca/^{24}Mg$	$^{208}Pb/^{12}C$	$^{66}Zn/^{12}C$	$^{63}Cu/^{12}C$
Bark	0,079451	0,000018	0,001596	0,001051	0,459979	0,000020	0,001336	0,000545
2010	0,036351	0,000006	0,000133	0,000160	0,271869	0,000017	0,000066	0,000170
2009	0,148140	0,000012	0,000618	0,000254	0,445275	0,000008	0,000054	0,000135
2008	0,102767	0,000015	0,000096	0,000153	0,510385	0,000008	0,000048	0,000114
2007	0,117924	0,000009	0,000056	0,000117	0,580625	0,000007	0,000041	0,000144
2006	0,111478	0,000022	0,000067	0,000228	0,512484	0,000020	0,000049	0,000173
2005	0,153622	0,000039	0,000120	0,000291	0,517973	0,000030	0,000058	0,000297
2004	0,220901	0,000068	0,000097	0,000260	0,597135	0,000031	0,000056	0,000154
2003	0,236417	0,000066	0,000095	0,000280	0,497736	0,000057	0,000058	0,000184
2002	0,220460	0,000034	0,000141	0,000194	0,515286	0,000044	0,000060	0,000113
2001	0,235611	0,000025	0,000156	0,000151	0,477758	0,000081	0,000051	0,000135
2000	0,253540	0,000032	0,000161	0,000491	0,419138	0,000084	0,000064	0,000168
1998	0,257173	0,000033	0,000146	0,000209	0,530727	0,000064	0,000057	0,000164
1997	0,236179	0,000024	0,000122	0,000246	0,471234	0,000062	0,000059	0,000354
1996	0,220640	0,000030	0,000110	0,000128	0,527305	0,000069	0,000069	0,000178
1995	0,224064	0,000035	0,000086	0,000269	0,516594	0,000078	0,000078	0,000159
1994	0,225064	0,000085	0,000132	0,000285	0,542646	0,000092	0,000097	0,000140
1993	0,214836	0,000052	0,000088	0,000176	0,439689	0,000104	0,000085	0,000145
1992	0,196566	0,000048	0,000075	0,000110	0,577381	0,000053	0,000076	0,000259
1991	0,196371	0,000064	0,000093	0,000352	0,532510	0,000042	0,000072	0,000318
1990	0,183738	0,000054	0,000098	0,000234	0,542059	0,000042	0,000074	0,000355
1989	0,170385	0,000061	0,000091	0,000282	0,548747	0,000040	0,000070	0,000194
1988	0,180386	0,000063	0,000071	0,000327	0,561221	0,000051	0,000082	0,001134
1987	0,180356	0,000074	0,000069	0,000177	0,566450	0,000035	0,000080	0,001199
1986	0,252006	0,000125	0,000119	0,000352	0,570139	0,000030	0,000086	0,000903
1985	0,233730	0,000099	0,000091	0,000184	0,542971	0,000033	0,000074	0,000631
1984	0,209248	0,000106	0,000096	0,000184	0,537402	0,000041	0,000128	0,000764
1983	0,262685	0,000110	0,000072	0,000232	0,531721	0,000023	0,000062	0,000503
1982	0,256783	0,000154	0,000088	0,000261	0,531442	0,000016	0,000049	0,000125
1981	0,233793	0,000213	0,000114	0,000463	0,537325	0,000043	0,000064	0,000293
1980	0,227208	0,000213	0,000103	0,000226	0,535236	0,000056	0,000064	0,000390
1979	0,279439	0,000285	0,000137	0,000339	0,624918	0,000054	0,000056	0,000536
1978	0,273926	0,000188	0,000088	0,000156	0,561181	0,000052	0,000066	0,001166
1977	0,291649	0,000168	0,000097	0,000382	0,682721	0,000069	0,000081	0,000801
1976	0,299650	0,000186	0,000094	0,000277	0,622225	0,000046	0,000069	0,000730
1975	0,284922	0,000191	0,000075	0,000446	0,582634	0,000021	0,000107	0,000270
1974	0,275405	0,000141	0,000069	0,000180	0,513620	0,000024	0,000094	0,000636
1973	0,289849	0,000158	0,000089	0,001135	0,563380	0,000031	0,000074	0,000270
1972	0,278606	0,000121	0,000086	0,000472	0,604826	0,000050	0,000080	0,000238
1971	0,292464	0,000147	0,000081	0,000321	0,604199	0,000109	0,000092	0,000432
1970	0,314144	0,000088	0,000096	0,000769	0,631293	0,000086	0,000114	0,000778

1969	0,269902	0,000080	0,000083	0,000505	0,585493	0,000115	0,000114	0,000541
1968	0,315109	0,000120	0,000131	0,000373	0,601769	0,000084	0,000144	0,000446

Table 9-4 Results from the element analysis. Only raw ratios are plotted.

9.3 Statistical analysis

This appendix provides a general description of the statistical analysis used in data evaluation. All the encountered equations and statistics are from Nemec (2011).

9.3.1 The Spearman rank-correlation test

The coefficient of the rank correlation test:

$$r_s = 1 - \frac{6\sum^n D_i^2}{n(n^2-1)} \qquad \textbf{Equation 9-1}$$

where D is the rank difference and n the number of data. The significance of correlation is evaluated by a one-tail hypothesis:

$$\begin{cases} H_0: r_s \leq 0 \\ H_1: r_s > 0 \end{cases} \quad \text{or} \quad \begin{cases} H_0: r_s \geq 0 \\ H_1: r_s < 0 \end{cases}$$

The test function:

$$t = |r_s| \sqrt{\frac{n-2}{1-r_s^2}} \qquad \textbf{Equation 9-2}$$

where r_s and n is rank correlation coefficient and number of data. Degrees of freedom:

$$DF = n - 2 \qquad \textbf{Equation 9-3}$$

9.3.2 Cramer-von Mises test for distribution normality

This test is designed for non-grouped data, and the hypotheses can be formulated (two-tail test):

H_0: The measurements conform to normal distribution

H_1: The measurements do not conform to normal distribution

The test function is formulated:

$$\omega^2 = \left[\sum^{n}\left(P_i - \frac{2i-1}{2n}\right)^2 + \frac{1}{12n}\right]\left(1 + \frac{1}{2n}\right) \qquad \textbf{Equation 9-4}$$

where P_i, n and *i* denote the corresponding cumulative frequency of standard normal distribution, number of data and the index value, respectively.

Its critical values for different levels of significance are listed in Table 9-5.

If $\omega^2 \geq \omega^2_{\frac{1}{2}\alpha}$ H_0 is rejected and H_1 is accepted.

If $\omega^2 < \omega^2_{\frac{1}{2}\alpha}$ H_0 is accepted.

	$\boldsymbol{\alpha = 0,10}$	$\boldsymbol{\alpha = 0,05}$	$\boldsymbol{\alpha = 0,025}$	$\boldsymbol{\alpha = 0,001}$
$\boldsymbol{\omega_\alpha}$	0,104	0,126	0,148	0,178

Table 9-5 Critical values for the Cramer-von Mises normality test. α denote the level of significance

Table 9-6 lists the ω^2 values calculated for various data in this study.

	$\boldsymbol{\omega^2}$
In-house wood standard	0.1143
ERM-CD100	0.0506
NIST-610	0.0282
Cellulose+BCR-2	0.0578
Cellulose+NIST-612	0.0465

Table 9-6 Test function values of the measured $^{207}Pb/^{206}Pb$ ratios of the standards measured during the Pb isotopic analysis.

9.3.3 Snedecor F-test for difference between variances

The following test will be used in conjunction with the student t-test for difference between means. The test function is:

$$F = \frac{S_1^2}{S_2^2} \qquad \textbf{Equation 9-5}$$

where S_1^2 and S_2^2 are the variances of the respective measurements. The larger and smaller variance is placed in the numerator and denominator, respectively.

$$DF_1 = n_1 - 1$$
$$DF_2 = n_2 - 1$$

where n_1 and n_2 represent the number of measurements corresponding to S_1^2 and S_2^2. Depending on their ratio, a one-tail hypothesis is formulated:

$$\begin{cases} H_0: S_1^2 \leq S_2^2 \\ H_1: S_1^2 > S_2^2 \end{cases} \quad \text{or} \quad \begin{cases} H_0: S_1^2 \geq S_2^2 \\ H_1: S_1^2 < S_2^2 \end{cases}$$

The critical value is then calculated for the desired significance level in excel using the equation:

$$=f.inv.rt \qquad \textbf{Equation 9-6}$$

Then,

If $F \geq F_\propto$ H_0 is rejected and H_1 is accepted.

If $F < F_\propto$ H_0 is accepted.

9.3.4 Student t-test for difference between means

Depending on the outcome of the Snedecor F-test above, the student t test function is:

If $F < F_{\propto}$ The test function is:

$$t = \frac{|\bar{x}_1 - \bar{x}_2|}{\sqrt{s^2\left(\frac{1}{n_1} + \frac{1}{n_2}\right)}} \qquad \text{DF}=n_1+n_2-2 \qquad \textbf{Equation 9-7}$$

$$s^2 = \frac{(n_1 - 1)S_1^2 + (n_2 - 1)S_2^2}{n_1 + n_2 - 2} \qquad \textbf{Equation 9-8}$$

If $F \geq F_{\propto}$ The test function is:

$$t = \frac{|\bar{x}_1 - \bar{x}_2|}{\sqrt{\left(\frac{S_1^2}{n_1} + \frac{S_2^2}{n_2}\right)}} \qquad \text{DF}=n_1+n_2-2 \qquad \textbf{Equation 9-9}$$

The one-tail hypothesis:

$$\begin{cases} H_0: \mu_1 \leq \mu_2 \\ H_1: \mu_1 > \mu_2 \end{cases} \quad \text{or} \quad \begin{cases} H_0: \mu_1 \geq \mu_2 \\ H_1: \mu_1 < \mu_2 \end{cases}$$

Then,

If $t \geq t_{\propto}$ H_0 is rejected and H_1 is accepted.

If $t < t_{\propto}$ H_0 is accepted.

9.3.5 Correlation analysis

The correlation analyses were performed by using the correlation function in Microsoft Excel 2010. The significance of the correlation coefficient (r_{CL}) can be evaluated by a one-tail hypothesis:

One-tail hypothesis:

$$\begin{cases} H_0: r_{CL} \leq 0 \\ H_1: r_{CL} > 0 \end{cases} \quad \text{or} \quad \begin{cases} H_0: r_{CL} \geq 0 \\ H_1: r_{CL} < 0 \end{cases}$$

The test function is:

$$t = |r_{CL}| \sqrt{\frac{n^* - 2}{1 - r_{CL}^2}} \qquad \textbf{Equation 9-10}$$

where r_{CL} is the correlation coefficient and n^* is number of pairs of overlapped elements. Then, if:

If $t \geq t_\propto$ H_0 is rejected and H_1 is accepted.

If $t < t_\propto$ H_0 is accepted.